EXPERIMENTAL DEVELOPMENTS TOWARDS A LONG-BASELINE LASER INTERFEROMETRIC GRAVITATIONAL RADIATION DETECTOR.

By

GRAHAM ALEXANDER KERR

Department of Natural Philosophy,

University of Glasgow.

Presented as a thesis for the degree of

Ph.D. in the University of Glasgow.

April 1986

ProQuest LLC.
789 East Eisenhower Parkway
P.O. Box 1346
Ann Arbor, MI 48106 – 1346

CONTENTS

ACKNOWLEDGEMENTS

First, and foremost, I would like to thank my supervisor, Jim Hough, whose help and guidance during the last few years have been invaluable.

I am grateful for the interest and support shown by Professor Ernest Laing, and the advice and encouragement of Professor Ron Drever.

To the other members of the Glasgow gravitational waves group - Harry Ward, Norna Robertson, Gavin Newton, Brian Meers, Stuart Hoggan and John Mangan - whose contributions to the overall experiment have been incalculable, I give my sincere thanks.

Excellent technical assistance, from within the group, was provided by Jim Pittillo, Angus McKellar, Allan Latta and John Jarvis, along with the entire staff of the departmental mechanical workshop.

Harry and Brian allowed the use of their printing hardware, and Ken Mackay assisted in cobbling together plotting routines for some of the graphs.

Finally, special mention must be made to my family and friends for their support and for enduring my darker moods during the writing of this thesis.

I would like to thank the SERC for financial assistance during the course of this work.

PREFACE

The Glasgow gravitational waves group, headed by J. Hough and R.W.P. Drever, is actively developing a ten metre prototype laser interferometer with the aim of building a larger (>1km) instrument which is intended to be used for the detection and observation of gravitational radiation. Construction of the prototype detector was initiated in 1978, and this thesis describes certain aspects of its development between October 1982 and September 1985.

Chapter 1 is an introductory review of gravitational wave theory, sources and detection techniques. This chapter is primarily intended for the orientation of the reader.

Chapter 2 discusses noise contributions to the detector, describes its operation and investigates the reduction of the limiting noise level. Much of this work was performed with the help of the entire group.

In Chapter 3, the reconstruction of a mainframe argon ion laser, which incorporates a separate cavity resonator, is described. Investigations into the subsequent improvements in the intrinsic noise of the laser are also described. This was performed with the assistance of N.A. Robertson, and the advice of J. Hough, C.N. Man and A. Brillet.

Chapter 4 discusses laser frequency stabilisation and analyses the reflection locking scheme used at Glasgow. The light loss due to stabilisation with an intra-cavity modulator is also analysed.

A new frequency stabilisation technique, which

removes the need for an intra-cavity device, is described in Chapter 5, and its performance analysed. The experiments, investigating this technique, were undertaken with the assistance of N.A. Robertson and J. Hough.

Chapters 6 and 7 involve the prototype detector, once more, and describe investigations into the reduction of residual laser frequency noise in the interferometer, by optical and electronic subtraction techniques, to improve the sensitivity of the detector. These experiments were carried out with the involvement of B. Meers, J. Hough, G.P. Newton and H. Ward. The analytical sections of Chapter 6 were undertaken at the instigation of J. Hough.

Chapter 8, summarises the development work and includes a discussion of techniques relevant to a kilometre detector.

The thesis concludes with an appendix which describes an experiment, carried out with the rest of the group, to place an upper limit on the level of gravitational radiation from the millisecond pulsar PSR1937+214.

SUMMARY

EXPERIMENTAL DEVELOPMENTS TOWARDS A LONG-BASELINE LASER INTERFEROMETRIC GRAVITATIONAL RADIATION DETECTOR.

Gravitational radiation (a wave-like disturbance in space-time, propagating with the speed of light) is predicted as a consequence of Einstein's General theory of Relativity. Indirectly verified by observations of the binary pulsar PSR1913+16, gravitational waves have still to be observed directly. Direct observation and study of these waves could provide detailed information on astrophysical events, unobtainable by the observation of any other form of radiation.

Currently one of the most promising techniques is the use of laser interferometry to sense the motions of suspended test masses. This type of detector is broad-band in nature and, as such, is particularly attractive. Of the two possible types of interferometer in use, some aspects of the development of one of these (an optical cavity interferometer) are extensively investigated.

Following a brief introduction to the theory of gravitational radiation and a review of gravitational wave sources and detection techniques, a detailed description of the design and operation of the Glasgow prototype detector is given.

The sensitivity of the interferometric detector can be impaired by many noise sources, and the thesis describes how progress in the reduction of two of these noise sources

improves the sensitivity. Firstly, a report is given on how progress in test mass design and the isolation of mechanical noise have improved sensitivity. The second noise source considered is the effect of fluctuations in the frequency of the illuminating laser light, and consideration of the influence of this noise source forms a large part of the thesis.

An argon laser was rebuilt, with a separate cavity resonator, to reduce the level of intrinsic frequency noise, along with other noise sources, and a new technique of stabilising the laser frequency was developed. This method, which uses the reflection locking r.f. sideband technique, does not require the use of an intra-cavity modulator, and thus enables the laser to operate with a higher power output.

The effects of residual laser frequency noise in the interferometer can be reduced by optical interference or by a technique which measures, and electronically subtracts, the frequency fluctuations. Both of these techniques are studied and their contributions to the improvement of detector sensitivity are reported.

With a view to the future, some techniques applicable to a longer detector (>1km) are discussed and, finally, an experiment with a split-bar detector, which places an upper limit on gravitational radiation from the millisecond pulsar PSR1937+214, is described.

CHAPTER 1.

"AN INTRODUCTION TO GRAVITATIONAL RADIATION."

In this chapter the concept of gravitational radiation is introduced, and the motivation behind the experimental pursuit of the detection and study of this radiation is discussed. Throughout the thesis the terms gravitational radiation and gravitational waves will be used interchangeably.

1.1 HISTORICAL BACKGROUND.

Since they were first predicted by A. Einstein [1,2] in 1917, gravitational waves have been a consequence of all major relativistic theories of gravity. Most theories predict similar strengths of gravitational wave fluxes from astrophysical sources, and, in the main, similar coupling to gravitational wave detectors. However different theories predict very different polarisation properties and speeds for the waves. This thesis will assume the validity of Einstein's general theory of relativity which describes gravitational waves as ripples in the curvature of spacetime, propagating with the speed of light. These ripples are characterised by two dimensionless gravitational wave amplitudes h_+ and $h_\times$, which may be regarded as scalar fields in spacetime. Much of the material that follows has been gathered from a number of books and review articles. [3→6]

1.2 GENERATION OF GRAVITATIONAL RADIATION.

Gravitational waves occur as solutions of Einstein's field equations, in the same way that electromagnetic waves are solutions to Maxwell's equations. Whereas accelerating charge produces radiation in the form of electromagnetic waves, the acceleration of mass produces radiation in the form of gravitational waves. However the efficiency of production of gravitational waves is very much smaller than that of electromagnetic waves, due to the fact that gravitational radiation is only produced by a system with a changing quadrupole moment. Dipole radiation is forbidden by conservation of momentum- i.e. mass has only one sign.

Newtonian theory describes the field of gravity in terms of the gravitational potential ϕ . The potential in the region of a fiducial point can be expanded as

$$\phi(x) = \phi_0 - \sum_j g_j x_j + \sum_{j,K} 1/2\ R_{jOKO}\ x_j x_K + \ldots . \qquad (1.1)$$

where x_j are the components of the vector $\underset{\sim}{x}$ from the fiducial point to the point of measurement, g_j are the components of local gravitational acceleration, and R_{jOKO} are numbers which measure the inhomogeneity in the gravitational field at the fiducial point. (R_{jOKO} is effectively the Riemann tensor of general relativity).

Here,

$$R_{jOKO} = \frac{\partial^2 \phi}{\partial x_j\, \partial x_K} \quad \ldots .\text{Newtonian.} \qquad (1.2)$$

Now the force acting on a mass m at a point $\underset{\sim}{x}$ is given by

$$\underset{\sim}{F} = -\underset{\sim}{\nabla}\phi \qquad (1.4)$$

* Eqn. 1.3 does not exist.

with components

$$F_j = -m\,\partial\phi/\partial x_j = mg_j - \sum_K mR_{jOKO}\,x_K \qquad (1.5)$$

Einstein's extension of Newton's work produced a contribution to R_{jOKO} such that

$$R_{jOKO} = \frac{\partial^2\phi}{\partial x_j\,\partial x_K} + \overset{(GW)}{R}_{jOKO} \quad \ldots\ldots\text{Einstein.} \qquad (1.6)$$

The form of $\overset{(GW)}{R}_{jOKO}$ is dictated by Einstein's theory. For instance a plane wave propagating in the z direction produces only two components....

$$\overset{(GW)}{R}_{xoxo} = -\overset{(GW)}{R}_{yoyo} = -1/2\ \ddot{h}_+\,(t-z/c) \qquad (1.7)$$

$$\overset{(GW)}{R}_{xoyo} = -\overset{(GW)}{R}_{yoxo} = -1/2\ \ddot{h}_x\,(t-z/c) \qquad (1.8)$$

(Dots denote derivatives w.r.t. t, c is speed of light.)

Here h_+ and h_x represent the momentary amplitude of the wave in the two orthogonal polarisations "+" and "x".

The relative forces F_j are perpendicular to the propagating (z) direction - similar to electromagnetic waves.

The gravitational field is a tensor field as opposed to the vector field of electromagnetism. Any tensor can be regarded as the conjunction of two vectors. The simplest arrangement, then, is the quadrupole, consisting of two opposed vector dipoles. The Riemann tensor represents a real distortion in the geometry of spacetime.

Consider figure 1.1.

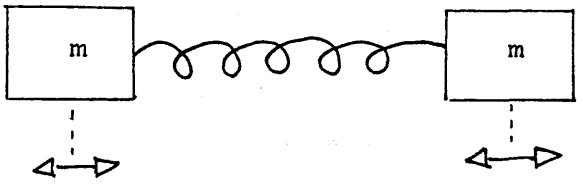

FIG. 1.1 SYSTEM OF TWO EQUAL MASSES JOINED BY A SPRING.

Each mass in figure 1.1 acts as an oscillating dipole. To a first approximation, the gravitational disturbance from one oscillating dipole cancels that of the other, but, because of the time required for the disturbance to propagate across the length of the spring, the two disturbances are slightly out of phase and exact cancellation does not occur. The accelerating system has a degree of asymmetry, and a flux of radiation is produced. The greater the amount of asymmetry in a system, the greater the efficiency of the production of gravitational radiation.

Figure 1.2 represents the relative forces of a gravitational wave by a line-of-force diagram. An object located in this force field will experience time-varying stresses due to the wave's relative gravitational forces, and those stresses will produce mechanical strains. This is illustrated in figure 1.3 which shows the mechanical distortion of a ring of test particles due to the passing of a gravitational wave. The magnitude of the tidal strain produced is typically of the order of the dimensionless wave amplitude h. Note that the polarisation state h_x is produced by a 45° rotation of h_+. Therefore, a 90° rotation goes through twice as many gravitational polarisation states as electromagnetic ones. Any quadrupolar wave

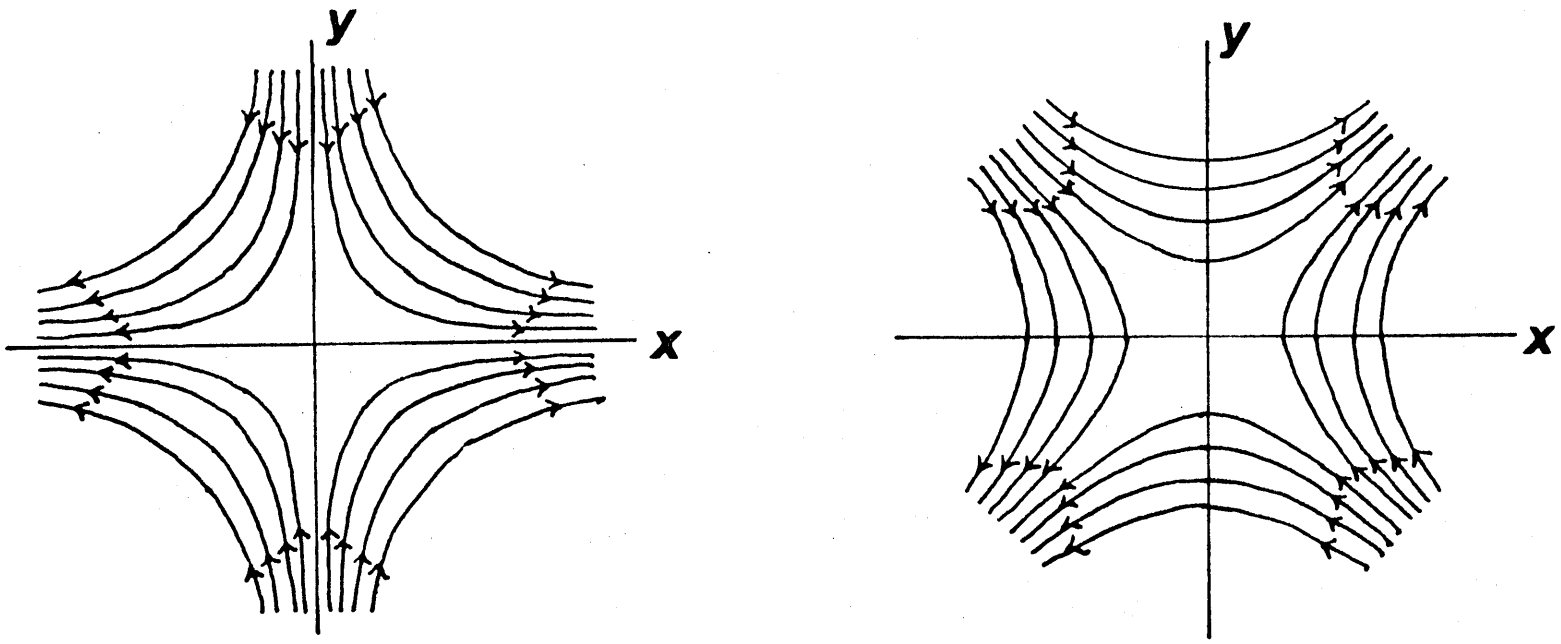

POLARISATION "+"

POLARISATION "X"

FIG.1.2: LINE-OF-FORCE DIAGRAM FOR THE RELATIVE FORCES PRODUCED BY A GRAVITATIONAL WAVE (PRESS, 1970). RELATIVE MEASURING POINT IS AT THE ORIGIN. THE DIRECTION OF THE RELATIVE FORCE IS INDICATED BY THE ARROWS; AND THE MAGNITUDE OF THE FORCE IS PROPORTIONAL TO THE DENSITY OF THE LINES.

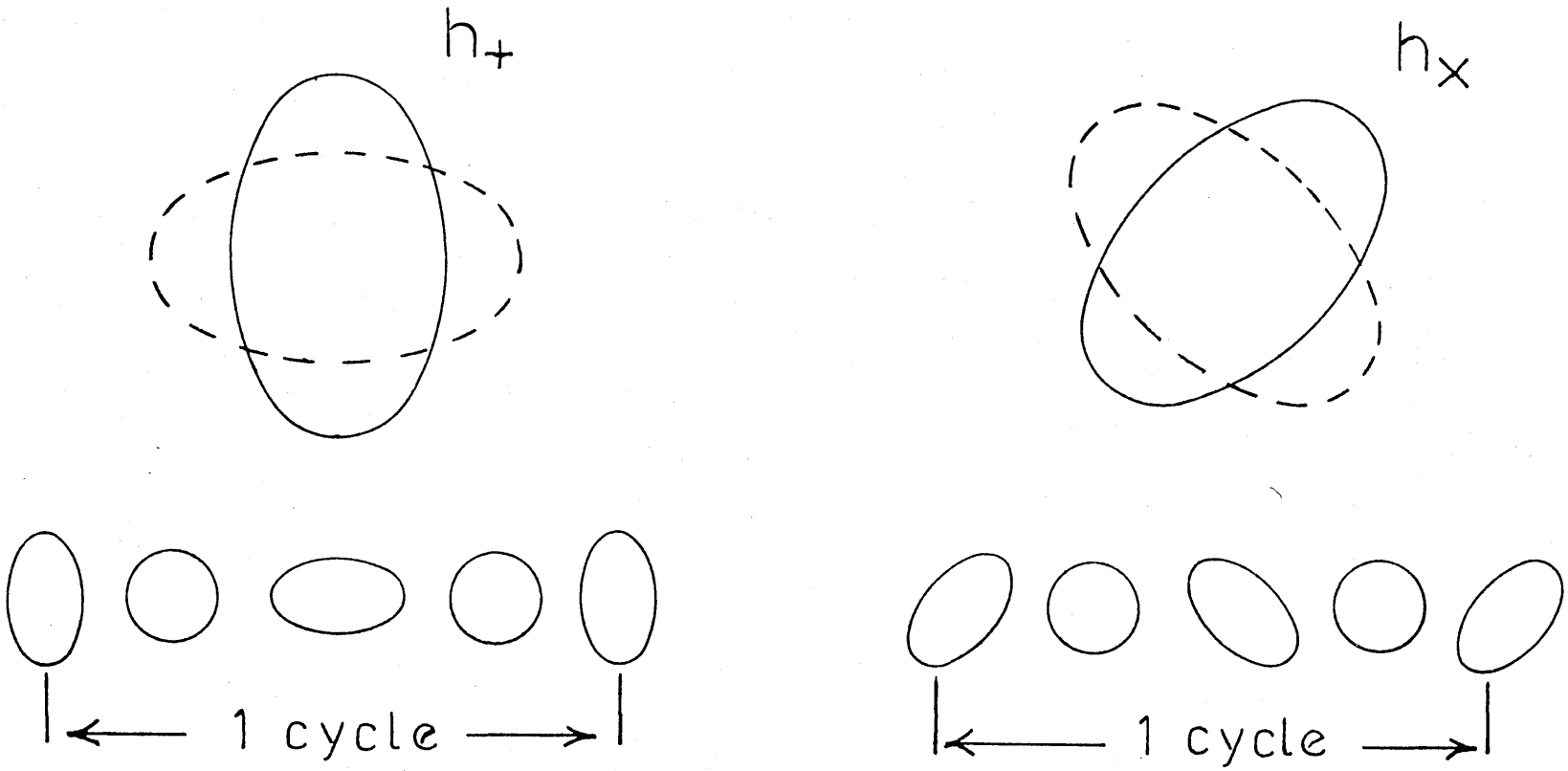

FIG.1.3: THE EFFECT OF A GRAVITATIONAL WAVE, PROPAGATING INTO THE PAGE, ON A RING OF PARTICLES (DOTTED LINES REPRESENT THE DISTORTION OF THE RINGS AFTER HALF A CYCLE). BOTH POLARISATIONS ARE ILLUSTRATED.

configuration can be constructed by a superposition of the two polarisation states. For instance circular polarisation is produced when h_+ and $h_\times$ are out of phase by 1/4 of a cycle.

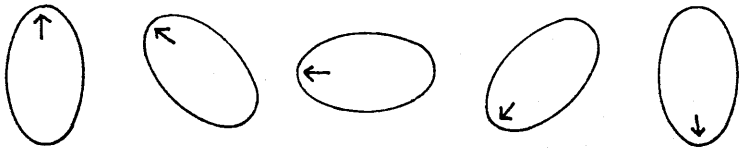

FIG. 1.4 EFFECT ON RING DUE TO CIRCULAR POLARISATION.

One cycle of the circularly polarised wave produces a rotation of 180° (cf. 360° for electromagnetic waves). This carries implications for the spin of the graviton - the quantum analogue of the electromagnetic photon. i.e. if the photon has spin 1 ($h/2\pi$), then the graviton has spin 2 (h/π).

The distortion of spacetime produced by a gravitational wave will exert a relative strain, $\Delta l/l$, on two test masses such that

$$\Delta l/l = h_+/2 = h_\times/2 = h/2 \qquad (1.9)$$

where l is the separation of the masses. This is the basis of gravitational wave detection. As will be seen, many detectors are similar in principle to the "generator" of figure 1.1.

It is obvious that a detection technique involving physically uncoupled masses is advantageous, in that the separation of l can be easily increased to improve sensitivity. The optimum separation being when l is 1/4 the length of the gravitational wave (section 1.6).

1.3 ENERGY CARRIED BY GRAVITATIONAL RADIATION.

As gravitational waves are predicted, by general relativity, to travel with the speed of light, the energy flux is equal to the product of the energy density and the speed of light. The energy flux, averaged over several cycles, is given by

$$\mathcal{F} = \frac{c^3}{16\pi G} \left\langle \dot{h}_+^2 + \dot{h}_\times^2 \right\rangle$$

$$= \frac{L_o}{16\pi} \left\langle (\dot{h}_+ /c)^2 + (\dot{h}_\times /c)^2 \right\rangle \quad (1.10)$$

where G is the gravitational constant and L_o is a constant of natural luminosity defined by

$$L_o = c^5/G = 3.63 \cdot 10^{59} \text{ ergs/sec}$$

$$= 2.03 \cdot 10^5 \, M_\odot c^2/\text{sec} \quad (1.11)$$

where $M_\odot$ denotes a solar mass.
(L_o is equal to the maximum intrinsic luminosity that any gravitational wave source can have).

This energy flux has similarities with electromagnetic theory: it is conserved (amplitude varies as $1/r$, flux as $1/r^2$); and it can be (at least partially) deposited in detectors.

1.4 AMPLITUDE OF GRAVITATIONAL RADIATION.

Einstein derived an expression for the gravitational wave field in terms of the second time derivative of the

quadrupole moment.

$$h_{jK}(t,\underset{\sim}{x}) = \frac{2G}{rc^4}\left[\ddot{I}_{jK}(t-r/c)\right] \qquad (1.12)$$

where $\underset{\sim}{x}$ is the Cartesian location of the observer from the source origin, $r=|\underset{\sim}{x}|$ is the distance from the source to the observer, and I_{jK} is the mass quadrupole moment of the source.

In terms of magnitude, this implies

$$h_+ \sim h_\times \sim h_{jK} \sim \frac{\left(\begin{array}{c}\text{SCWARTZCHILD RADIUS } GM_{KIN}/c^2 \\ \text{ASSOCIATED WITH THE MASS} \\ \text{EQUIVALENT } M_{KIN} = E_{KIN}/c^2 \text{ OF THE} \\ \text{QUADRUPOLE K.E. OF THE SOURCE}\end{array}\right)}{\text{SOURCE-OBSERVER DISTANCE}} \qquad (1.13)$$

This indicates how weak expected gravitational wave amplitudes are likely to be. For example, a source with mass equal to that of our sun $M_\odot$, and with $M_{KIN} \ll M_\odot$, at the centre of our galaxy has amplitude

$$h_+ \sim h_\times \sim h_{jK} \ll \left(\frac{G\,M_\odot}{c^2\,r}\right) \simeq 5 \cdot 10^{-18} \qquad (1.14)$$

1.5 SOURCES OF GRAVITATIONAL RADIATION.

Although there have been proposals for laboratory generators of gravitational radiation,[7,8] the amplitudes predicted are so small that it is unlikely that they would be detectable in the foreseeable future. The most likely sources of gravitational radiation (and the most rewarding) are astrophysical generators.

Astrophysical sources of gravitational radiation can, in general, be classified into three separate groups according to the types of signals produced:

(1) Burst, or Impulsive, sources.

(2) Continuous, or Periodic, sources.

(3) Stochastic sources.

It is possible, however, for some sources to change their classification. For example, a compact binary will change from being a continuous source to being an impulsive source as it evolves and dies.

The strength of the signals produced are usually expressed in terms of the gravitational wave amplitude, h, at the detector, the characteristic frequency, f, of the signal, and (for impulsive and stochastic sources) the characteristic bandwidth, Δf.

If quadrupole radiation is the dominant contributor to gravitational radiation, then the luminosity is given in terms of the third time derivative of the mass quadrupole moment.

$$L_{jk} = \frac{G}{5c^5} \langle \dddot{I}_{jk} \dddot{I}_{jk} \rangle \qquad (1.15)$$

For sources of characteristic size R_o and mass M, with an internal velocity v, then 1.15 gives a reasonable approximation of luminosity L

$$L \sim \left(\frac{c^5}{G}\right)\left(\frac{R_g}{R_o}\right)^2\left(\frac{v}{c}\right)^2 \qquad (1.16)$$

where $R_g = GM/c^2$ is the gravitational radius of the source. It is apparent that the strongest sources are likely to be compact ($R_o \sim R_g$), highly relativistic ($v \sim c$) objects. Such a source will release a large fraction of its internal energy, as a burst of gravitational radiation, in a very short time ($\sim R_g/c$).

How promising a potential source is, is a combination of the predicted signal strength and rate of occurrence. A diagrammatical summary of some predicted source strengths is shown in figure 1.5. The upper line marked "cherished beliefs" is an upper limit to gravitational radiation from all sources, assuming the validity of some fundamental laws of physics (e.g conservation of energy) and beliefs about the universe.[6]

(a) Impulsive Sources.

Several scenarios have been suggested for the emission of bursts of gravitational radiation. Among the most promising of these, are the collapse of massive stars to compact neutron stars, the final coalescence of compact binary systems , and collisions involving black holes. Such bursts are expected to have a bandwidth $\Delta f \sim f$, the characteristic frequency of the signal, wherein most of the energy is contained. Some impulsive sources are tabulated, together with expected strengths and rates of occurrence, in table 1.6.

(i) Supernovae Collapse.

The formation of a neutron star (or black hole) in the dense core of a type II supernova is expected to produce a relatively large flux of gravitational radiation. These supernovae usually occur in the arms of spiral galaxies, and are believed to be explosions of massive stars ($\gtrsim 8M_{\odot}$) which collapse to neutron stars in less than a second. The core of the neutron star then bounces with a period of a millisecond. However, the

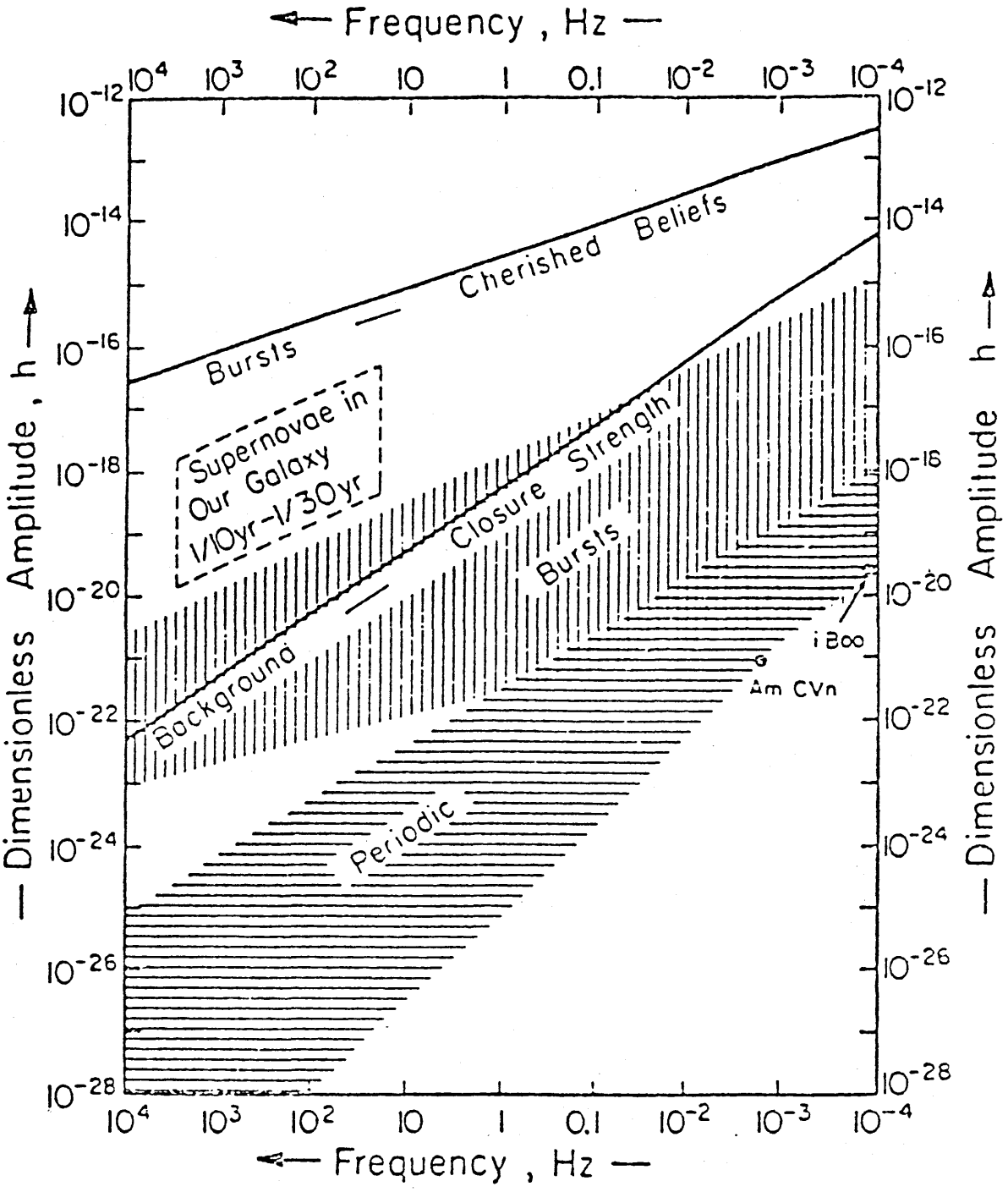

FIG.1.5: A GRAPHICAL REPRESENTATION OF THE STRENGTHS OF SOME OF THE EXPECTED SOURCES OF GRAVITATIONAL WAVES, MEASURED AT THE EARTH, THORNE (1980).

TABLE 1.6: SOME POSSIBLE IMPULSIVE SOURCES OF GRAVITATIONAL RADIATION.
(ALL SOURCES HAVE DURATIONS OF THE ORDER OF 1/f)

SOURCE	AMPLITUDE	FREQUENCY(Hz)	RATE	DETECTION METHOD
BLACK HOLE EVENTS:				
-IN GALACTIC NUCLEI/QUASARS	10^{-16}-10^{-19}	10^{-4}-10^{-1}	$<$50/YEAR	DOPPLER TRACKING &
-IN GLOBULAR CLUSTERS	10^{-19}-10^{-21}	1-10^{2}		LASER INTERFEROMETER IN SPACE.
STELLAR COLLAPSE:				
-IN OUR GALAXY	10^{-17}-10^{-20}	10^{2}-10^{4}	1/10 - 1/30 YR	LASER INTERFEROMETER ON
-AT DISTANCE OF VIRGO CLUSTER	10^{-21}-10^{-22}	10^{2}-10^{4}	FEW PER YEAR	EARTH; COOLED BAR DETECTOR.
FINAL COALESCENCE OF COMPACT BINARIES	10^{-21}-10^{-22}	10-10^{3}	FEW PER YEAR	LASER INTERFEROMETER ON EARTH; COOLED BAR DETECTOR.
STARQUAKES IN NEUTRON STARS	10^{-22}-10^{-23}	10^{2}-10^{3}	$\sim$ 1/YEAR	LASER INTERFEROMETER ON EARTH.
BLACK HOLE/BLACK HOLE & BLACK HOLE/NEUTRON STAR COLLISIONS	$10^{-16}(M/100M_{\odot})$ @65kpc	10^{-4}-10^{3}	1/10YEAR	MOST METHODS
	$5 \cdot 10^{-19}(M/100M_{\odot})$ @15Mpc		10/MONTH	

amount of radiation emitted depends critically on the asymmetry and velocity of the collapse. These explosions may involve stars of up to $100M_{\odot}$, and up to 1% of the core rest energy has, in the past, been predicted to be released as gravitational radiation. Most recent estimates[9] of the energy released as gravitational waves in a supernova give typical energies of between $3 .10^{-2} M_{\odot} c^2$ and $10^{-5} M_{\odot} c^2$. A collapse in our galaxy is estimated to produce a gravitational wave amplitude of 10^{-17} -10^{-20}.

(ii) Births of Black Holes.

When a massive star collapses to form a neutron star, the shock wave produced ejects the stellar envelope. However, if the shock wave is too weak to remove the envelope, then the core collapses ($\sim$1sec.) to form a black hole. During collapse, a flux of neutrinos diffuses out of the core along with gravitational radiation[10] (-if the collapse is asymmetric). The expected strength of gravitational radiation, from such a source, is likely to be small, however, if there is no rapid rotation, or strong magnetic distortion, to produce a non-spherical collapse.

Theories of the release of gravitational radiation from rapidly rotating black holes (Kerr holes) are still in their infancy, but indications are that amplitudes will be small[11] (Eardley 1983). One possibility is, however, that the collapsing core will be unstable to non-axisymmetric modes and will evolve into a rotating triaxial shape, or even break up into two, or more, smaller cores[12] (Clark and Eardley 1977). In its asymmetrical configuration, the core can efficiently emit gravitational waves.

Studies of gravitational wave patterns will reveal details of black holes and black hole events that could not be discovered by any other method.

(iii) Neutron Star Binaries.

Indirect evidence for the existence of gravitational waves has been found from measurements of the binary pulsar PSR 1913+16 (Taylor and Weisberg 1982)[13]. Using the pulsar as a very accurate clock, the decay of the orbit has been measured and found to be consistent with decay due to gravitational radiation release.

For the final decay of a neutron star binary system, the gravitational wave signal emitted, as the two stars coalesce, is predicted to be a "chirp" of rising frequency and amplitude, with a duration of many milliseconds. Clark and Eardley (1977)[12] have estimated the efficiency of gravitational wave production for such a system to be $\sim$ 0.005%. This would correspond to a source in the Virgo cluster of galaxies producing a maximum gravitational wave amplitude of $h \sim 10^{-21}$.

(iv) Neutron Starquakes.

The rotational frequency of neutron stars occasionally change, very suddenly. This is widely regarded as a "starquake"[14], releasing a large amount of strain energy that the star had been unable to release during a rapid collapse. The characteristic frequency of the gravitational wave component of this radiation is expected to be in the region 10^{2}-10^{4} Hz, with a 1 Hertz bandwidth. The event rate for such events is predicted to be the order of one per year with amplitudes of 10^{-22}-10^{-23}.

(v) Binary Black Hole Populations.

A "possible but unlikely" source of gravitational waves, that has been proposed to give amplitudes near the "cherished beliefs" limit (fig. 1.5), is that of a massive galactic halo of black hole and neutron star binaries, which are the pre-galactic remains of Population III stars (Zimmermann and Thorne 1980)[9]. Bond and Carr (1984)[15] have argued that a large fraction of the "missing mass", necessary to close the universe, may be present in binary black hole remnants of Pop.III stars ($M > 100M_{\odot}$). Gravitational waves emitted during coalescence of these binary systems would take the form of individual bursts or contribute to the stochastic background radiation, depending on the initial separation of the binaries. Amplitudes of $h \sim 10^{-16}$ $(M/100M_{\odot})$, with bursts times of 10^{-2} $(M/100M_{\odot})$ seconds, have been predicted. Event rates have been estimated as one coalescence per decade, for sources within 65kpc of the galactic centre, and 10/month for weaker signals $\{h \sim 4 .10^{-19}(M/100M_{\odot})\}$ from sources out to 15Mpc. The characteristic frequency of signals from these sources is likely to be in the region 50-500 Hz.

(b) Periodic Sources.

Periodic gravitational waves are likely to be produced by such sources as binary star systems and rotating neutron stars (pulsars). Table 1.7 shows the predicted characteristic frequencies and amplitudes of gravitational wave emission from several periodic sources. The amplitudes involved are smaller, in general, than those

TABLE 1.7: SOME POSSIBLE SOURCES OF CONTINUOUS AND STOCHASTIC GRAVITATIONAL RADIATION.

SOURCE	AMPLITUDE	FREQUENCY(Hz)	DETECTION METHOD
(PULSARS)	$(10^{-22}-10^{-30})$	$(10^{-2}-10^{4})$	
VELA PULSAR	$5 \cdot 10^{-26}$	23	LASER INTERFEROMETER
CRAB PULSAR	10^{-25}	60	ON EARTH.
ROTATING WHITE DWARFS	$10^{-21}-10^{-23}$	$10^{-2}-1$	LASER INTERFEROMETER IN SPACE.
POST-SUPERNOVAE WHITE DWARF PULSATIONS	$\sim 10^{-22}$	10^{-2}	LASER INTERFEROMETER IN SPACE.
(BINARY STARS)			
IOTA BOOTES	$\sim 5 \cdot 10^{-21}$	$8.6 \cdot 10^{-5}$	
AM CVn	$\sim 10^{-20}$	$2 \cdot 10^{-3}$	LASER INTERFEROMETER IN SPACE.
GEMINGA	$\sim 10^{-19}$	$3 \cdot 10^{-2}$	
(STOCHASTIC BACKGROUND)			
PREGALACTIC BLACK HOLES	$10^{-14}-10^{-19}$	$10^{-4}-10^{-1}$	DOPPLER TRACKING; LASER INTERFEROMETER IN SPACE.
COALESCENCE OF BINARY BLACK HOLE PAIRS FOR POP.III STARS	$10^{-22}-10^{-24}$	10^{3}	LASER INTERFEROMETER ON EARTH.

typically produced by impulsive sources, but, as a continuous source has no real bandwidth limit, extra integration time can be used to bring these sources within reach. For ground based detectors, low frequency noise is likely to be so large that only rotating neutron stars, with their higher characteristic frequency, are likely to be detectable.

Rotating Neutron Stars.

The most well known, and referred to, periodic source is the Crab pulsar which has a rotational period of 33 milliseconds. With an estimated luminosity of 10^{32} ergs/sec, the amplitude strain at the earth would be around $h \sim 10^{-28}$, at a characteristic frequency of 60Hz (twice the rotation frequency). The most sensitive search, to date, at this frequency, has been carried out by a bar detector with a sensitivity of $h=3.7 \ .10^{-20}$, for an integration time of 1 month (Hirakawa et al 1977).[16]

Pulsars of higher rotational velocity than the Crab pulsar are more desirable, from the point of view of ground based detectors, as characteristic frequencies below 100Hz compete with low frequency noise sources and make detection more difficult. The discovery of the millisecond pulsar PSR 1937+214 initially gave rise to hopes that it was emitting a detectable flux of gravitational waves (- see Appendix), but this turned out to be unlikely from its very slow spin-down rate.

However the discovery of pulsars as fast as this one ($\tau \sim 1.5 \ .10^{-3}$ secs) bodes well for sources that may be discovered in the future and which may have spin-down rates

greater than that of PSR 1937+214. Large quantities of energy may then be given off as gravitational radiation from these pulsars. -A combination of the rotational period of millisecond pulsar and the ellipticity of the Crab pulsar would produce an ideal source.

As the gravitational wave luminosity depends largely on the characteristic frequency of the source, a radiating star will quickly spin down to a rotational period where the luminosity is poor. The time of strong gravitational wave emission, then, will be very short unless the star is subjected to a compensating spin-up torque that restores the energy and angular momentum lost in the emission of gravitational radiation. This may be the case if the star is accreting extra matter from a nearby companion. Although initial predictions suggested that a rapidly-rotating, accretion-driven neutron star would not produce a large flux of gravitational radiation (due to poor magnetic field induced ellipticity), recent theories are more promising.[17] At a rotational frequency of around 1kHz, the reaction forces, due to gravitational wave emission, produce an axial distortion which enhances the GW luminosity. Viscous forces in the star damp the resulting instability, and an equilibrium state is reached with modes developing that are characterised by structural deformities in the star. Wagoner (1983)[17] predicts an emission of gravitational waves from a few hundred Hertz to 1kHz, with an amplitude

of

$$h = 3 \cdot 10^{-27} \left(\frac{1\text{kpc}}{r}\right) \left(\frac{1\text{kHz}}{mf}\right)^{1/2} \left(\frac{L_\gamma}{10^{-8}\ \text{erg cm}^{-2}\ \text{sec}^{-1}}\right) \quad (1.17)$$

where L_γ is the observed x-ray flux of the source and is proportional to the rate of accretion, and m is the mode number of the oscillation.

There is mounting evidence for the existence of large populations of accreting neutron stars (e.g Skinner et al 1982)[18] where spin-up to rotational frequencies has occurred. These are potentially good sources of periodic gravitational radiation.

(c) Stochastic Background Sources

A stochastic background of gravitational radiation - similar to the microwave background - may be present due to the coalescence of binary black hole pairs from Population III stars in the early universe, or from fluctuations in the density of primeval spacetime which produced the galaxies, or indeed from the "big bang". In principle this background could be so strong that its energy density is adequate to close the universe (Thorne 1979)[6] -see fig. 1.5. However, it is most likely that the stochastic background would be many orders of magnitude weaker than the closure strength. Carr (1980)[19] has postulated several mechanisms by which massive Pop.III stars could produce a stochastic background of amplitude $h \sim 3 \cdot 10^{-24} - 10^{-22}$ at frequencies around 1kHz. A search for such radiation could take the form of a cross-correlation experiment between two detectors (Hough et al 1975).[20]

1.6 THE EVOLUTION OF GRAVITATIONAL WAVE DETECTORS.

1.6(a) 1st Generation Detectors.

The first experimental schemes for the detection of gravitational waves were carried out by J. Weber of the University of Maryland [21] (1960, 1969). Weber's first experiments involved the use of a large aluminium cylinder of length 1.5 metres, and weight 1.5 tonnes. The bar of aluminium essentially acted like two masses joined by a spring (i.e. the corresponding receiver to the proposed transmitter of fig. 1.1). The two halves of the bar may be regarded as two separate masses joined by the spring constant of the aluminium. The incidence of a suitably polarised gravitational wave on the bar will excite, primarily, the fundamental resonance of the cylinder (in this case 1.6kHz), and the amplitude and phase of the oscillation provides information about the gravitational wave. The sensing of the motion of the bar was carried out by piezoelectric transducers bonded around the middle of the bar. The bar was suspended by a wire and housed in a vacuum tank.[22]

Using two separate detectors , at Maryland and Argonne, separated by 1000km, Weber searched for, and claimed to find, coincident pulses from the detectors with a sensitivity of $h \sim 4 \ .10^{-16}$. The ensuing controversy, surrounding his results, stimulated several other groups, around the world, to try and repeat his findings. Most of these experiments were similar in design to that of Weber's, although Braginskii et al (1972)[23] employed

capacitive sensing, as opposed to piezoelectric sensing.

The University of Glasgow group constructed split-bar detectors using piezoelectric transducers sandwiched between the two separate bar-halves (Drever et al 1973).[24] These detectors had a greater mechanical to electrical coupling efficiency which enabled a wider bandwidth to be used, and allowed a greater accuracy in pulse timing. Searches for gravitational radiation, with two such detectors, at a sensitivity greater than that of Weber's, produced no evidence in his support. (These types of bars were also used by Allen (1975)[25] and by Aplin[26] (1972)). Similar bar experiments, around the world, also produced negative results,[27] at strain sensitivities as low as $3 \cdot 10^{-17}$.

The cross-correlation experiment of Hough et al[20] set an upper limit to a continuous gravitational wave flux at 1kHz of $6.8 \cdot 10^{3}$ Wm^{-2} Hz^{-1}.

Aside from the bar experiments, other ideas for gravitational wave detectors were also evolving. By monitoring vibrations of the Earth, Forward et al (1961)[28] set an upper limit to gravitational waves at a frequency of 0.0001 Hz.

Searches for periodic radiation from pulsars were also made.[29] The experimental results of Mast et al (1974) confuted the "positive" results of Sadek and Meidev (1972),[30] who claimed to have detected gravitational radiation from the pulsar CP 1133, by measuring the normal modes of the Earth.

The limit to sensitivity of most of the early bar

experiments was imposed by thermal noise in the bar material, and noise limitations in the motion sensing system[84]. The limit set by thermal noise may be appreciated by a simple harmonic oscillator treatment.

The thermal energy in the fundamental mode of the bar is approximately kT, which can be set equal to the energy in an oscillator.

$$\Delta E = kT = 1/2\ m\ \omega^2 \Delta x^2 \qquad (1.18)$$

where k is Boltzmann's constant, T is the absolute temperature of the bar, ω is the angular frequency of the bar resonance, and Δx is the amplitude of the oscillations.

For a measuring time, τ, shorter than the storage (or damping) time, τ_s, of the bar, 1.18 is modified by a factor (τ / τ_s) such that the amplitude of the thermal oscillations detectable is given by

$$x = \left(\frac{2kT}{m\ \omega^2}\right)^{1/2} \left(\frac{\tau}{\tau_s}\right)^{1/2} \qquad (1.19)$$

which implies that the effect of the noise may be reduced by large bar storage times and short measuring times.

The storage time of of the bar is related to the quality factor, Q, of its material by

$$\tau_s = 2Q/\omega \qquad (1.20)$$

Incorporating this into 1.19 gives

$$\Delta x_T = \left(\frac{kT\,\tau}{m\,\omega\,Q}\right)^{1/2} \qquad (1.21)^*$$

The efficiency of coupling between the energy stored in the bar and the measuring transducer is described by a dimensionless coupling constant, β (≤ 1), and the overall

* Note eqns 1.22, 1.23 do not exist.

sensitivity of the detector depends on this coupling factor and on the intrinsic noise of the transducer and detection system.

For short pulses of gravitational radiation the thermal limit is

$$h \sim 2 \cdot 10^{-19} \left(\frac{T}{300K}\right)^{1/2} \left(\frac{\tau}{10^{-3}\,s}\right)^{1/2} \left(\frac{1m}{l}\right) \left(\frac{10^3\,kg}{m}\right)^{1/2} \left(\frac{1kHz}{\frac{\omega}{2\pi}}\right)^{1/2} \left(\frac{10^7}{Q}\right)^{1/2} \qquad (1.24)$$

When limited by thermal noise, there are four main ways of improving sensitivity:

(a) Cool the bar to lower temperatures,

(b) Increase the mass of the bar,

(c) Use a bar with a higher quality factor,

(d) Increase the size of the bar.

1.6(b) 2nd Generation Detectors.

(1) Low Temperature Bar Experiments:

In general, there followed two alternative approaches to increasing the sensitivity of the 1st generation bar detectors. Because of the difficulty in manufacturing large bars of very high Q materials, some experimenters used small bars ($\leq$ 100kg) with quality factors as high as 10^9, while other groups used large, massive bars of aluminium ($\sim$ 5 tonnes) with Q's of the order of 10^6-10^7. Both these methods involved the use of cryogenic technology to cool the bars to around a few Kelvin. Institutions carrying out the former of these two methods include Moscow State University; and institutions implementing the second approach include Stanford University, Louisiana State University, and the University of Rome. (An intermediate approach was adopted by the University of Western Australia who constructed a medium

sized bar (1000kg) of niobium ($Q=6 \cdot 10^7$)).

Especially at low temperatures, a source of noise that is very important is sensor noise. The effect of actually measuring the displacement of the bar introduces additional noise itself. Braginskii et al (1972)[23] have measured the sensitivity limitation to resonant bar detectors from thermal noise in the piezoelectric transducers used to sense the motion of the bar. Less disruptive sensors, such as superconducting diaphragms and SQUIDS, are being developed. Analysis of a SQUID sensing system, by Hough et al (1977),[31] suggest that the sensors own noise, along with the "back-reaction" noise of the measurement, may impose a severe barrier to the sensitivity of low temperature detectors. As sensor noise decreases with increasing measuring time, there is an optimum observation time obtained by balancing this noise source with thermal noise.

Apart from thermal noise, a more "fundamental" limit to sensitivity is set by the Uncertainty Principle, which limits the accuracy to which the separation of the two masses (i.e. the two bar-halves) can be measured. For a bar of mass m, and a measuring time τ, the limit can be shown to be

$$\Delta x = \left(\frac{2\hbar}{m\omega} \right)^{1/2} \qquad (1.25)$$

where $\hbar$ is Planck's constant divided by 2π, and ω is the frequency of the bar resonance. This implies a quantum limit sensitivity of

$$h \sim 6 \cdot 10^{-21} \left(\frac{10^3\ \mathrm{kg}}{m}\right)^{1/2} \left(\frac{1\mathrm{m}}{l}\right) \left(\frac{10^3\ \mathrm{Hz}}{\omega/2\pi}\right)^{\frac{1}{2}} \qquad (1.26)$$

The limit due to the uncertainty principle can also be deduced from the limit imposed by sensor noise. Heffner (1962)[33] has used an argument based on quantum mechanics to derive an expression for the ultimate noise temperature of a linear amplifier which, Giffard (1976)[34] has shown, limits the minimum detectable motion to that of the quantum limit.

Remarkably, there exist proposals for circumventing the quantum limits. The techniques involved are known as quantum non-demolition techniques (QND), and include schemes such as "quantum counting" and "back-action evasion". Back-action evasion techniques attempt to measure only one phase of the bar's motion, with the noise that results from the measurement appearing in the other phase. A general theory of QND techniques has been developed by Unruh (1979)[35], and by Caves et al (1979)[36]. In practice, these proposals look very difficult to implement, at present, and it is unlikely that they will be used in the very near future. At present, thermal and amplifier noise are still likely to be the main limits to bar detector sensitivity.

(2) Free mass and nearly-free mass detectors:

Detectors which fall into this category are, perhaps, more attractive than present bar detectors as they are broad-band in nature. Also, sensitivity can be improved by increasing the separation l ($\lesssim \lambda_g/2$) to large distances. The intention is to increase the size of the signal to be measured, rather than decrease the background effects.

(a) Laser Interferometers:

The separation of test masses (hung as pendulums) is monitored very accurately by the use of a highly stabilised light source. To avoid the need for absolute length measurements, three such masses are used (arranged in an L-shape); and the the difference in the lengths of the two arms of the "L" is measured. This is illustrated in figure 1.8. Mirrors are located on each of the test masses, such that each arm of the "L" acts like an arm of a Michelson interferometer - which is illuminated with laser light. A change in the length difference of the two arms produces a change in the intensity of the interfered light at the photodiode. A gravitational wave propagating vertically, of suitable polarisation, would produce differential changes in the lengths of the two arms, resulting in phase changes in the stored light, giving rise to an observable signal at the photodiode. If the gravitational wave period is short compared with the periods of the pendulum suspensions ($\sim$ 1Hz), then the masses respond as if they were almost free, resulting in a differential signal corresponding to the gravitational wave amplitude.

The first such system was contructed by Moss and Forward (1971, 1978)[37,38], at Hughes Reseach Laboratories, who achieved a displacement sensitivity of 1.3×10^{-14} m, in a 1Hz bandwidth.

At present, there are two different types of laser interferometers being developed[82], although the principle is essentially the same in both cases.

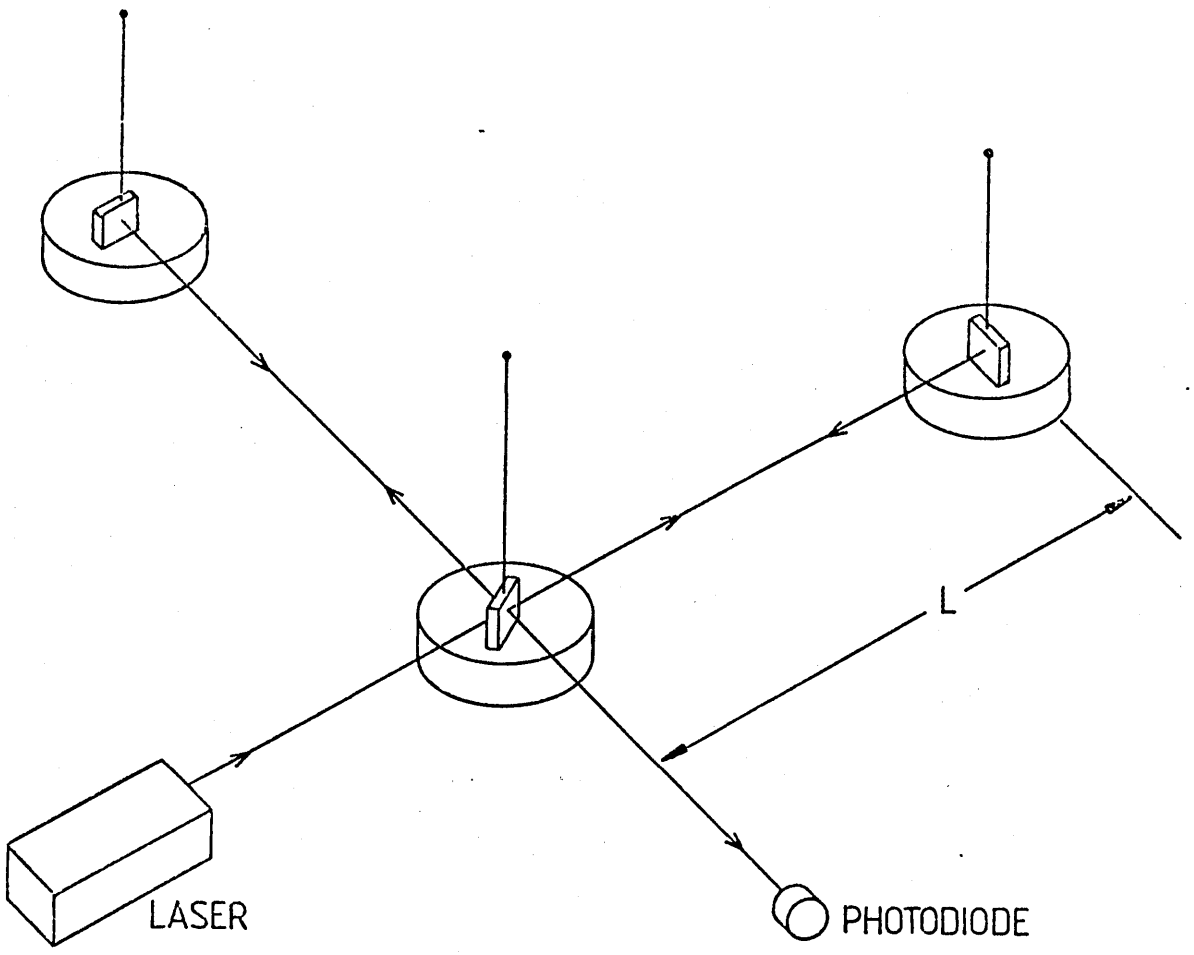

FIG.1.8: SCHEMATIC DIAGRAM OF A SIMPLE LASER INTERFEROMETER.

(i) Delay-Line Interferometer.

To increase the potential strain sensitivity of this type of detector, the obvious tactic to employ is to increase the baseline of the detector, l. A method of effectively simulating a longer baseline was initially suggested by Weiss (1972)[39]. The suggestion was the use of optical delay lines to deflect the light many times between the test masses and thus increase the phase shift in the light due to the relative displacement of the two interferometer arms.

It is instructive to consider some of the limits of this detection technique. From ref. 32, the quantum limited uncertainty in measuring the separation of two test masses, each of mass m, is given by

$$(\delta x_1)^2 = \frac{2\hbar}{m\omega^2\tau} \qquad (1.27)$$

For an interferometer with two orthogonal arms, the uncertainty in relative displacement is δx such that

$$\delta x = \left(\delta x_1^2 + \delta x_2^2\right)^{1/2} \qquad (1.28)$$

where δx_1 and δx_2 are the uncertainties in the relative separation of each arm.

This gives

$$\delta x = \left(\frac{4\hbar}{m\omega^2\tau}\right)^{1/2} \qquad (1.29)$$

which implies a strain sensitivity of

$$h \sim \frac{\delta l}{l} \sim 10^{-23}\left(\frac{10^2\,\mathrm{kg}}{m}\right)^{1/2}\left(\frac{10^3\,\mathrm{Hz}}{\omega}\right)\left(\frac{10^{-3}\,\mathrm{s}}{\tau}\right)^{1/2}\left(\frac{1\,\mathrm{km}}{l}\right) \qquad (1.30)$$

The practical limit to this type of detector,

however, is likely to be from shot noise in the number of photons detected at the output of the interferometer.

Consider a delay-line interferometer, as shown in figure 1.9. The output intensity of light from this Michelson interferometer is just

$$I = 1/2\ I_o\ (1 - \cos\phi) \qquad (1.31)$$

where I_o is the input intensity of the laser light, and the phase difference between the two beams $\theta = \pi - \phi$.

Now, for a single-pass, zero-loss, interferometer, the number of photons appearing at the output per second is

$$N = I_o/(2h\nu)\ .\ (1-\cos\phi) \qquad (1.32)$$

With an average mirror reflectivity of R and n reflections,

$$N = \frac{I_o R^n \tau \epsilon}{2h\nu}\ (1-\cos\phi) \qquad (1.33)$$

where τ is the measuring time and ϵ is the quantum efficiency of the photodiode.

For a differential change in length, δl, a relative phase change, $\delta\phi$, is produced such that

$$\delta\phi = (n+1)(2\pi/\lambda)\ \delta l \qquad (1.34)$$

where λ is the wavelength of the laser light.

A change in the relative displacements of the masses produces a change in the number of photons per unit time at the output.

i.e. $$\delta N = \frac{I_o \pi R^n (n+1)\ \sin\phi\ \tau \epsilon}{h\nu\lambda}\ \delta l \qquad (1.35)$$

Counting statistics suggests that the number of output photons/unit time follows a Poisson distribution.

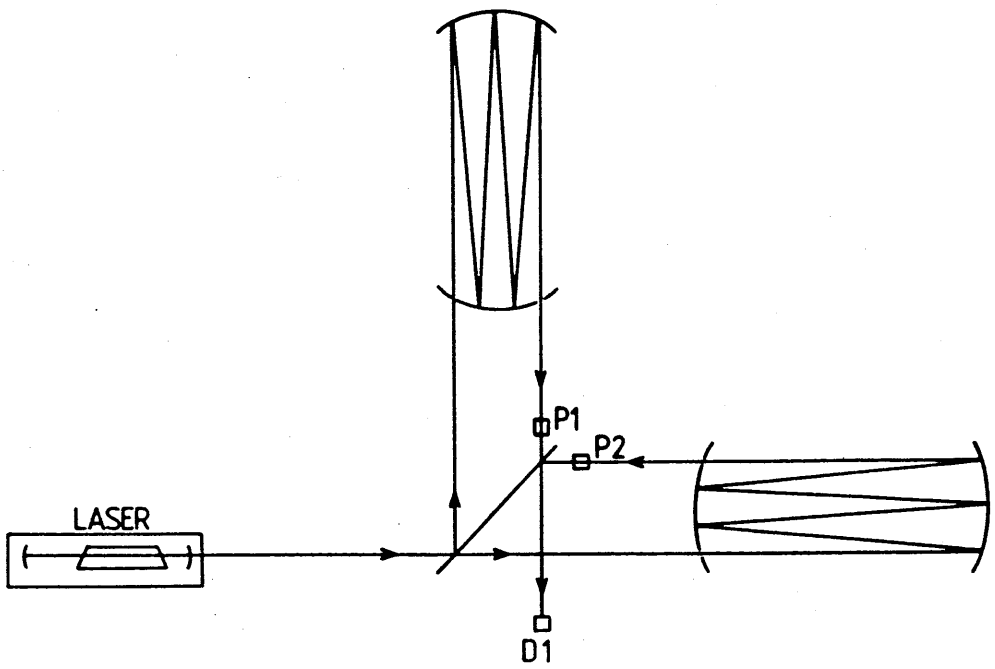

FIG.1.9: MICHELSON INTERFEROMETER USING MULTIPLE-PASS DELAY LINES TO ENHANCE THE PHOTON NOISE LIMITED SENSITIVITY. P1 AND P2 ARE PHASE ADJUSTING MODULATORS, AND D1 IS THE PHOTODIODE WHICH DETECTS THE OUTPUT LIGHT.

i.e. Probability of N counts $P(N;\bar{N}) = \dfrac{e^{-\bar{N}}\,\bar{N}^{N}}{N!}$ (1.36)

where N! represents factorial N and $\bar{N}$ represents the mean value of N. This has a standard deviation $\bar{N}^{1/2}$ which gives the detection condition,

$$\delta N \gg \bar{N}^{1/2} \tag{1.37}$$

Thus, a combination of 1.34, 1.35 and 1.36 gives an expression for the smallest detectable motion,

$$\delta l \gg \left(\frac{hc\lambda}{4\pi^2 \tau \epsilon I_0 R^{\wedge}(n+1)^2 \cos^2(\phi/2)} \right)^{1/2} \tag{1.38}$$

$$\text{using } \frac{1-\cos\phi}{\sin^2\phi} = \frac{1}{2\cos^2(\phi/2)}$$

Now, 1.38 suggests that resolution is best close to an interference fringe null (i.e. $\phi \to 0$).

Maximising $R^{\wedge}(n+1)^2$ results in

$$(n+1) = \frac{2}{1-R} \tag{1.39}$$

For optimum sensitivity ($\phi \sim 0$) this implies

$$\delta l_{MIN} \sim \left(\frac{hc\lambda(1-R)^2}{16\pi^2 \tau \epsilon I_0 R^{\wedge}} \right)^{1/2} \tag{1.40}$$

And, using $R^{\wedge} \sim \exp(n\log_e R) \sim 0.13$, this is

$$\delta l_{MIN} \sim \left(\frac{hc\lambda(1-R)^2}{2\pi^2 \tau \epsilon I_0} \right)^{1/2} \tag{1.41}$$

For $\lambda =$ 514.5 nm, and with unit quantum efficiency of the photodiode, the minimum detectable displacement in a 1Hz bandwidth is

$$\delta l_{MIN} \sim 10^{-16} \frac{(1-R)}{\sqrt{I_0}} \quad (m/\sqrt{Hz}) \tag{1.42}$$

Thus,

radiation. These techniques will be discussed further in chapter 8.

One method of circumventing the shot noise limit has been proposed by Caves (1981)[41] who suggested the use of "squeezed" photon states. By altering the distribution of vacuum fluctuations between two orthogonal phases, the photon counting fluctuations may be reduced at the expense of increased, but less important, fluctuations in radiation pressure on the test masses. Again, this seems difficult to apply, at present, due mainly to technological difficulties, but may be of importance in the future.

Other noise sources are also likely to limit the sensitivity of the detector, but these are not fundamental in nature, and should be surmountable with sufficient experimental ingenuity. These noise problems will be discussed in the following chapters.

The type of interferometer shown if figure 1.8 is known as a delay-line, or Michelson, interferometer. This method was studied at Glasgow, using delay-line interferometry to sense the motion of a split-bar detector. There are currently two groups working on delay-line interferometers, one at the Max Planck Institute in Munich, (2 detectors with baselines of 3m and 30m), and the other at MIT, (one detector with a 1m baseline).

(ii) Optical Cavity Interferometers.

After initial experiments, at Glasgow and Munich, with delay-line interferometry, the potentially serious effect of incoherent scattering of light at the multireflection mirrors (and elsewhere in the system) was

discovered. If scattered light is detected at the output, after having traversed a different path to that of the main beam, it will be out of phase from it by a large amount, giving a phase fluctuation in the output beam dependent on the amplitude of the scattered light. In practice, this may limit the sensitivity of the detector. Schilling et al (1981)[42] suggested that the effect may be reduced by modulating the wavelength of the light by a chosen amount such that the major components of the scattered light average to zero over the integration time of the measurement. This effect is also reduced by precise stabilisation of the laser frequency.

An alternative approach, adopted by the Glasgow group, was to try and make the path travelled by scattered light small compared with the main beam.[40] This produced an alternative type of laser interferometer where every traverse of an interferometer arm is superimposed on the previous beam traverses. This type of interferometer is thus based on optical cavities (Fabry-Perot cavities). The following chapters will describe this technique in detail, as applied in a prototype detector, of 10m baseline, at Glasgow. A second group, at California Institute of Technology, under the direction of R.W.P. Drever, have also adopted this method and close links have been formed with this group.

(b) Doppler Tracking of Spacecraft.

A detection scheme that is hoped will be useful for low frequency sources, is the monitoring of satellites by Doppler tracking. This technique offers very long baselines

and freedom from seismic noise, which makes it attractive for sources with frequencies below 10Hz.

In this scheme, there are usually two free masses (e.g. two spacecraft, or the Earth and a spacecraft), one of which carries a microwave oscillator of frequency ν_0, and the other a transmitter of signals at frequency ν, close to ν_0. This produces a tracking signal, $(\nu - \nu_0)/\nu_0$, which will change (due to Doppler effect) when a gravitational wave passes.

Estabrook and Wahlquist (1975)[43] have shown that the magnitude of the Doppler shifted signal is given by

$$\text{Signal} \sim h \sin(2\pi l/\lambda_g) \qquad (1.44)$$

where l is the separation of the spacecraft and λ_g is the wavelength of the gravitational wave.

Hellings (1983)[44] has searched for pulsed and stochastic gravitational radiation by Doppler tracking of the spacecraft Voyager I. His negative results had a sensitivity of $h \sim 3 \cdot 10^{-14} f^{-1/2}/\sqrt{\text{Hz}}$, in the frequency range $10^{-4} - 5 \cdot 10^{-2}$ Hz, limited by phase distortion of the radio signals by the interstellar medium.

Noise sources for this technique include frequency noise in the master oscillator, and dispersion effects of the interstellar medium. Sensitivities of $h \sim 10^{-15}$ in the frequency range $10^{-4} - 10^{-2}$ Hz are hoped for in the future.

Investigators in this field include a group at the Jet Propulsion Lab. in California.

(c) Space Laser Interferometers.

There have been several proposals for optical

detectors in space (e.g. Weiss et al 1976)[45], and it is likely that future space experiments will consist of low power laser interferometers with baselines as large as 10^6 m. These will probably only be viable, however, after the ground based interferometers have been perfected.

An important noise source for these detectors will be interference from cosmic ray fluxes, which are stronger in space than they are on Earth, and from the solar wind.

Intended to detect low frequency sources, they have a potential sensitiviy of $h \sim 10^{-22}/\sqrt{Hz}$ at frequencies as low as 10^{-6} Hz.

Investigators in this field include a group at the Joint Institute of Laboratory Astrophysics in Colorado.

(d) Skyhook Detector.

An interesting space detector has been proposed by Braginskii and Thorne (1985)[46]. Christened "Skyhook", the design consists of two masses separated by a long (25km), thin cable with a spring section in the middle. The system would be arranged to orbit the Earth. The relative motions of the masses would be transmitted to the spring by the cable; and a sensor would monitor the resulting spring motion. This detector would operate in the region 10^{-1} -10^{-2} Hz, and, if noise problems can be overcome, would have a potential sensitivity of $h \sim 3 \cdot 10^{-17}$.

1.7 SUMMARY AND STATUS OF DETECTION TECHNIQUES.

The Stanford bar detector, cooled to 4K, is currently the most sensitive instrument, in the kilohertz

region of the spectrum, with a sensitivity of $h \sim 5.0 \cdot 10^{-19}$ for millisecond pulses, and a bandwidth of 13Hz. The laser interferometer groups at Glasgow, Caltech and Munich are all approaching this level of performance, and are likely to be comparable with Stanford in the next year or two. It is hoped considerable extensions of the baselines of the interferometers will take place and that in the next five years, or so, several long baseline detectors ($\gtrsim$ 1km) will come "on air". These detectors will be potentially good enough to detect astrophysically interesting events in the frequency range above 100Hz. Below 100Hz, good sensitivity depends on the success of ground noise isolation systems which hold many non-trivial engineering problems. Plans exist, also, for large scale bar experiments, in the U.S.A, involving arrays of bars tuned to slightly different frequencies to broaden the detection bandwidth.[47]

Detectors in space are currently the most hopeful method of detecting events with periods greater than a hundred seconds. In the short term, multifrequency Doppler tracking experiments are the most realisable of these, with existing technology. Space laser interferometers, however, could produce greater sensitivities but are unlikely to be used in the near future.

It is necessary, then, to pursue the development of several different types of detectors, covering different frequency ranges. Initial gravitational wave events will, most likely, be discovered as a result of coincidence experiments with two or more groups around the world. The direction of burst sources could be inferred from phase

differences, or arrival times, of coincident pulses; and correlation of pulses with optical observations could test for any velocity difference between electromagnetic and gravitational waves. The direction of periodic sources can be deduced from Doppler measurements of the source period. Measurement of the gravitational wave polarisation would test the various gravitation theories and produce information about the nature of the sources.

In conclusion, the detection and study of gravitational radiation will bring the following rewards: (i) It will act as a testing ground for relativistic gravity theories, and more importantly (ii) it will open up an avenue for astronomical exploration which will reveal important information about the mechanisms of the sources. Gravitational radiation is largely unique in this respect, as it is virtually unattenuated by the dense matter that absorbs and scatters electromagnetic radiation and elementary particles. Only the study of gravitational radiation is likely to reveal "detailed" information on violent astrophysical phenomena, such as the collapse of massive stars; and on structure of black holes. Gravitational waves are also one of the few probes of the early universe. There is, therefore, a requirement for gravitational radiation detectors, with large bandwidths and high sensitivities, to study the waveforms emanating from known (and yet to be discovered) astrophysical phenomena.

CHAPTER 2.

"THE PROTOTYPE OPTICAL CAVITY DETECTOR."

Having discussed the rewards of successful gravitational radiation observation and the main detection techniques currently being developed, the remainder of this thesis is devoted to certain aspects of the design and development of the ten metre prototype detector at Glasgow University.

2.1 DETECTION PRINCIPLES.

The prototype detector is an interferometer incorporating two, orthogonal, high finesse, Fabry-Perot cavities forming the two equal sides of an L-shape. The cavity mirrors are mounted on three test masses, suspended as pendulums, so that for frequencies much higher than the pendulum suspension frequency (approx. 1Hz), the masses behave as if they were essentially free. As has been stated, the influence of gravitational waves is such that they produce differential expansion and contraction of the cavity lengths.

The interferometer is illuminated by light from an argon laser, and successive light traverses in each cavity are superimposed, giving the resonance condition that a round-trip consists of an integral number of wavelengths. Cavity resonance is maintained by forcing the laser frequency to follow the length deviations of one cavity while altering the length of the second cavity to

compensate for fluctuations in the laser frequency. Thus slight changes in cavity length induce relatively large changes in the phase of the stored light, and relative motions of the cavities (such as those caused by gravitational waves) are monitored by observing the feedback signal which holds a cavity on resonance, or by looking at the combined interference output of the cavities (fig. 1.8).

As with delay-line interferometers, the fundamental limit to sensitivity lies with the noise due to photon counting error in the detected light output.

2.2 PHOTON NOISE LIMIT TO SENSITIVITY.

From 1.32, the number of photons appearing at the output of a single-pass interferometer is given by the expression

$$N = \frac{I_o \tau \epsilon}{2h\nu} (1 - \cos\phi) \qquad (2.1)$$

where the symbols are as previously defined. A change in the relative lengths of the two cavities, δl, produces a relative change in the phase of the output light, $\delta\phi$, such that

$$\delta\phi = K \delta l \qquad (2.2)$$

where K is a constant of proportionality. Thus the corresponding change in the number of photons appearing at the output of the interferometer is

$$\delta N = \frac{I_o \tau \epsilon}{2h\nu} \sin\phi \; K \delta l \qquad (2.3)$$

From 1.37, the detection condition, $\delta N > \bar{N}^{1/2}$, applies to give

$$\delta_1^2 \geq \frac{h\nu}{I_0 \tau \epsilon K^2 \cos^2(\phi/2)} \qquad (2.4)$$

Optimum sensitivity is obtained when $\phi \sim 0$. Hence,

$$\delta_1 \geq \left(\frac{2h\nu\Delta f}{I_0 \epsilon K^2} \right)^{1/2} \qquad (2.5)$$

where Δf ($=1/2\tau$) is the observational bandwidth of the measurement.

Each arm of the detector can now be treated as a separate Fabry-Perot interferometer. Assuming one cavity is held fixed with respect to the laser light, the phase change due to the displacement of the masses appears on the light from the other cavity, and the output of the detector can be treated as coming from that cavity. Let A_i be the amplitude of the light incident on the interferometer. The amplitude of the light returning from the cavity can be shown to be (section 4.3)

$$A_0 \exp(i\phi) = \frac{A_i t_1^2 r_2 \exp(i\delta)}{(1 - r_1 r_2 \exp(i\delta))} \qquad (2.6)$$

where δ is the phase offset per double-pass of the cavity, r_1 and r_2 are the amplitude reflection coefficients of the input and output mirrors of the cavity respectively, and t_1 is the amplitude transmission coefficient of the input mirror.

Thus the maximum amplitude of light from the cavity is just

$$A_{MAX} = \frac{A_i t_1^2 r_2}{(1 - r_1 r_2)} \qquad (2.7)$$

The output intensity is obtained by multiplying 2.6 with its complex conjugate to give

$$I_o = \frac{I_i (t_1^2 r_2)^2}{(1-2r_1 r_2 \cos\delta + (r_1 r_2)^2)} \qquad (2.8)$$

which can be rewritten as

$$I_o = \frac{I_i T_1^2 (F/\pi)^2 (R_2/R_1)^{1/2}}{1 + 4(F/\pi)^2 \sin^2(\delta/2)} \qquad (2.9)$$

where $$F = \frac{\pi \sqrt{r_1 r_2}}{(1-r_1 r_2)} \qquad (2.10)$$

is the finesse of the cavity, and R_1 $(=r_1^2)$, R_2 $(=r_2^2)$ and T_1 $(=t_1^2)$ are the corresponding intensity coefficients to r_1, r_2 and t_1.

Now, from 2.6,

$$\frac{\exp i(\delta-\phi)}{A_o} = \frac{1-r_1 r_2 \exp(i\delta)}{A_i t_1^2 r_2} \qquad (2.11)$$

Expanding the exponential, and equating real and imaginary parts results in

$$\frac{1}{A_o} \simeq \frac{1-r_1 r_2}{A_i t_1^2 r_2} \qquad (2.12)$$

and $$\frac{(\phi-\delta)}{A_o} \simeq \frac{r_1 r_2 \delta}{A_i t_1^2 r_2} \qquad (2.13)$$

which implies $$\phi = \delta\left(\frac{1}{1-r_1 r_2}\right) \qquad (2.14)$$

For small changes in the length of the cavity,

$$\delta = (4\pi/\lambda)\,\delta l \qquad (2.15)$$

Thus, the corresponding phase deviations of the output light, $\delta\phi$, are given by

$$\delta\phi = \frac{4\pi}{\lambda}\left(\frac{\delta l}{1-r_1 r_2}\right) \qquad (2.16)$$

Comparison with 2.2 reveals that the constant of proportionality, K, is given by

$$K = \frac{4\pi}{\lambda}\left(\frac{1}{1-r_1 r_2}\right) \qquad (2.17)$$

So, using 2.10,

$$K^2 = \left(\frac{4\pi}{\lambda}\right)^2 \frac{F^2}{\pi^2\sqrt{R_1 R_2}} \qquad (2.18)$$

Combining this with 2.9 produces

$$I_o K^2 = \frac{I_i T_1^2 (1/R_1)(4\pi/\lambda)^2 (F/\pi)^4}{1 + (4F^2/\pi^2)\sin^2(\delta/2)} \qquad (2.19)$$

The ultimate shot noise limit is arrived at by assuming zero absorption in the cavity mirrors (i.e $T_1 = 1-R_1$). Then, using $R_1 \simeq R_2$, 2.19 becomes

$$I_o K^2 \simeq I_i (4\pi/\lambda)^2 (F^2/\pi^2) \qquad (2.20)$$

Hence, from 2.5, the minimum detectable motion, for cavity storage times less than the gravitational wave period, is given by

$$\delta l \geqslant \left(\frac{hc\lambda\Delta f}{8\epsilon F^2 I_i}\right)^{1/2} \qquad (2.21)$$

Comparison of 2.21 with 1.41 shows that the photon noise limited sensitivity of an optical cavity interferometer is similar to that of a delay-line interferometer.

In passing, it is interesting to note that this limit is equally dependent on the wavelength and power of the illuminating light, which is why, at present, argon lasers operating at a wavelength of 514.5 nm give the best opportunity of good sensitivity.

The cavity storage time, τ_s, is related to the finesse of the cavity by

$$F = \frac{c\,\pi\,\tau_s}{2l} \qquad (2.22)$$

So for millisecond pulses a finesse of $\sim$ 450 is appropriate, which, with an input power of 1W and a quantum efficiency of 0.5, gives a shot noise limited sensitivity, for a 1km baseline, of

$$h \sim \frac{\delta l}{l} \sim 3 \times 10^{-22} \left(\frac{1W}{I_i}\right)^{1/2} \left(\frac{0.5}{\epsilon}\right)^{1/2} \left(\frac{1km}{l}\right) \; (/\sqrt{Hz}) \qquad (2.23)$$

In practice, there will always be some absorption of light by the cavity mirrors which, together with non-optimum alignment and mode-matching, is reflected in the contrast, or visibility, V ($\leq$ 1), of the Fabry-Perot fringes. It is then appropriate to modify 2.21 by a factor $f(V,\phi_o)$ which depends on the visibility of the fringes and, to a certain extent, on the depth of phase modulation, ϕ_o, used for frequency stabilisation of the laser.[48] Now,

$$h(\text{shot noise}) \sim \left(\frac{hc\lambda\Delta f}{8\epsilon F^2 I_i l^2}\right)^{1/2} \cdot f(V,\phi_o) \qquad (2.24)$$

The factor $f(V,\phi_o)$ is typically around 3-5, but for low absorption mirrors (losses less than 1 part in 10^4) giving good visibility, it is expected to approach unity.

For the situation where the cavity finesse is high enough to produce a storage time, τ_s, greater than the period of the gravitational wave, τ_g, 2.21 is again modified by a factor[48] $[1+(2\pi\tau_s/\tau_g)^2]^{1/2}$.

Note that 2.24 is applicable to the case where the entire power out of the detector is used to monitor sensitivity (i.e. cavity outputs are interfered). If the cavities are monitored separately, this limit is higher by

a factor $\sqrt{2}$.

2.3 RADIATION PRESSURE.

Fluctuations in the intensity of the laser light will produce corresponding fluctuations in the displacements of the masses by the radiation pressure exerted by the light. The influence of laser intensity noise, on the masses, due to macroscopic effects can, in general, be balanced out, to a high degree, if the parameters of each arm of the interferometer are the same. However, the intensity fluctuations due to shot noise are anticorrelated in the two arms of the detector, and therefore cannot be minimised by recombination of the beams.

Whereas the photon noise error of section 2.2 decreases with increasing laser power, the effect on the radiation pressure is the opposite. Caves (1981)[41] has shown that these two effects can be treated as orthogonal components of an overall quantum noise error. From this, he has shown that there is an optimum laser power which minimises the total error by balancing the contributions from shot noise and radiation pressure.

i.e. $$I_{OPT} \simeq \frac{mc\lambda\pi}{4F^2\tau^2} \qquad (2.25)$$

where m is the mass of the test mass, F is the finesse of the cavity, and τ is the duration of the measurement.

For a finesse of 450 and a mass of 100kg, the optimum power in a millisecond bandwidth is $\sim$ 60kW. It can be seen, then, that shot noise will be the dominant

contribution until very high laser powers are achieved.

Caves has also shown that the minimum error obtainable, by balancing radiation pressure with shot noise, is the order of the standard quantum limit derived in section 1.6.

2.4 EXPERIMENTAL NOISE SOURCES.

To reach a shot noise limited sensitivity in an amount of laser power greater than a milliwatt requires the understanding and elimination of several non-fundamental noise sources. The most troublesome of these noise sources are discussed below, together with some of the measures necessary to overcome them.

2.4(a) INTENSITY NOISE.

The intensity noise fluctuations of an argon laser are many orders of magnitude above those due to shot noise. These fluctuations will be reproduced in the photocurrents of the detecting photodiodes, and would be the dominating noise source in the interferometer.

To overcome this, the servo loop, used to stabilise the laser frequency, utilises radiofrequency (r.f) phase modulation of the light at a frequency ($\gtrsim$ 10MHz) where the intensity fluctuations of the laser are comparable with the shot noise level. As the light out of the detector is coherently detected, laser intensity noise only couples to the sensitivity via a static offset error in the locking point null of the servo loop. The amount of intensity noise coupling can then be approximated by

$$\frac{\delta l}{l} \simeq \frac{\delta I}{I} \frac{\Delta l}{G} \qquad (2.26)$$

where Δl is the original path difference in the interferometer with the feedback loop open, $\delta I/I$ is the value of the fractional intensity fluctuations of the laser, and G is the open-loop gain of the servo loop.

In the frequency range of interest $\delta I/I$ is typically $\sim 10^{-5}$ $/\sqrt{Hz}$, which implies

$$\delta l \simeq 10^{-5} \Delta l \, G^{-1} . \Delta f^{1/2} \qquad (2.27)$$

It is, therefore, necessary to use as high a loop gain as possible to minimise locking errors.

$\delta I/I$ can be reduced further by passive improvements to the laser itself and by active servo systems, feeding back to, either, the laser power supply or to an arrangement of optical modulators outside the laser cavity.[49]

2.4(b) FREQUENCY NOISE.

Frequency noise of the laser will couple to sensitivity through a residual path difference, Δl, between the two arms of the interferometer. Then, if the frequency noise is $\Delta\nu$, the minimum detectable motion, for an interfered output, is

$$\frac{\delta l}{l} = \frac{\Delta\nu}{\nu} \Delta l \qquad (2.28)$$

Now Δl depends mainly on the finesse of the cavities, so 2.28 can be rewritten as

Combined Output... $$\frac{\delta l}{l} = \frac{\Delta F}{F} \frac{\Delta\nu}{\nu} \qquad (2.29)$$

where ΔF denotes the difference in finesse of the

cavities.

Thus, the very high demands on frequency stabilisation may be reduced somewhat by careful matching of the cavity finesses.

If the cavities are separately monitored then the stability condition is more severe (i.e. $\delta l/l = \Delta\nu/\nu$). However, as the frequency deviations are observed in both outputs, they can be electronically subtracted, from the sensitivity monitoring output, to an extent dependent on the factor, G, of the subtraction. Then

Separate Cavity Outputs... $$\frac{\delta l}{l} = \frac{1}{G}\,\frac{\Delta\nu}{\nu} \qquad (2.30)$$

To reach a strain sensitivity of $\sim 10^{-21}$, then, would require something like a frequency stability of 10^{-5} Hz plus 20dB of electronic subtraction.

Laser frequency noise will be considered in more detail in chapter 4, and both of the above methods of minimising the coupling of frequency noise will be demonstrated in chapters 6 and 7. As with intensity noise, some improvement in the intrinsic noise of the laser is obtainable by passive improvements (chapter 3).

2.4(c) BEAM GEOMETRY FLUCTUATIONS.

Fluctuations in the position and angle of the laser beam, together with pulsations of the beam width, can produce phase noise in the output of the detector if the wavefronts of the two interfered beams are not perfectly matched.[50] For example, if the beams are interfered at a small angle α, and the laser exhibits lateral beam

fluctuations δx, then this leads to a spurious signal

$$\delta_1 \simeq \alpha \delta_x \qquad (2.31)$$

It has been shown that the amount of lateral fluctuations from a free-running argon laser can limit the sensitivity of an interferometer to as high as 10^{-15} m/$\sqrt{\text{Hz}}$.[48] It is necessary, therefore, to introduce certain optical elements in to the design of interferometers to alleviate the effects of beam geometry fluctuations.

At the Max Planck Institute in Garching, a technique has been developed whereby the incident beam is passed through an optical resonator, or "mode-cleaner", before it enters the detector. The non-perfect beam can be represented by a fundamental TEM_{00} mode contaminated by low order transverse modes which are a result of the fluctuations in the geometry of the beam. As the mode-cleaning cavity is made resonant for the fundamental mode only, the fluctuations of the beam are suppressed by a factor related to the finesse of the cavity.[51]

Another method, presently in use at Glasgow, consists of an active servo system which feeds back to a quartet of steerable mirrors in the path of the beam.[52] Two of these mirrors are mounted on low-frequency, wide-ranging, coil elements which control large fluctuations in the beam angle and position, and the remaining two have their orientation controlled, in two dimensions, by high frequency, piezoelectric transducers. The motions of the laser beam are monitored by two, position sensitive, quadrant photodiodes. This method has been shown to have the potential to suppress fluctuations

at $\sim$ 1kHz by a factor of 100. Provision is also made for the additional use (if necessary) of a mode-cleaner in the Glasgow system.

A technique initially suggested by R. Weiss, at MIT, involves passing the laser beam through a length of single-mode optical fibre before it enters the interferometer. The effect is similar to that of a mode-cleaner, in that it suppresses the higher order transverse beam modes. The attraction of this technique is that it is a purely passive device and is, therefore, simple to implement. This technique has also been adopted, lately, by the group at the Max Planck Institute.[53] However, problems remain with this method as it is difficult to transmit high amounts of laser power through the fibre.

Again, some improvement in the intrinsic laser geometry fluctuations can be obtained by passive modifications to the laser, as will be seen in the following chapter.

2.4(d) SCATTERED LIGHT.

As mentioned in chapter 1, one of the main reasons for adopting an optical cavity detector was the belief that it would be less sensitive, than a delay-line interferometer, to noise introduced by scattered light.

By its nature, scattered light is largely uncorrelated in the two arms of the detector, and manifests itself in fluctuations of the phase of the output light. If the fractional amplitude of scattered light is σ, and its phase angle relative to the main beam is θ, then the

resultant phase change at the photodiode is given by, (Schnupp et al, 1985)[55]

$$\phi = \sigma \sin\theta \qquad (2.32)$$

Frequency fluctuations of the laser, $\delta\omega$, will produce phase fluctuations, $\delta\theta$, such that

$$\delta\theta = \delta\omega\tau \qquad (2.33)$$

where τ is the light travel time for the path difference between the main and scattered beams. Differentiation of 2.32 with respect to θ results in

$$\delta\phi = \sigma \cos\theta\tau\delta\omega = 2\pi\sigma\tau\cos\theta\,\delta\nu \qquad (2.34)$$

There are two main ways, then, of reducing the effects of scattered light: (i) minimize the amount of scattered light (by insertion of baffles etc into beam pipes) and (ii) improve the stability of the laser frequency.

A gravitational wave may be expected to produce a phase change

$$\delta\phi_{g\omega} = (4F/\lambda)\,\delta l \qquad (2.35)$$

And if $\delta\phi_{g\omega} \sim \delta\phi$, then scattered light imposes a limit to detectable motion of

$$\delta l = (\lambda/4F)\,\delta\phi \qquad (2.36)$$

The equivalent gravitational wave strain is

$$h = \frac{2\delta l}{l} = \frac{c\pi}{Fl}\sigma\tau\cos\theta\,\frac{\delta\nu}{\nu} \qquad (2.37)$$

The worst case condition occurs for $\cos\theta = 1$. Estimating the amplitude of scattered light to be 0.1%, the poorest limit to sensitivity, set by scattered light, for a 1km detector of finesse 450, with frequency stabilisation of 10^{-5} Hz/$\sqrt{\text{Hz}}$ and a scattering time of a millisecond (- order of the storage time), is

$$h \sim 10^{-23} \left(\frac{\tau}{10^{-3}\,s}\right)\left(\frac{\sigma}{10^{-3}}\right)\left(\frac{\delta\nu}{10^{-5}}\right)\left(\frac{450}{F}\right)\left(\frac{10^{3}}{l}\right) \quad (/\sqrt{Hz}) \qquad (2.38)$$

Optical cavity detectors lend themselves to good frequency stabilisation, and as successive beams overlap, the path difference of scattered beams is very much reduced.

Aside from improving frequency stabilisation, there also exist proposals for the reduction of scattered light effects by modulation techniques designed to break the coherence of the main and scattered beams (Man et al, 1978, and Schnupp et al, 1985).[54,55]

2.4(e) REFRACTIVE INDEX FLUCTUATIONS.

To provide acoustical isolation, and to limit the effects of refractive index fluctuations, the test masses and beam paths are located inside a vacuum chamber. Fluctuations in the pressure of the vacuum, however, may result in a significant variation of the optical path length of the interferometer. The standard of vacuum, then, has to be maintained to a high degree.

If the beam inside a cavity is modelled as a cylinder of length l and diameter w, then, for a density of gas molecules n, the number traversing the beam in an measuring time τ is

$$N = \frac{n\pi\bar{c}wl\tau}{4} \qquad (2.39)$$

where $\bar{c}$ is the mean velocity of the molecules.

Brownian motion produces a fluctuation, δN, in the number of molecules crossing the beam such that

$$\frac{\delta N}{N} = \frac{1}{\sqrt{N}} = \left(\frac{4}{n \pi \bar{c} w l \tau} \right)^{1/2} \qquad (2.40)$$

Now, the change in refractive index, $\Delta\mu$, of the gas is related to the change in the number of molecules, ΔN, by

$$\frac{\Delta\mu}{\mu - 1} = \frac{\Delta N}{N} \qquad (2.41)$$

And,

$$\frac{(\mu - 1)}{(\mu - 1)_A} = \frac{P}{P_A} \qquad (2.42)$$

where P is the pressure of the vacuum, and the subscipt "A" refers to atmospheric conditions.

The change in optical path, Δl, produced by a refractive index fluctuation is given by

$$\Delta l = l \Delta\mu = l(\mu - 1) \frac{\Delta N}{N} \qquad (2.43)$$

From 2.42,

$$(\mu - 1) \simeq 3 .10^{-4} . \frac{P}{10^5} = 3 .10^{-9} .P \qquad (2.44)$$

Using the low pressure approximation, n= P/ kT, and combining 2.43 and 2.44, produces an expression for the sensitivity limit due to refractive index fluctuations.

$$h \sim \frac{\Delta l}{l} \sim 3 .10^{-9} \left(\frac{1{\cdot}6kTP}{\bar{c} w l \tau} \right)^{1/2} \qquad (2.45)$$

For a 1km baseline, and with similar optical cavity design to the present ones, $w \sim (\lambda l)^{1/2} \sim$ 2cm.

A pressure of 10^{-6} Torr (i.e. $1.3 .10^{-4}$ Pa) would then imply a sensitivity limit of $\sim 3 .10^{-23} / \sqrt{Hz}$.

2.4(f) THERMAL NOISE.

The mechanical design of the test masses and their suspensions is important from the point of view of preventing strong coupling of mechanical noise to the detector sensitivity. Thermal noise is not as dominant a noise source for interferometers as it is for bar detectors, due to the fact that an interferometric detector does not require to operate at the resonant frequency of the test masses.

Thermal noise can couple to the sensitivity by two routes: (i) Thermal excitation of the pendulum suspensions, and (ii) Thermal vibrations of the internal modes of the masses about their centres of mass.

Both types of noise can be treated similarly, in the manner of Weiss (1972)[39], as a stochastic driving force which excites the mechanical system. This force has a spectral density given by

$$\Delta F^2/\Delta f = 4kT\beta \qquad (2.46)$$

where k is Boltzmann's constant, T is the absolute temperature of the damping medium, and β is the damping coefficient associated with the frequency of excitation.

The damping coefficient, β, can be expressed in terms of the quality factor, Q, the resonant frequency, ω_o, and the mass, m, by

$$\beta = m\omega_o/Q \qquad (2.47)$$

Treating the excited system as a harmonic oscillator results in a value for the amplitude of displacement of the test mass, Δx, given by

$$\frac{\Delta x^2}{\Delta f} = \frac{4kT}{m\,\omega_o^3\,Q}\left[\frac{1}{\left(1-\frac{\omega^2}{\omega_o^2}\right)^2+\left(\frac{\omega^2/\omega_o^2}{Q}\right)}\right] \qquad (2.48)$$

As the frequencies of the two separate noise contributions are arranged to appear at the two limiting frequency cases ($\omega >> \omega_o$ and $\omega << \omega_o$), they can be treated separately.

(a) Pendulum mode: The pendulum suspensions of the masses have their periods arranged such that their resonant frequency is much lower than the frequency of the gravitational wave window. Then, $\omega >> \omega_o$, and if Q>>1,

$$\frac{\Delta x^2}{\Delta f} = \frac{4kT}{m\,Q}\,\frac{\omega_o}{\omega^4} \qquad (2.49)$$

This implies a limit to sensitivity, for a long baseline detector, of

$$h_{SUSP} \sim \frac{\delta l_{SUSP}}{l} \sim 1.10^{-24}\left(\frac{\omega_o}{2\pi\ .1\ Hz}\right)^{1/2}\left(\frac{2\pi\ .1kHz}{\omega}\right)^2 \left(\frac{100kg}{m}\right)^{1/2}\left(\frac{10^6}{Q}\right)^{1/2}\left(\frac{1km}{l}\right) \quad (/\sqrt{Hz}) \qquad (2.50)$$

(b) Internal modes of the masses: To prevent strong coupling from the lowest normal mode of a test mass, the frequency of the mode should be much higher than the gravitational wave window. For $\omega << \omega_o$, and Q>>1,

$$\frac{\Delta x^2}{\Delta f} = \frac{4KT}{\omega_o^3\,m\,Q} \qquad (2.51)$$

which implies,

$$h_{INT} \sim \frac{\delta l_{INT}}{l} \sim 2.10^{-23}\left(\frac{2\pi\,10kHz}{\omega_o}\right)^{3/2}\left(\frac{10kg}{m}\right)^{1/2}\left(\frac{10^5}{Q}\right)^{1/2} \left(\frac{1km}{l}\right) \quad (/\sqrt{Hz}) \qquad (2.52)$$

The effects of thermal noise can, therefore, be minimised by using high Q materials and suspensions. (Pendulum suspensions with Q's as high as 10^7 have been shown to be achievable [56]).

2.4(g) SEISMIC NOISE.

Isolation against noise introduced by motion of the ground is primarily provided by the pendulum suspensions. The amount of seismic isolation afforded by a single-degree-of-freedom pendulum suspension is given by (Weiss 1972)[39]

$$\omega >> \omega_0 , \quad \left| \frac{\Delta x_1}{\Delta x_0} \right|^2 = \left(\frac{\omega_0}{\omega} \right)^4 + \left(\frac{\omega_0}{\omega} \right)^2 \left(\frac{1}{Q^2} \right) \qquad (2.53)$$

where Δx_1 is the mass displacement, and Δx_0 is the the ground displacement.

For Q high,

$$\frac{\Delta x_1}{\Delta x_0} \simeq \left(\frac{\omega_0}{\omega} \right)^2 \qquad (2.54)$$

which implies a 12dB-per-octave roll-off, $(\omega_0/\omega)^2$, until the frequency $\omega_0 Q$, when the roll-off becomes $(\omega_0/\omega Q)$.

The benefit of good isolation at high frequencies is gained at the cost of large motions at the resonant frequency, ω_0, of the pendulum. As will be seen, it is then necessary to introduce extra damping of the cavities, around this frequency, to maintain resonance of the light.

Around 1kHz, Weiss suggests a "quiet" ground motion of

$$\Delta x_0 \gtrsim 10^{-15} \ \mathrm{m}/\sqrt{\mathrm{Hz}} \qquad (2.55)$$

This implies a coupling of ground motion to a suspended test mass, for a 1Hz pendulum mode, of

$$\Delta x_1 \gtrsim 10^{-21}\ m/\sqrt{Hz} \qquad (2.56)$$

Further isolation may be provided by stacks of alternating lead and rubber mounted between the ground and pendulum support. 1 stage of lead and rubber acts as a heavy mass on a spring for shear forces on the lead. A total of n stages acts like a multipole low-pass filter with the transmissibility, $(\Delta x_1/\Delta x_0)$, falling as $1/f^n$.

It is necessary to keep the lead small enough such that its internal modes are well above the gravitational wave window. Also, the resonant frequency of the entire stack must have its resonant frequency well below this window.

For the extension of the gravitational wave window to low frequencies (<100 Hz), it will probably be necessary to employ an active seismic isolation system which uses feedback to, effectively, lower the resonant frequency of the pendulum.[57]

Several other noise sources, considered by Weiss (1972),[39] include displacement noise from cosmic ray showers and gravitational gradients. These other noise sources appear unlikely to have a prohibitive effect on the target sensitivity of a long baseline detector.

2.5 DESIGN AND OPERATION OF THE PROTOTYPE DETECTOR.

2.5(a) EARLY DEVELOPMENT.

The construction of the 10m prototype interferometer was initiated in 1978. The entire vacuum chamber, which

houses the test masses and the beam paths, is supported by a steel frame (Dexion 260) resting, at four points, on stacks of lead and rubber which provide initial isolation from ground motions. The original design of the interferometer incorporated 3-mirror ring cavities (to prevent light from the cavities returning to the laser), and the arrangement was such that it facilitated only separate cavity monitoring - i.e. there existed no facility for recombining the beams. The first investigations of performance were undertaken in 1981, and produced a best sensitivity of $\sim 3 .10^{-15}$ m/$\sqrt{\text{Hz}}$ at 1kHz.[58]

The understanding of the contributing noise sources, gained by the experiences of this early detector set-up, led to a major reconstruction of the detector. This included aspects such as futher seismic isolation (provided by lead and rubber stacks between the vacuum chamber and the each test mass suspension point), improved frequency and positional stabilisation of the laser light, and the adoption of 2-mirror cavities to reduce light losses and improve fringe contrast.

With this last modification, the light returning from the cavity is coincident with the incoming beam. To separate the input and output beams, and to provide optical isolation, a polarising beamsplitter/quarter-wave plate arrangement is used to introduce a 90^{o} difference between the polarisations of the beams. - Further isolation is provided by Faraday rotators in the input beam path. This is shown in figure 2.1 along with the other main optical elements of the interferometer. The arrangement shown is

FIG. 2. 1. DIAGRAM OF INTERFEROMETER SHOWING POLARISATION SCHEME.

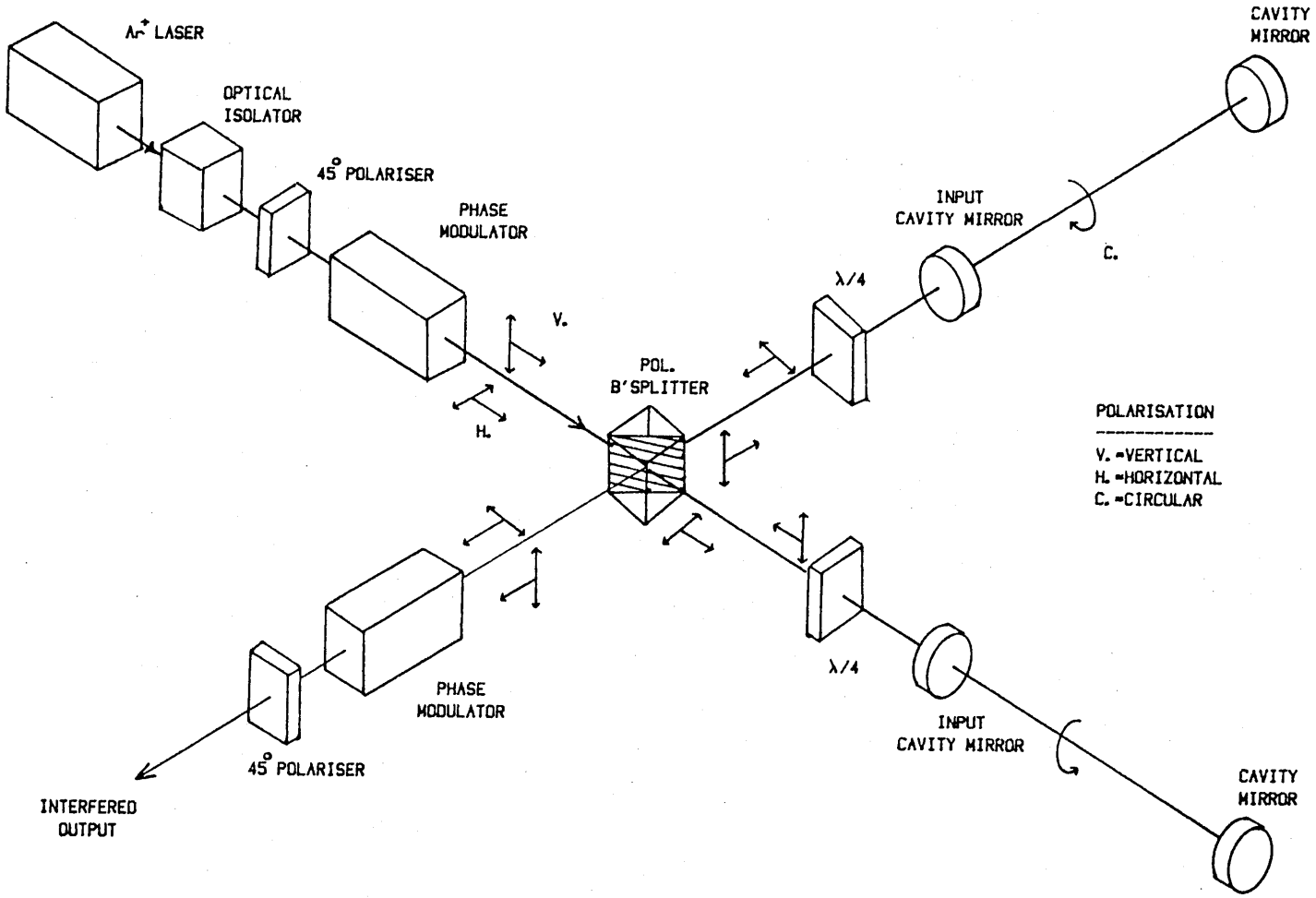

the "combined output" set-up where the phase modulator, in the path of the output beam, is used for an r.f. modulation technique which allows the phase difference between the beams to be measured (chapter 6). The input phase modulator is used as part of the laser frequency stabilisation loop which is discussed and described in chapter 4.

2.5(b) TEST MASS SUSPENSIONS.

The support for each pendulum suspension is separated from the vacuum chamber by 5 stages of lead and rubber ($f_o \sim$ 10Hz). The top of the stack is arranged such that it can be rotated and tilted by d.c. motors which can be operated from outside the vacuum chamber. These motors can offset any large drifts made by the lead/rubber stacks.

To maintain the alignment and resonance of the cavities, the orientations of the test masses have to be extremely stable (-angular stability $<< 10^{-4}$ rads). Figure 2.2 shows the basic design of a test mass and how it is suspended and orientated. Each mass is hung by three steel wires (1/100 inch thick) suspended from a flat, rigid triangle which is, in turn, suspended by a single thicker wire. Mechanical steering forces are applied to this triangle, by tilt and rotational loudspeaker transducers, via a servo system. These transducers pull against opposing spring constraints.

The orientation of a mass is monitored by reflecting a helium-neon laser beam from a mirror(s) mounted on the mass (not shown) and detecting it with a position-sensitive photodiode. The signals from the photodiode are amplified

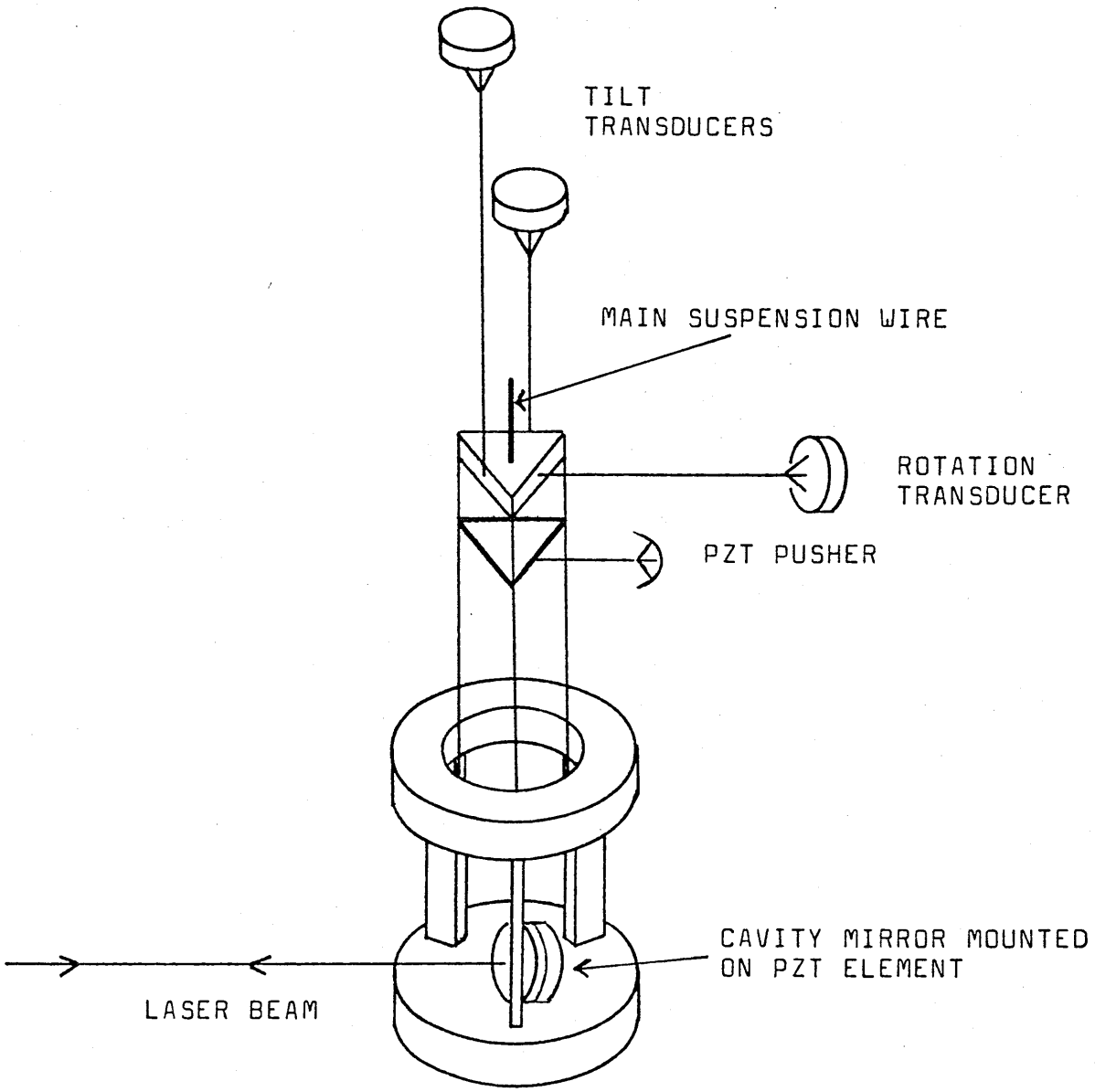

FIG.2.2: CONSTRUCTION AND SUSPENSION OF A TEST MASS

THE ORIENTATION OF THE MASS IS STABILISED BY FEEDING BACK ONTO THE SUSPENSION POINTS VIA THE TILT AND ROTATION LOUDSPEAKER TRANSDUCERS. CAVITY LENGTH CAN BE MODULATED AT HIGH FREQUENCIES BY THE PZT CAVITY MIRROR, AND AT LOW FREQUENCIES BY THE PZT PUSHER WHICH PUSHES, ONTO THE LOWER OF THE TWO TRIANGLES, ALONG THE CAVITY.

and filtered before being fed back to the transducers. The angular stability obtained is the order of a microradian. The orientation controls act at frequencies below 30Hz and are strongly filtered above this frequency to prevent the introduction of noise into the frequency band of interest.

After the reconstruction, the test masses installed were all of similar design. Each test mass consisted of two aluminium discs separated by three, rectangular, aluminium pillars. This gave a total mass of 12kg. A cavity mirror, mounted on a piezoelectric element, was situated on the lower of the two discs. In the frequency stabilising cavity (primary), this element is used to apply calibration displacement signals; and in the other (secondary) cavity, it is used to alter the cavity length to follow the laser frequency.

Part of the signal used to stabilise the secondary cavity (<20Hz) is applied to the mass by a bimorph PZT element which pushes onto a second lower triangle in the mass suspension (fig. 2.2). Two of these elements act in unison for each cavity to damp the large swinging motions at the pendulum frequency.

Fine tuning of the test mass position, for cavity alignment, is obtained by altering the d.c. bias to the loudspeaker transducers.

The suspension of the central test mass is as described above, but the test mass itself is of a more complicated construction. Apart from containing the input mirrors, for the cavities, and the central polarising beamspitter, the lower deck of the mass also houses the

output phase modulator, the isolating quarter-wave plates, and two auxiliary beamsplitters sited between the central splitter and the cavity mirrors. These additional splitters split off 10% of the light returning from the cavities, to be used for the cavity stabilisation loops. One of these outputs (secondary) is also used for monitoring of the detector sensitivity. A small fraction of the input beam is directed towards the position-sensitive photodiodes, used for beam geometry control, located on the top deck of the central mass. [The top deck also houses a mode-cleaning cavity, and the design of the mass is such that it would be possible to stabilise the light to this cavity first before it enters the elements on the lower deck]. A more complete diagram of the interferometer is shown in figure 2.3.

2.5(c) CAVITY CONTROL LOOPS.

(i) Primary Loop.

The circuit elements for the laser stabilisation loop are shown in figure 2.3. Light leaving the laser is phase modulated by a Brewster-cut, electro-optic crystal (Gsanger) driven by $\sim$ 0.5W of r.f. power at 24MHz. The cavities have a finesse of $\sim$ 600 and a linewidth of 25kHz. The modulation frequency, then, is considerably in excess of the transmission bandwidth of the cavity. The input mirror of the cavity is flat while the end mirror has a radius of curvature of 15m. The light returning from the cavity has no r.f. phase modulation, and when interfered with light reflected directly from the input mirror

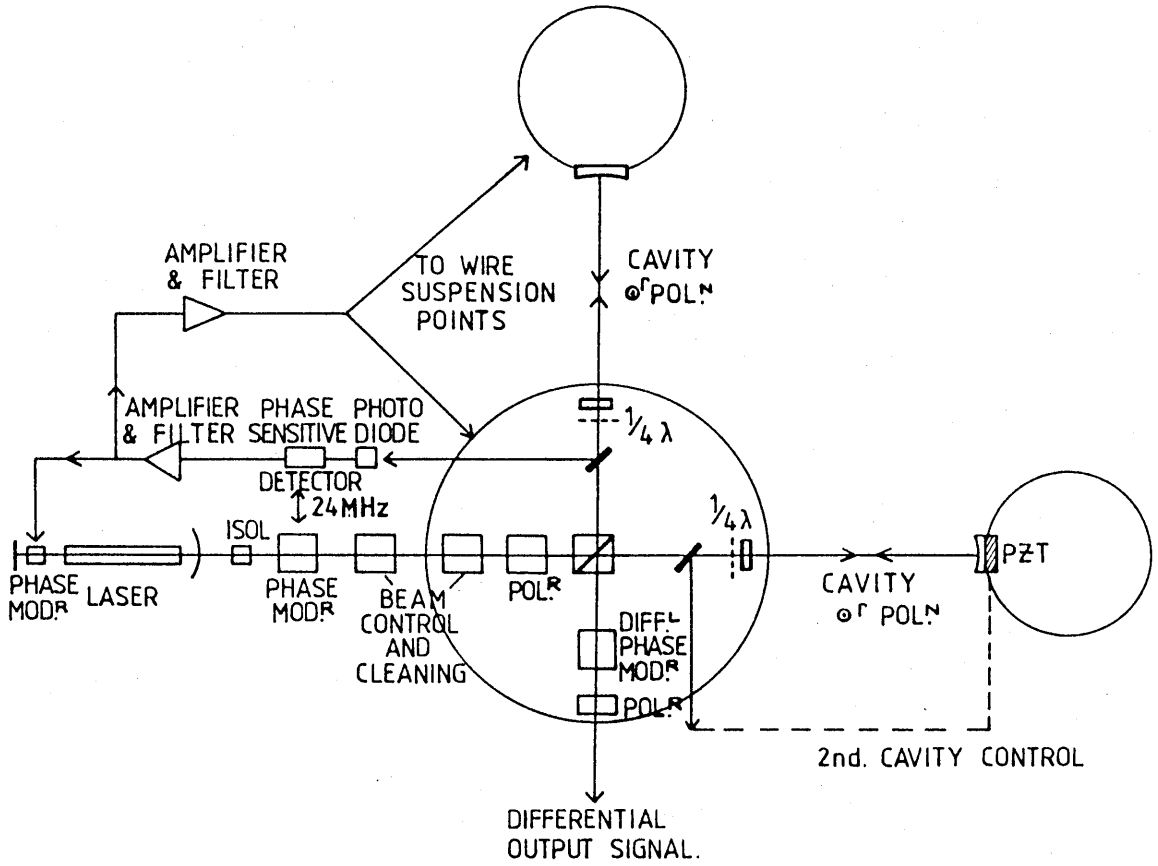

FIG.2.3: SCHEMATIC DIAGRAM OF THE INTERFEROMETER. THE CIRCUIT ELEMENTS FOR THE STABILISATION OF THE PRIMARY LOOP ARE SHOWN.

produces an amplitude modulated signal proportional to the phase deviations of the incident light with respect to that stored in the cavity. The output light is detected by a photodiode and the signal heterodyned with a reference 24MHz signal by a phase sensitive detector (PSD). The resulting error signal, amplified and filtered, is fed (via differential 250V amplifiers) to an electro-optic modulator inside the laser cavity. This is an ADP crystal which exhibits Pockels effect such that it alters its refractive index in a manner proportional to the voltage change across it. The optical length of the laser cavity, and hence the frequency of the output light, can be changed by altering the volts applied to the modulator. The modulator used typically has a quarter-wave voltage of 400V, and the laser cavity has a length of $\sim$ 2m. This implies a potential frequency change of 1.10^{5} Hz/volt for differential drive. The unstabilised laser frequency moves many megahertz at low frequencies but less at higher frequencies. The driving amplifier is arranged in a by-pass format to provide optimum performance (This is dealt with more fully in chapter 5). The bandwidth of the loop is wide ($\sim$ 1MHz) which enables a high loop gain ($\sim 10^{5}$ at 1kHz) to be achieved.

As shown in figure 2.3, part of the signal is also fed to the suspension points of the masses to damp their low frequency excursions. The bimorph PZTs, used as the feedback transducers, have a driven motion of 2.10^{-7} m/V which gives them a dynamic range of $\sim 40\lambda$. This is enough to cope with the largest mass deviations and to maintain

cavity resonance. So the laser is stabilised to the primary cavity at high frequencies and vice-versa at low frequencies. The driving circuit for the primary PZT pushers is shown in figure 2.4.

(ii) Secondary Loop.

The error signal for the stabilisation of the secondary cavity is derived in exactly the same way as that of the primary, using the same r.f. modulation scheme. Here again, the light returning from the cavity falls on a photodiode and is coherently detected. The resulting signal, this time, is amplified and filtered and fed to the piezoelectric transducer which drives the end mirror of the cavity. As with the primary cavity, some of the feedback signal is used to damp the low frequency motion of the masses.

The piezoelectric transducer used for driving the cavity mirror was a ceramic tube (Vernitron PZT-5H) with a motion of $4.2 \cdot 10^{-9}$ m/V.

The bandwidth of the secondary loop is limited by the resonance of the transducer structure ($\sim$ 20kHz), and as a result the loop gain achieved ($\sim$ 10 at 1kHz) is much smaller than that of the primary loop. Figure 2.5 shows the the driving circuitry for the secondary stabilisation loop. The unity gain frequency of the loop is around 5kHz. Thus at frequencies of $\sim$ 2.5kHz and lower, the motion required of the PZT driven mirror, to maintain resonance, is a measure of the detector sensitivity.

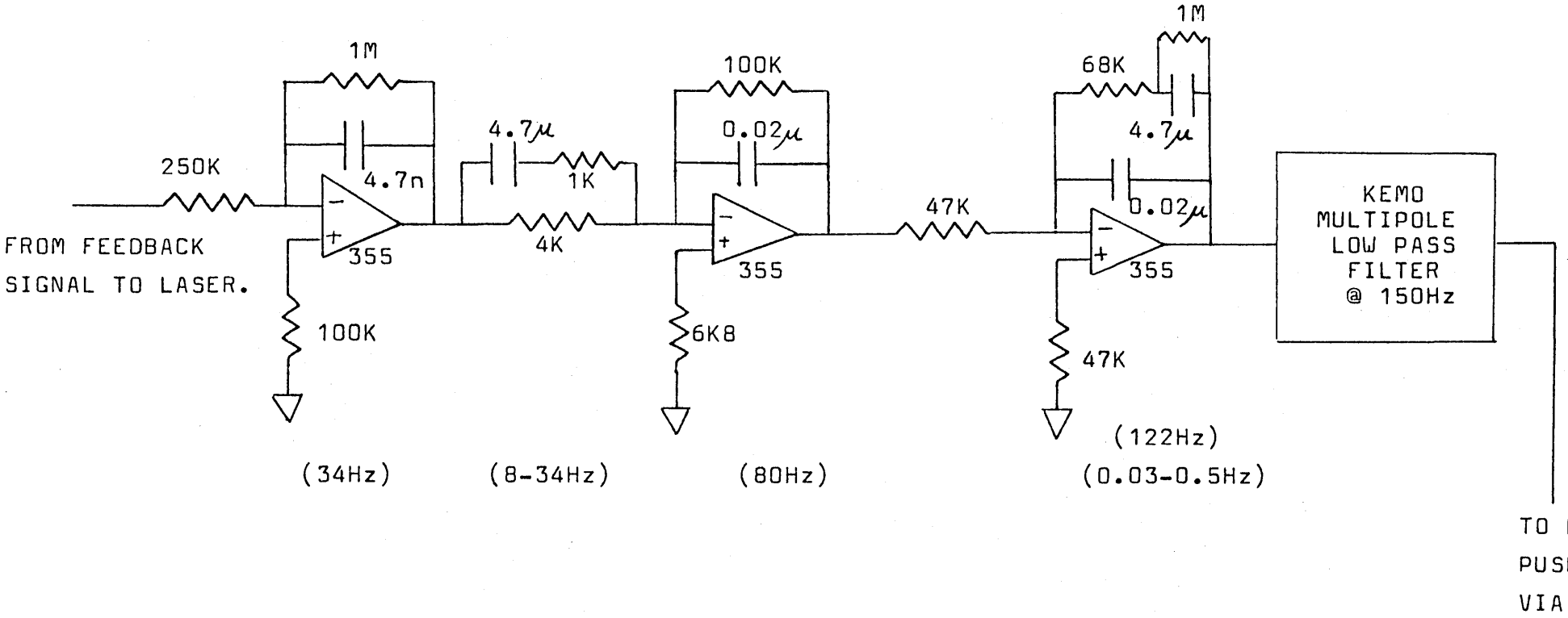

FIG.2.4: DRIVING CIRCUIT FOR THE PRIMARY PZT PUSHERS.

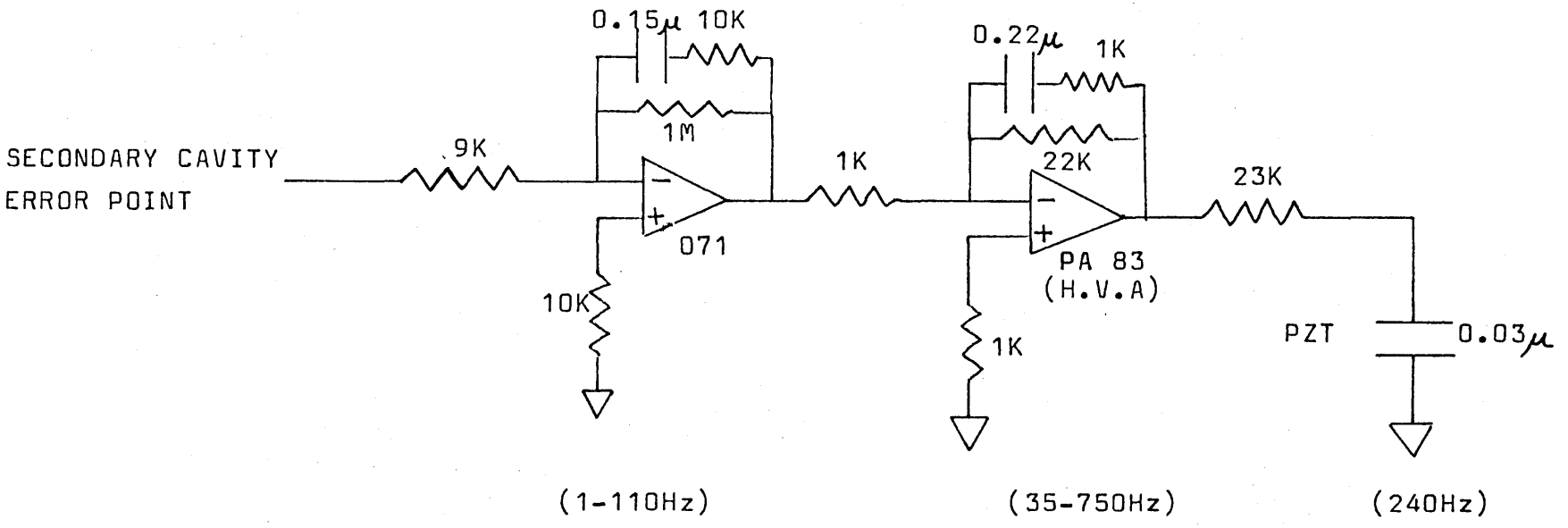

FIG.2.5: EARLY DRIVING CIRCUIT FOR SECONDARY CAVITY STABILISATION.

2.6 INITIAL DETECTOR PERFORMANCE.

Early in the operation of the rebuilt system, large oscillatory components were observed in the phase error signals from the cavity feedback loops. These oscillations were found to originate from the test mass orientation servos. Investigations revealed that certain resonant modes of the loudspeaker transducer wires could induce sympathetic resonances of the triangles from which the mass is suspended. As a result, the transducer wires were replaced by stiff, aluminium rods which eliminated noise from the longitudinal "violin modes" of the wires. The transverse resonances of the rod were then quenched by coating the triangle with damping compound, and loading it with a section of lead and rubber. These modifications improved the reliability of performance of the detector, particularly at low frequencies. A sensitivity spectrum of the detector, at this stage, is shown in figure 2.6. The spectrum indicated that the noise level was much reduced at low frequencies. However, the large number of peaks in the spectrum suggested that many of the noise problems were still of mechanical origin.

2.7 NOISE CONTRIBUTIONS FROM TEST MASS DESIGN.

2.7(a) END MASS MECHANICAL NOISE:

Noise due to the physical structure of a test mass may be excited by seismic and acoustic noise; and thermal excitation of the mass resonances may become important at

FIG.2.6: EARLY SPECTRUM OF THE DISPLACEMENT NOISE OF THE RECONSTRUCTED INTERFEROMETER, AS MEASURED BY THE MOTION OF THE SECONDARY CAVITY PZT MIRROR.

kilohertz frequencies.

To analyse the spectrum of mechanical noise from the test masses, one of the end masses was incorporated as part of an "optical bench" Michelson interferometer. Illuminated by light from a He-Ne laser, the PZT mirror of the test mass was driven by white noise. The beat signals produced on the output light of the Michelson interferometer were detected by a photodiode and Fourier analysed. Figure 2.7 shows the spectrum of noise produced by the experiment. The end mass was found to be resonant at many discrete frequencies over a large bandwidth covering much of the frequency band of interest. The most severe of these resonances are indicated in figure 2.7.

The first step, in the reduction of the effects of these resonances, was the introduction of a new design of test mass. The new end masses are made of aluminium ($m \sim 3kg$), and are almost spherical in design (diam. $\sim$ 18cm), with an almost pure resonant frequency of 20kHz. The front of the mass is machined flat to hold two (4cm diam.) PZT elements which are secured to the mass by epoxy resin. The two PZT elements are ceramic rings (Vernitron PZT-5H) placed in series. Each ring has an associated motion per volt of $6 \cdot 10^{-10}$ m/V which, when driven differentially, give the transducer a total motion of $1.2 \cdot 10^{-9}$ m/V. The cavity mirror is held against the PZT elements by an arrangement of 3 beryllium copper leaf-springs and a high viscosity vacuum grease. A hole bored through the centre of the sphere allows the beam to enter and leave the cavity. These masses are suspended in the same manner as described in

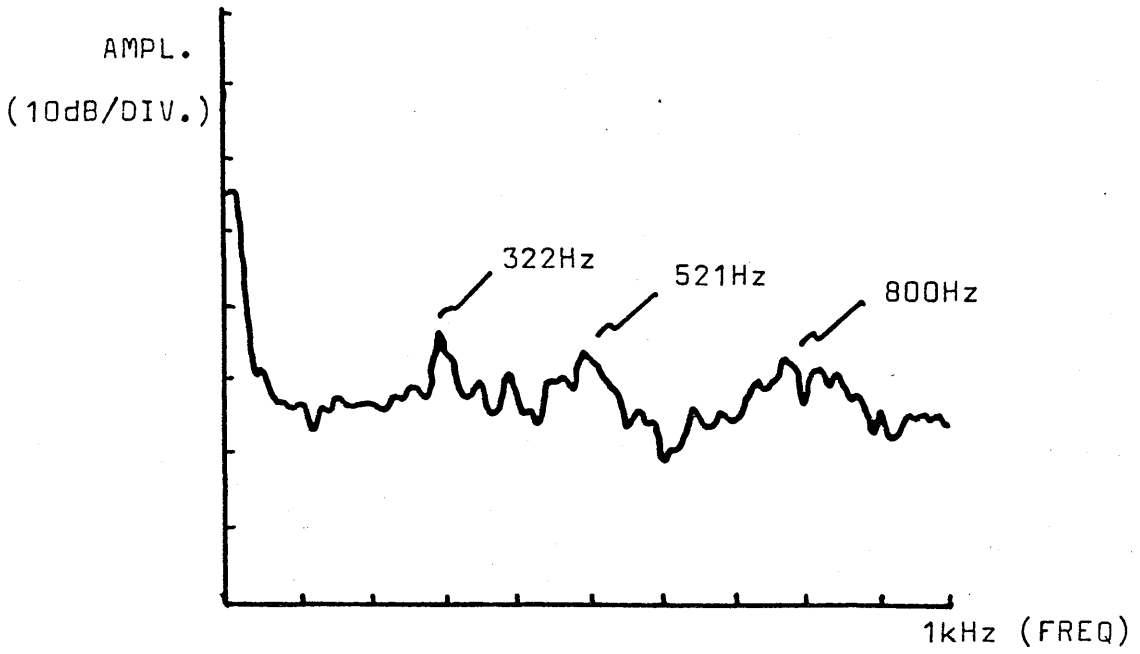

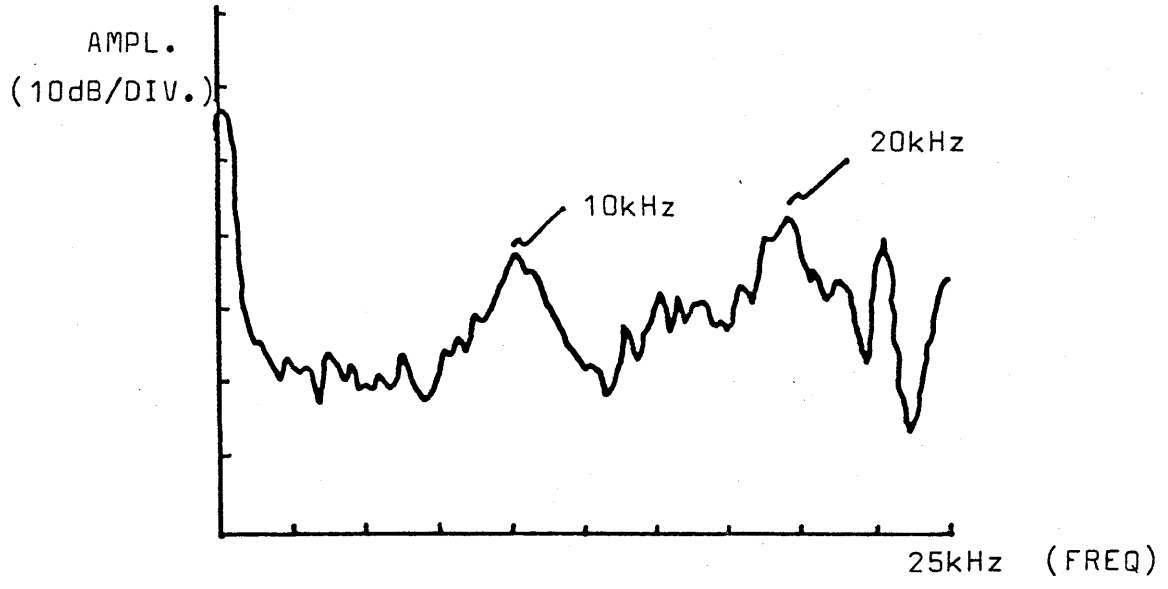

FIG.2.7: RESONANT STRUCTURE OF END MASS WHEN MECHANICALLY DRIVEN WITH WHITE NOISE.

section 2.5(b).

The resonant structure of the new mass was examined by the same method as the previous mass, and the Fourier spectrum of the mechanical noise is shown in figure 2.8(a). The spectrum is flat up to a first resonance at 20kHz, the fundamental mode of the sphere.

The quality factor of the new masses was examined by stabilising the laser to the primary cavity, and exciting the PZT of the mass. The resonant structure of the mass was discernable on the feedback volts to the laser intra-cavity modulator. The Fourier spectrum of noise associated with the test mass resonance is shown in figure 2.8(b). The resonance itself can be seen to be reasonably pure, although the dip occurring at the tip of the peak is indicative of the coupling of more than one mode. The Q of the test mass was measured by driving the PZT with a square wave and measuring the decay of the resonance on a fast storage oscilloscope. This resulted in a value of Q of ~ 200 which, although not particularly large, is sufficient to limit the coupling of thermal noise to around $\delta l \sim 10^{-19}$ m/$\sqrt{\text{Hz}}$. The Q of the mass is degraded in part by the supports which connect the leaf-springs to the mass, the addition of the piezoelectric transducer, and, possibly, by the introduction of the grease layer between the mirror and the PZT.

The performance of the detector, with the new end masses, is shown in the extended spectrum of figure 2.9. At low frequency ($\sim$ 200Hz) the displacement noise is two orders of magnitude better than had previously been

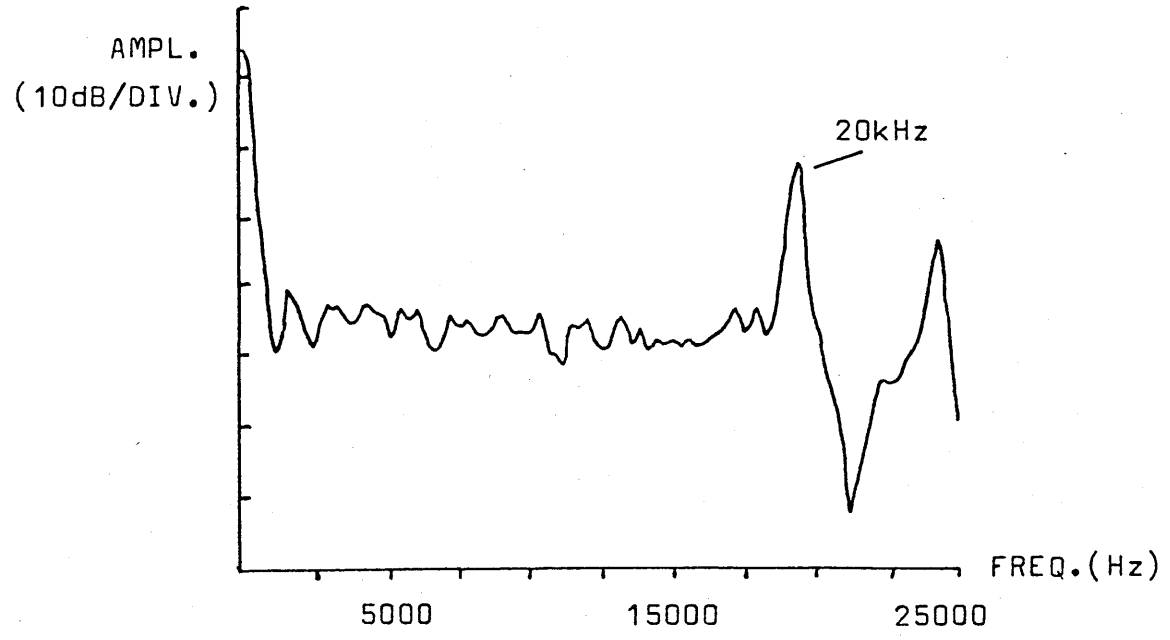

FIG.2.8(a): FOURIER SPECTRUM OF MECHANICAL NOISE OF NEW TEST MASS (c.f. FIG.2.7). NOTE THAT SPECTRUM IS ESSENTIALLY FLAT UP TO ~ 20kHz.

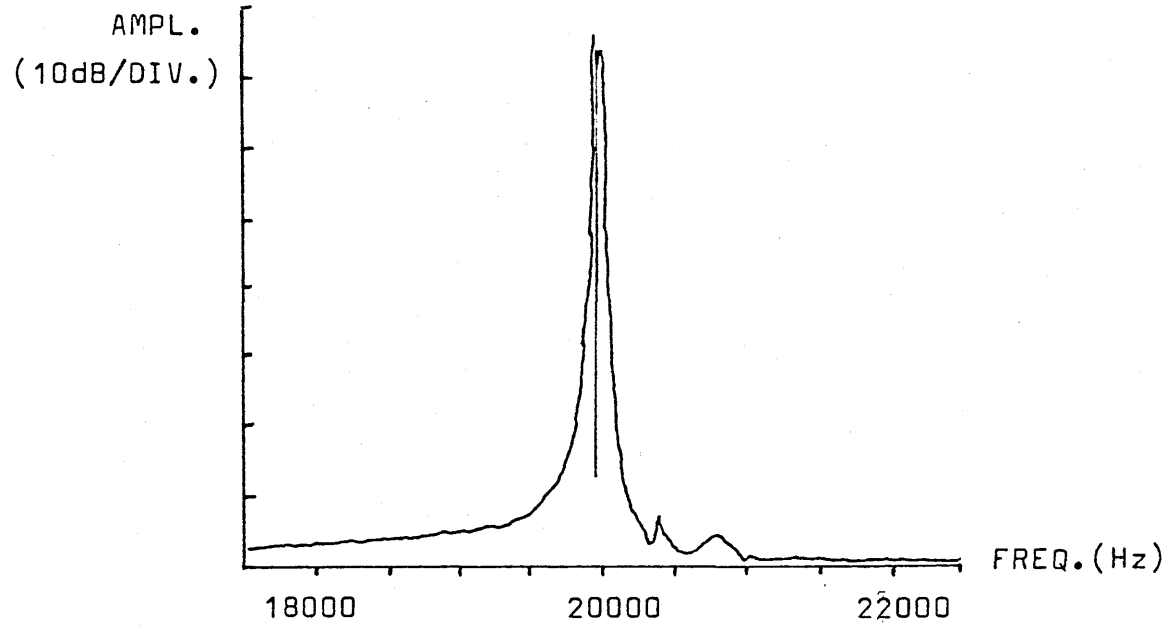

FIG.2.8(b): FOURIER SPECTRUM OF MECHANICAL NOISE AROUND THE TEST MASS RESONANCE. THE QUALITY FACTOR OF THE RESONANCE IS OF THE ORDER OF 200.

FIG.2.9: EXTENDED SPECTRUM OF THE SENSITIVITY OF THE INTERFEROMETER WITH THE NEW END MASSES INSTALLED.

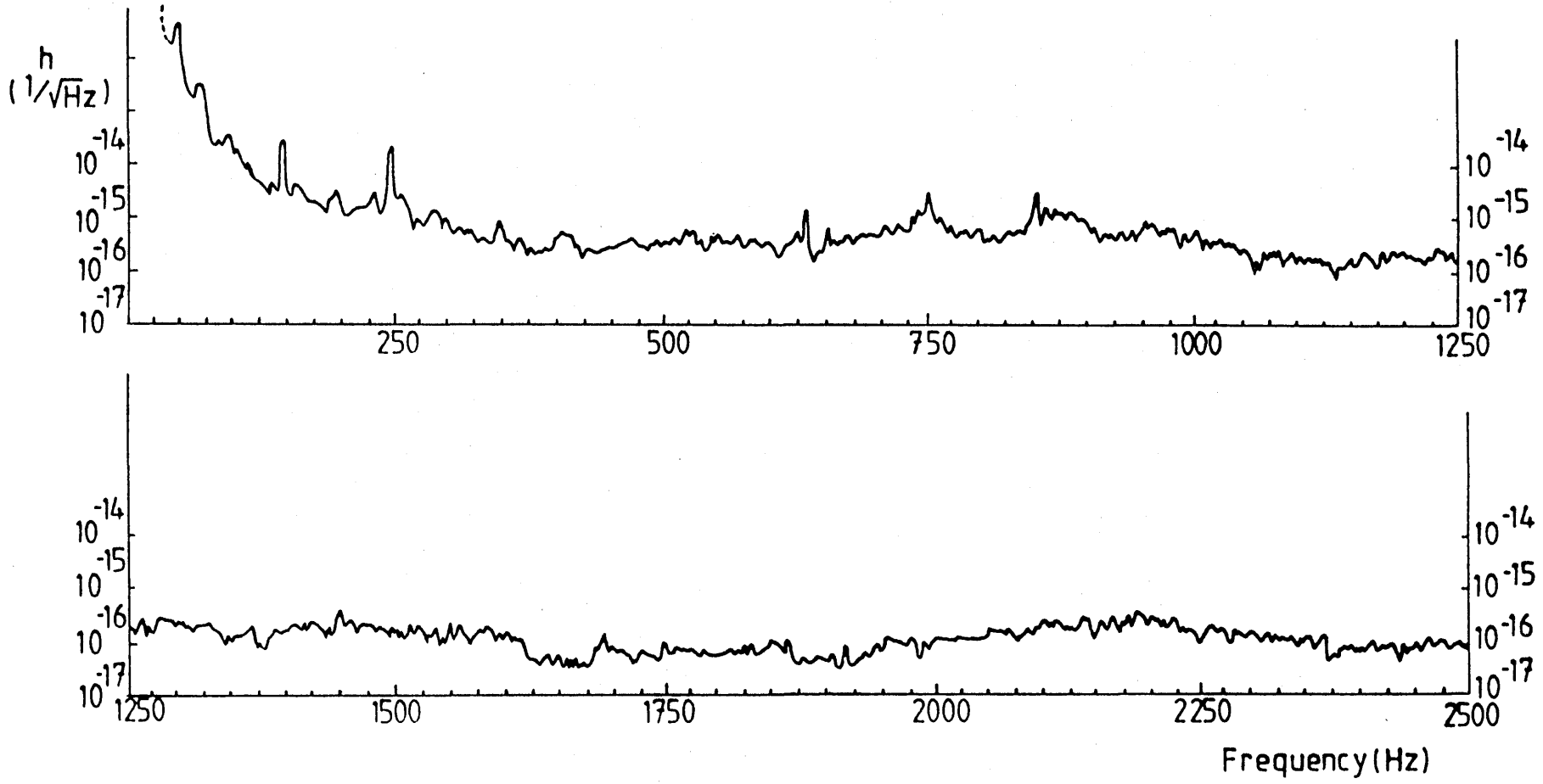

observed. Over a frequency band around 1.8kHz, the sensitivity is close to $3 \cdot 10^{-16}$ m/$\sqrt{\text{Hz}}$; - almost a factor of 10 better than previous results. With a visibility of $\sim 40\%$, and the small amount of light used in the cavity stabilisation ($\sim 300\,\mu$W), the limit due to shot noise, at this stage, would have been around $1 \cdot 10^{-16}$ m/$\sqrt{\text{Hz}}$.

2.7(b) CENTRAL MASS MECHANICAL NOISE.

With the improvements made to the end masses, it seemed reasonable to suppose that much of the remaining noise in the system was due to mechanical resonances of the central mass. To test for this, a PZT mirror, forming part of the unused mode-cleaning cavity on the top deck of the mass, was driven by white noise (to artificially excite these resonances), while monitoring the secondary cavity sensitivity signal. This experiment suggested that much of the dominant noise in the spectrum was due to excitation of these resonances. Figure 2.10 shows a superposition of two sensitivity spectra, with and without artificial excitation of the central mass. The similar structure in both, especially between 1.5 and 2kHz, is clearly significant. When looked at over a wide frequency range, the system reached the photon noise level at around 17kHz and above. Again it appeared that the excess noise below 17kHz was mainly due to mechanical resonances.

With the complicated design of the central mass, it was not surprising to find that it had resonances within this frequency band. Simplification of this mass, although desirable, is not particularly practicable. However, a way

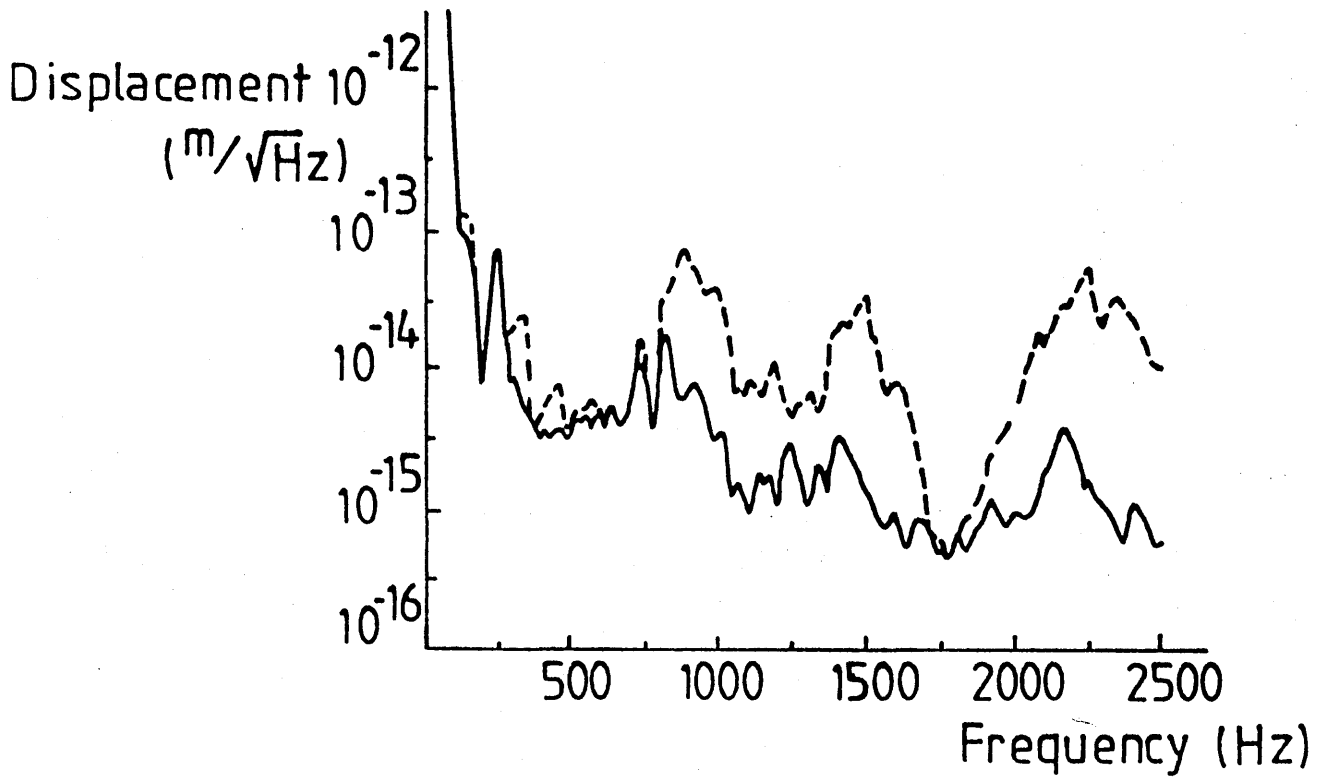

FIG.2.10: SPECTRUM OF THE DISPLACEMENT NOISE IN THE INTERFEROMETER. DOTTED TRACE IS WITH WHITE NOISE EXCITATION OF THE CENTRAL TEST MASS.

round the problem is to move each of the two central cavity mirrors onto its own separately suspended test mass of good quality factor and high internal resonant frequency. (Then the amount of noise induced by the central mass is no longer multiplied by the cavity finesse).

These extra masses were constructed with the same shape as the end masses but (due to space limitations of the central vacuum tank) are physically smaller (diam. $\sim$ 8cm). To compensate, somewhat, for their lack of size, they are made of a heavier material than the end masses (phosphor bronze) which has a similar Q to that of aluminium, and which gives them a mass of $\sim$ 2kg.

Suspended by an arrangement of 4 steel wires from a "crucifix" of aluminium, which is itself suspended by two wires from the main suspension point, the masses are unconstrained for horizontal motions along the cavity axis.

The sensing of the mass orientation is performed in the same manner as the end masses, but the feedback control is done differently. At each of the 4 points of the crucifix is located a 1cm diameter, rare-earth magnet, to which driving electromotive forces are applied from coils situated behind, and close to, the magnets. These can be clearly seen in the photograph of the central mass in plate 2.11.

By altering the current through the coils, the forces applied to the magnets changes, and thus the orientation of the mass change . Opposite points of the crucifix are driven differentially, and the set position of the masses may be altered by changing the mean level of current

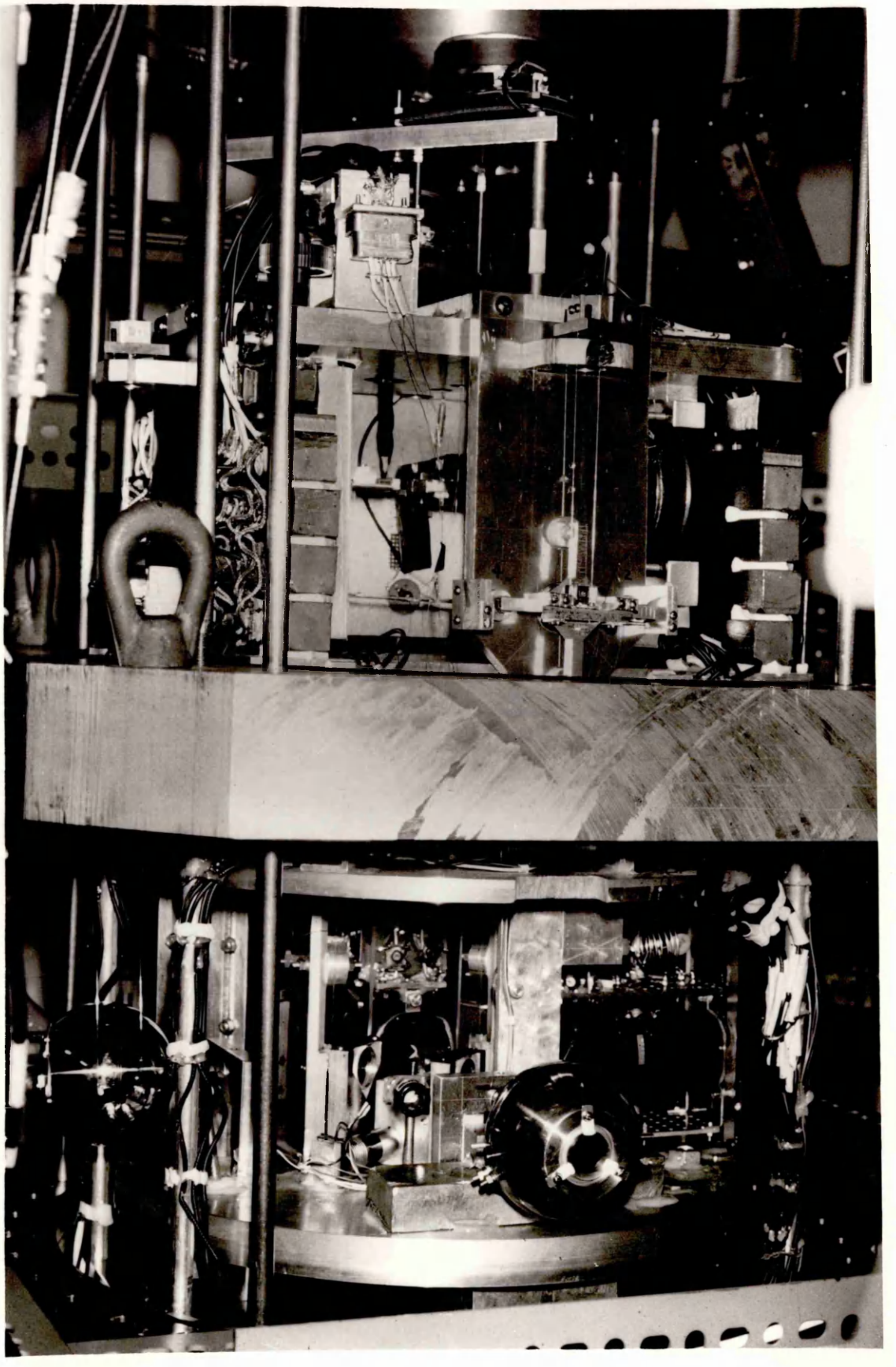

PLATE 2·11: THE CENTRAL MASS AREA OF THE INTERFEROMETER SHOWING THE SMALL SEPARATED TEST MASSES.

flowing in the coils. The pointing accuracy of these feedback controls is similar to those of the end masses. The centre of the crucifix is connected to a bimorph PZT for low frequency cavity damping. A schematic diagram of the interferometer, illustrating the new mass arrangement, is shown in figure 2.12.

The inclusion of these masses produced an immediate reduction in the level of displacement noise in the interferometer, as shown in the comparative spectra of figure 2.13. The sensitivity spectrum is now essentially flat at a level of 1.5×10^{-16} $m/\sqrt{Hz}$ from approximately 1 to 2.5kHz, and is close to the photon noise limit set by the small amount of laser power.

Subsequent measurements, with increased laser power, did not produce a further improvement in the sensitivity, at this stage, which suggested that the detector was not yet limited by photon noise.

Investigations of a variety of different noise source couplings indicated that the effect of laser noise was close to the base level of figure 2.13. One attack on this noise front involved the reconstruction of an argon laser, and is described in the following chapter.

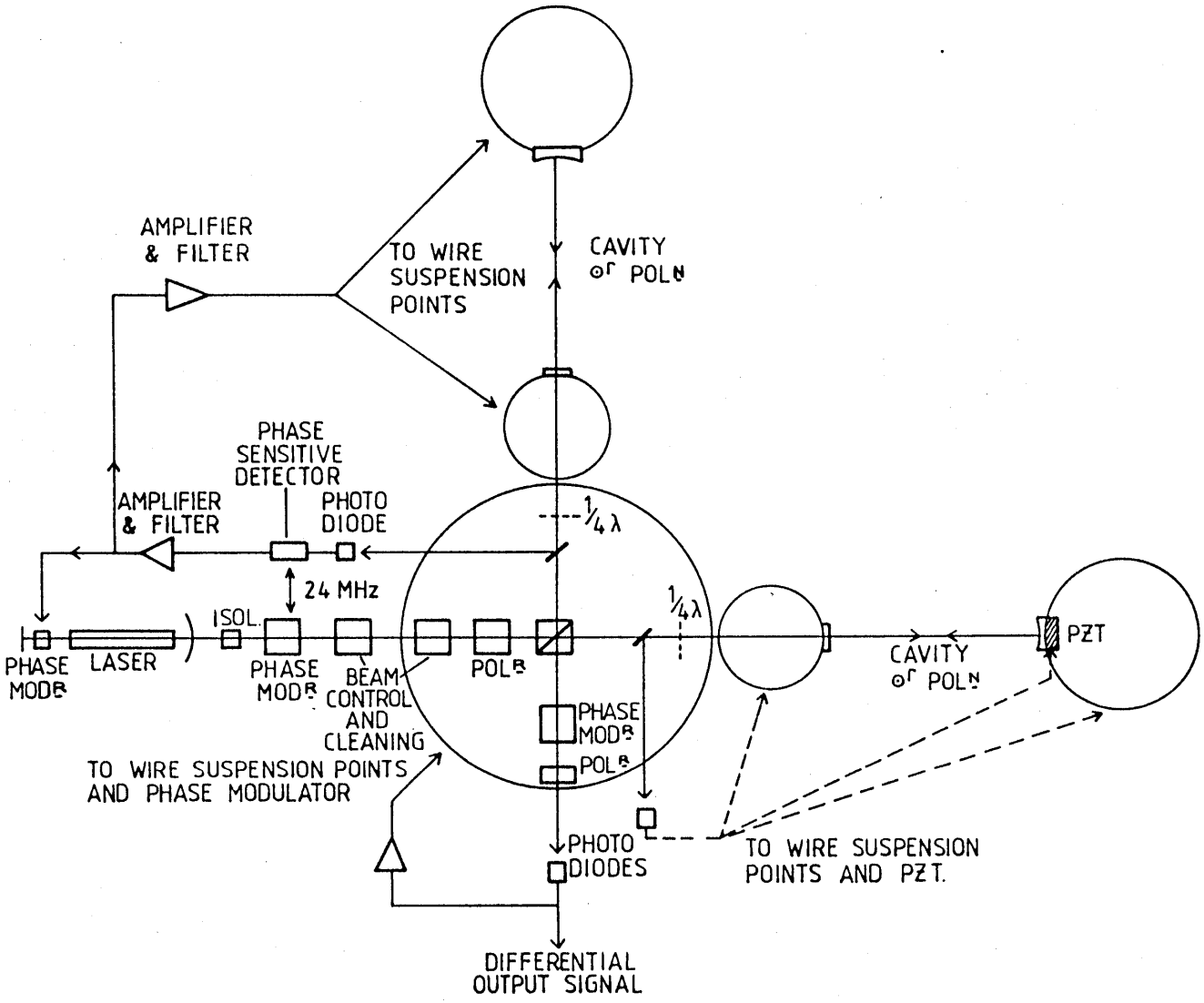

FIG.2.12: SCHEMATIC DIAGRAM OF THE INTERFEROMETER SHOWING THE SEPARATELY SUSPENDED CENTRAL TEST MASSES.

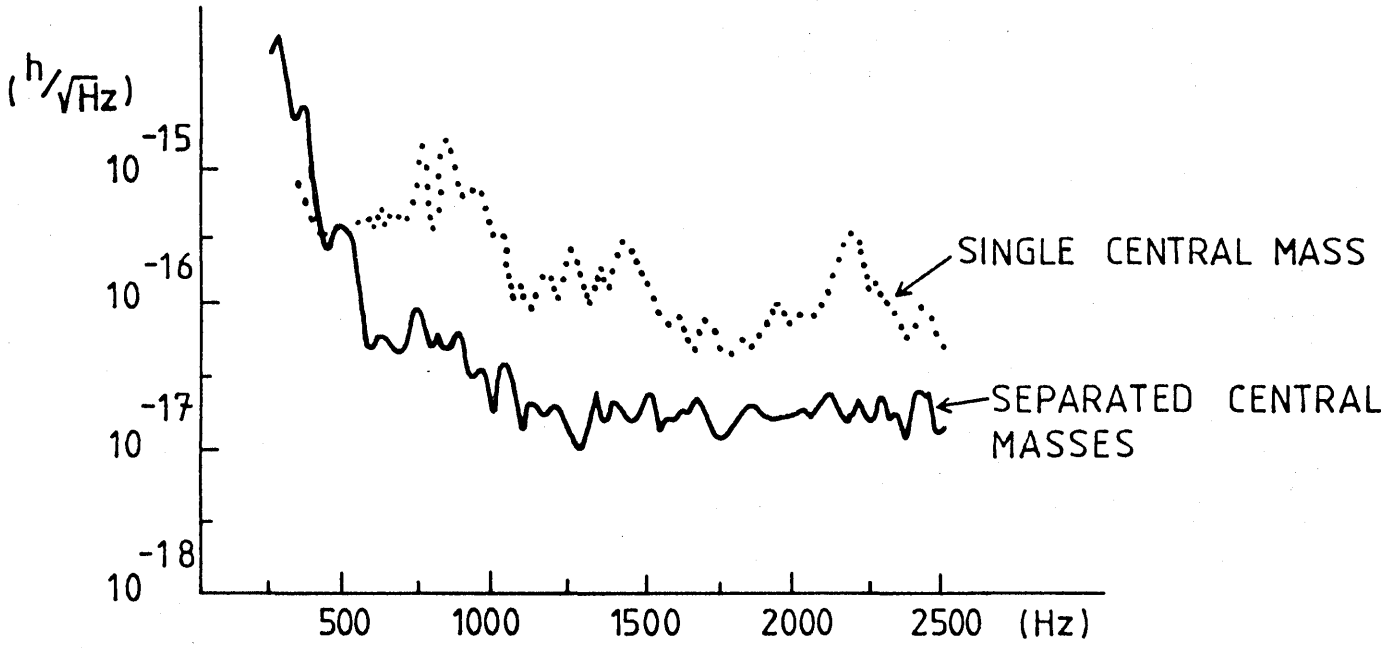

FIG.2.13: COMPARATIVE SPECTRA OF NOISE IN THE INTERFEROMETER BEFORE AND AFTER INCORPORATION OF SEPARATE TEST MASSES AT THE CENTRE OF THE SYSTEM.

CHAPTER 3.

"AN ARGON ION LASER INCORPORATING A SEPARATE CAVITY RESONATOR."

The previous chapter indicated that a high degree of short term stability is required, in the parameters of the laser light, in order to achieve a sensitivity for the detector which is limited only by shot noise in the light detected. Good stability performance is obtained by a combination of low intrinsic laser noise and high loop gain in the servo system used for stabilisation. Even with the most sophisticated electronic designs, the frequency stability demanded of the light requires gain factors which are extremely difficult to achieve. The reduction of the intrinsic laser noise of commercial lasers is, therefore, almost a prerequisite for good stabilisation.

The theoretical noise level of any laser is, ultimately, determined by the fact that the laser consists of a number of discrete particles interacting with the radiation field, and this interaction is governed by the laws of quantum electrodynamics. In addition, the atoms in the upper laser state are capable of de-exciting via spontaneous emission which is, in general, incoherent and thus subject to blackbody radiation statistics. In practice, however, any noise observed in the laser output is mainly due to macroscopic effects such as thermal changes, resonator instabilities, microphonics, and power supply noise.

3.1 PLASMA NOISE.

Plasma noise arises due to fluctuations, localised or otherwise, in the density of the plasma, both spatially and temporally, which can exist in the laser discharge (resulting in fluctuations in refractive index). This noise is introduced primarily through the laser power supply but is also partly due to temperature fluctuations and acoustic noise. The negative resistance characteristic of a glow discharge, plus the variation in impedance of the discharge as a function of pressure, make it possible for the discharge to amplify acoustic waves.[59] Plasma noise results in fluctuations of laser power, frequency, and beam geometry.

3.2 RESONATOR NOISE.

Short term frequency stability is mainly a function of mechanical and microphonic vibrations of the laser cavity. Two contributing sources of vibration are the turbulent cooling water flow and external acoustic noise in the laboratory. Vibrations of the laser cavity, as well as causing fluctuations in the frequency of the fundamental laser modes, induce contaminating higher order transverse modes (i.e. modes other than TEMoo) into the electric field distribution resulting in fluctuations of the position, orientation and shape of the laser beam. In addition, changes in the length of the laser cavity cause the longitudinal modes to shift in frequency within the

gain curve causing power fluctuations and more pronounced mode-hopping. Mode-beating can also occur between co-existing transverse modes if the laser is not running purely in the fundamental transverse mode.

For mirrors separated by optical path L, the frequency separation between neighbouring longitudinal modes is

$$\Delta\nu = \nu_{q+1} - \nu_q = (q+1)c/2L - qc/2L = c/2L. \qquad (3.1)$$

where c is the velocity of light in a vacuum. A frequency independent measure of the stability of a laser, which is useful for the comparison of the magnitudes of various noise sources, may be given by

$$S = \delta\nu/\nu . \qquad (3.2)$$

where $\delta\nu$ is the frequency band over which the optical output may fluctuate and ν is the centre frequency of the optical output.

Fig. 3.1 shows the construction of a typical argon ion laser. Argon lasers are particularly inefficient among modern lasers. The efficiency η of the conversion of electrical energy to optical energy is, at best, only 0.05%. This means for an output of 1 Watt it is necessary to put in the order of 2 kW, and nearly all of this must be dissipated on the walls of the plasma container which may be only $5cm^3$ in volume ($\sim$ 2.5mm bore diameter, 1m length). To remove the excess heat, cold water is circulated around the plasma tube. For a mainframe laser this waterflow is typically 23 litres/minute at a pressure of 3.5 kg/cm^2 (50 p.s.i). As a result of this, the plasma tube, and subsequently the cavity resonator, receive considerable

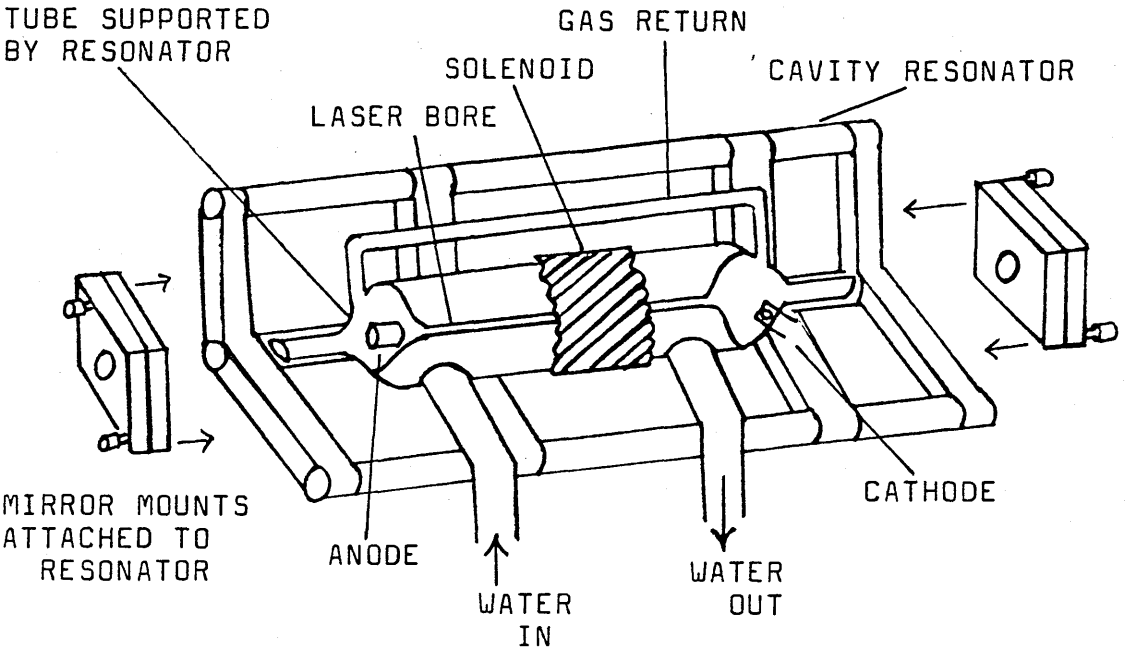

FIG.3.1: SCHEMATIC DIAGRAM OF A TYPICAL ARGON ION LASER. FREQUENCY STABILITY IS MAINLY DETERMINED BY THE STABILITY OF THE LASER CAVITY. WATER NOISE COUPLES IN BY EXCITATION OF THE CAVITY RESONATOR WHICH SUPPORTS THE PLASMA TUBE.

mechanical/acoustical excitation. This disturbance is transferred to the laser light.

It is difficult to reduce excitation of the lasing medium induced by the water flow but it can be seen that much improvement may result by decoupling the cavity resonator from the plasma tube. The following section outlines the reconstruction of a commercial argon ion laser - a Coherent CR18 model fitted with an Innova tube.

3.3 RESONATOR CONSTRUCTION.

Some improvement in frequency noise is obtainable by rigidly mounting the cavity mirrors to the optical table supporting the laser body (Billing et al 1979)[50]. Other experimenters have employed the idea of a separate cavity resonator.[60] In designing a laser cavity resonator consideration has to be given to certain features. The critical element in any resonator is the material used to separate the laser mirrors. It is desirable that this material has a high mechanical damping factor, a high degree of mechanical rigidity, and a low thermal expansion. A material often used to separate laser mirrors is Invar which has a thermal coefficient of expansion of 0.9×10^{-6}/K. However this material is magnetostrictive. Jaseja et al (1962)[61] have found a shift of 140kHz in the output of a He-Ne laser operating at 1.15 μm (i.e $S = 5 \times 10^{-10}$), caused by the Earths magnetic field. A field of 1 gauss can cause a shift of 2MHz in a He-Ne laser operating at 632.5nm. The high current densities necessary in an argon laser mean

that the laser power leads, which are necessarily close to the laser resonator, are likely contributors of stray magnetic fields. Invar, therefore, was rejected and fused silica, with a thermal expansion of less than $0.4 \cdot 10^{-6}/K$ and high mechanical rigidity, was the spacer material chosen.

It was decided to constuct the resonator with the mirrors separated by three silica rods, each 2.5 m long and 5cm in diameter. The mirrors were held on plates of aluminium at each end, and additional aluminium plates were used at intermediate points along the rods, to restrict the rod resonances. For a thermal drift of 1K the mirror separation would change by 10^{-6} m. This implies a long term frequency stability of better than 0.3 GHz/K (i.e. an upper limit of 5 longitudinal mode-hops per degree temperature change). As any hop in the mode of the laser would automatically knock a frequency stabilisation system out of lock, it is desirable to keep these to a minimum. Therefore, it was decided to mount the laser cavity mirrors on aluminium mounts of dimensions such that their thermal expansion would oppose that of the silica rods and so keep the length of the cavity as constant as possible.

A theoretical limit on laser frequency fluctuations is set by thermal oscillations of the silica rods separating the mirrors.[62] The excitation energy of each mode in the crystal lattice is given by

$$E_T = kT \qquad (3.3)$$

where k is Boltzmann's constant and T is the ambient temperature. Assuming elastic deformation, that is

$$E_T = \tfrac{1}{2} F_T . dl \qquad (3.4)$$

where F_T is the force the rod experiences due to thermal excitation of the lattice and dl is the associated change in the length of the rod.

$$\text{i.e } F_T = 2kT/dl \qquad (3.5)$$

Equating this force with the elastic restoring force of the rod results in

$$S = \delta\nu/\nu = dl/l = [\, 2kT/EV]^{1/2} \qquad (3.6)$$

where V is the volume of material in the rod, and E is Young's modulus of elasticity.

For the silica rods of the resonator, this sets a limit to S of 10^{-15}.(i.e a frequency fluctuation of 1 Hz. This corresponds to a relative motion of the two laser mirrors of $4 .10^{-15}$ m. It is apparent that the contribution of this noise source is relatively insignificant compared to acoustic and seismic noise effects on the resonator (-typical value of $\delta\nu$(mechanical) is > 1MHz).

A schematic diagram of the resonator arrangement is shown in fig. 3.2. The structure is supported at three points (on the clamping plates CP1 and CP3). The amount of deflection exerted on a single rod by endplates EP1 and EP2 is given by

$$\delta_{EP} = M_{EP}\, g l^3/9EI \qquad (3.7)$$

and for CP2 by

$$\delta_{CP} = M_{CP}\, g l^3/576EI \qquad (3.8)$$

where M_{EP} and M_{CP} are the masses of an endplate and clamping plate respectively, l is the distance from a supporting plate to the deflecting plate, g is the acceleration due to gravity, E is Young's modulus, and I is the second moment

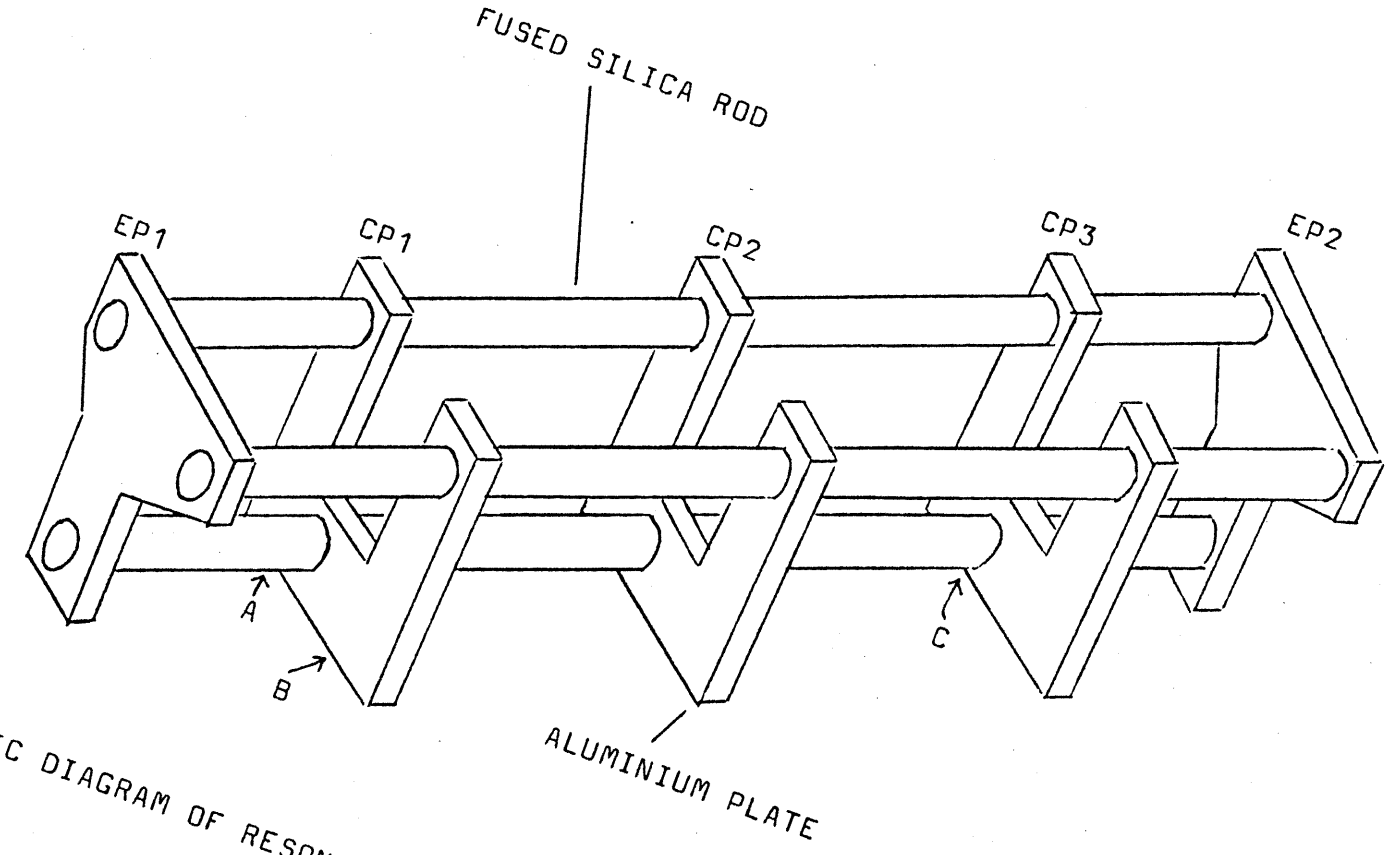

FIG.3.2: SCHEMATIC DIAGRAM OF RESONATOR STRUCTURE. (POINTS OF SUPPORT ARE INDICATED BY A, B AND C).

of area of the rod. (This assumes the masses of the plates are distributed evenly between the three rods). With the parameters of this resonator the amount of deflection is small ($\sim 10^{-5}$ m).

Similarly, the maximum stress induced by an endplate is given by

$$s_{MAX} = M_{EP}\, l\, \delta_{EP}/3I \qquad (3.9)$$

and for the central clamping plate by

$$s_{MAX} = M_{CP}\, l\, \delta_{EP}/24I \qquad (3.10)$$

These produce similar values of ~ 250 N/m^2 which is very small compared with the breaking stress of the rods ($s_B = 4 \cdot 10^7$ N/m^2).

Structural vibrations are easily coupled into the laser frequency making a significant contribution to $\delta\nu/\nu$. The resonant frequencies of the mechanical system have to be kept as high as possible. Since these are proportional to $(E/\rho)^{1/2}$, where ρ is the density of the rods, it is advantageous to have this ratio high. Of all available materials, silica has one of the highest E/ρ ratios.

The angular frequency of the first longitudinal resonance of a section of rod is given by

$$w_L = (\pi/l) \cdot [E/\rho]^{1/2} \qquad (3.11)$$

The intermediate clamping plates ensure that the first resonance is kept above 3 kHz.

The transverse resonances couple to the laser frequency only as a second order effect but are still of importance.[63] Transverse vibrations of a section of rod clamped at both ends have a fundamental resonance at an angular frequency given by

$$w_T = (4.73)^2 \cdot [E/\rho]^{1/2} \cdot [I/Al^4]^{1/2} \qquad (3.12)$$

where A is the cross-sectional area of the rod. This gives a lowest transverse resonance of the structure of $\sim$250 Hz.

Plate 3.3(a) shows the rebuilt argon ion laser. The aluminium endplates which hold the laser mirrors have much of their metal cut away to reduce the sensitivity of the resonator to acoustic noise. The laser mirrors, mounted on piezoelectric motion drives, are held in two-dimensional gimbal mounts. The rods are damped by coating them with a viscous damping compound (Duxseal) and lagging them with lead sheeting. They are then further isolated from acoustical excitation by wrapping them in a sandwiched polyurethane and lead combination (Soundmat LF).

The entire resonator rests on a massive optical table and is supported by three phosphor-bronze hemispheres, of 2cm diameter, located on the underside of the two outer clamping plates. To minimize the transfer of noise from the flow of cooling water to the resonator, which might occur via the optical table, the plasma tube (contained in the original laser body) is placed inside but not touching any elements of the resonator, resting on trays of lead shot. The lead shot serves to dissipate any excitation which might couple between the tube and the resonator.

Initial operation of the rebuilt laser led to the observation of air current noise. With the beam path partially open, inside the laser cavity, localised fluctuations in air currents alter the refractive index of the optical path resulting in large low frequency

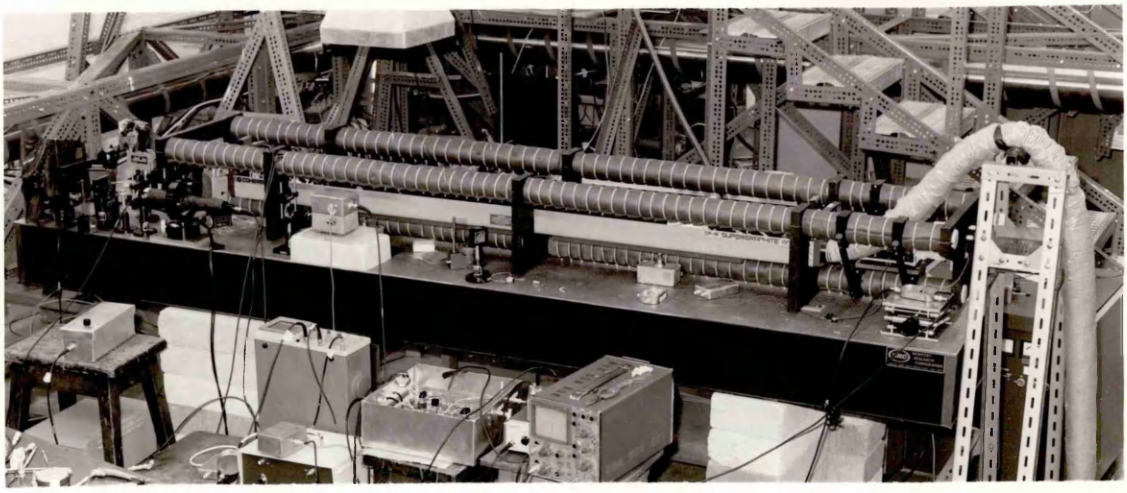

PLATE 3·3(a) : VIEW OF ARGON LASER
WITH REBUILT RESONATOR

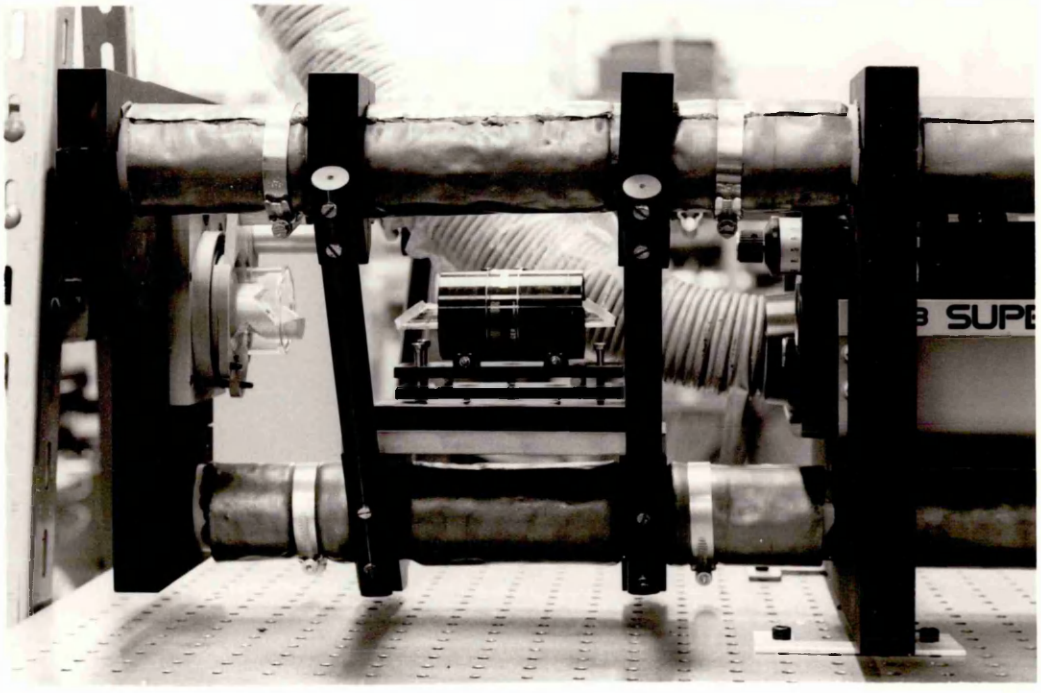

PLATE 3·3(b) : THE INTRA-CAVITY MODULATOR
ARRANGEMENT

fluctuations in frequency, intensity and direction of the laser beam. To overcome this, the beam paths are enclosed in glass tubing with a loose coupling of polythene film to minimise noise exchange between the discharge tube and resonator.

To facilitate the use of an intra-cavity device for frequency stabilisation, a supporting structure designed for this purpose is attached to part of the resonator. A kinematically designed aluminium table, which supports the modulator, is secured to the resonator by four laminate rods (Tufnol carp brand).This structure can be seen in plate 3.3(b).

3.4 SHORT TERM FREQUENCY STABILITY OF THE FREE-RUNNING ARGON LASER.

The frequency fluctuations of the free-running laser were obtained by frequency locking a tunable Fabry-Perot cavity to the laser and calibrating the measured control signal applied to the PZT transducer which tunes the cavity.

A schematic diagram of the experimental arrangement is shown in fig. 3.4. With the laser running with single frequency, the output of the Fabry-Perot cavity (monitored by photodiode 2) contains not only signals due to laser frequency fluctuations but also the laser intensity fluctuations which would normally mask these. The intensity signal is also monitored by photodiode 1, allowing the intensity noise component to be subtracted off by a low

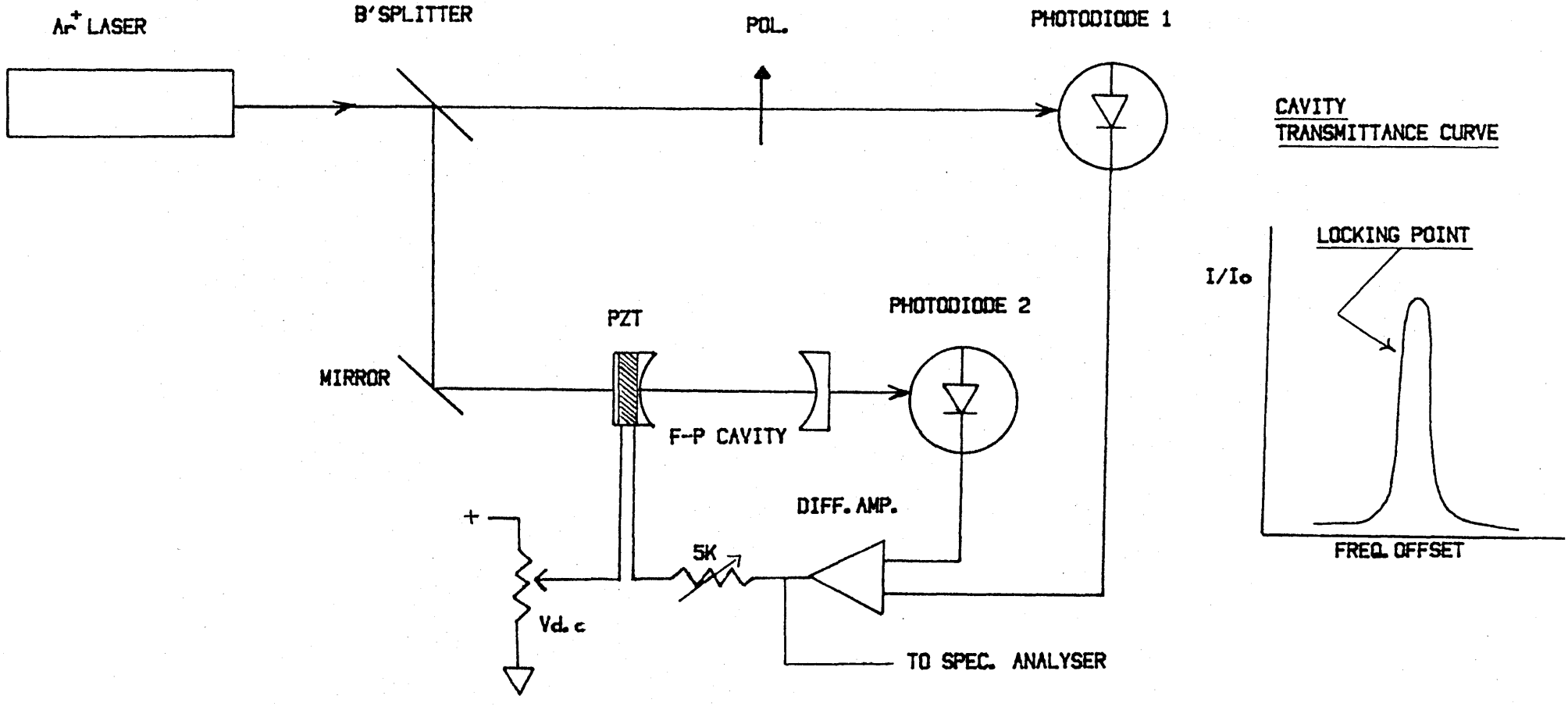

FIG. 3.4 SCHEMATIC DIAGRAM OF APPARATUS FOR MEASUREMENT OF FREQ. NOISE.

noise differential amplifier, (PAR 113), which has a common mode rejection of greater than 40dB over a bandwidth of several kilohertz. The light falling on photodiode 1 may be attenuated by a polariser, enabling a locking point to be chosen on the cavity's transmittance curve. The point on the curve with greatest gradient allows the maximum dynamic gain of the servo loop. Any slight changes in laser frequency, then, produce large changes in the intensity of the light transmitted by the cavity (which is only seen by photodiode 2). The signal from the differential amplifier is applied (with suitable amplification and filtering) to the tuning PZT of the Fabry-Perot cavity allowing it to "track" the laser frequency.

A variable d.c. voltage can also be applied to the PZT to enable the cavity to be tuned over its free spectral range onto a transmission fringe. With the cavity locked to the laser frequency, the signal fedback to the PZT is a true measure of the laser frequency noise provided the Fabry-Perot is not noisy.

The Fabry-Perot cavity - a commercial confocal cavity (Tropel 216) - has a free spectral range of 300MHz and a linewidth of 1.5MHz. The cavity has a first mechanical resonance at $\sim$ 5kHz and it was necessary to damp this with a 5kΩ potentiometer in series with the capacity of the PZT ($\sim$ 30nF) for optimum loop gain in the servo.

The improvement in frequency noise performance obtained with the new resonator is shown in fig. 3.5. As might be expected, most of the improvement is seen at low frequencies ($<$ 1kHz). The main peaks due to water induced

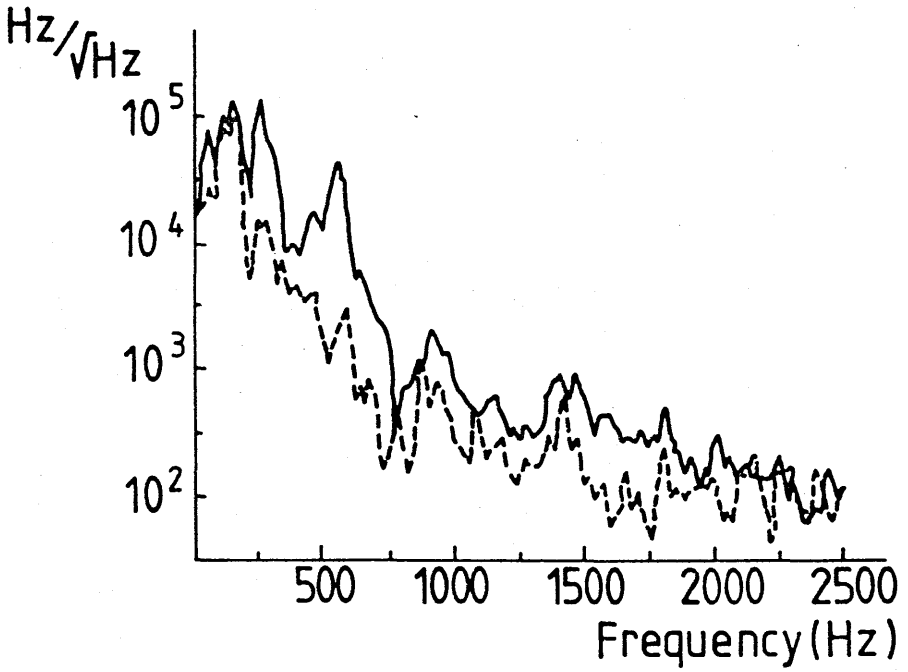

FIG.3.5: TYPICAL FOURIER SPECTRA OF NATURAL FREQUENCY FLUCTUATIONS OF LASER. (SOLID CURVE: TUBE IN STANDARD RESONATOR, AND DOTTED CURVE: TUBE IN SEPARATELY BUILT RESONATOR).

noise have been suppressed by factors approaching 25dB. Many of the other peaks are related to harmonics of the 50Hz mains power supply and are believed to be intrinsic to the laser.

3.5 DIRECTIONAL STABILITY OF THE FREE-RUNNING LASER.

The use of the reconstucted laser has also significantly reduced the fluctuations in laser beam geometry. A measure of the directional fluctuations of the light was obtained by measuring the beam displacement with a quadrant position-sensitive photodiode used in a differential mode to render insignificant the effect of laser intensity fluctuations.[50,52]

Fig. 3.6 shows the measuring method for positional fluctuations of the beam. This method is derived from the active beam stabilisation system developed at Glasgow.[52] Any motion of the laser beam induces changes in the difference current obtained from opposite quadrants of the photodiode. Fluctuations in two dimensions can then be monitored.

Following the notation of Meers et al,[52] the difference current for a measurement dx is given by

$$di = 2\eta P(t)dx/\pi w \qquad (3.13)$$

where η is the photodiode's efficiency of converting light power to current, w is the spot size of the beam, and P(t) is the laser power on the photodiode. The limit to detectable motion is set by shot noise in the diode current and this gives a minimum detectable displacement of

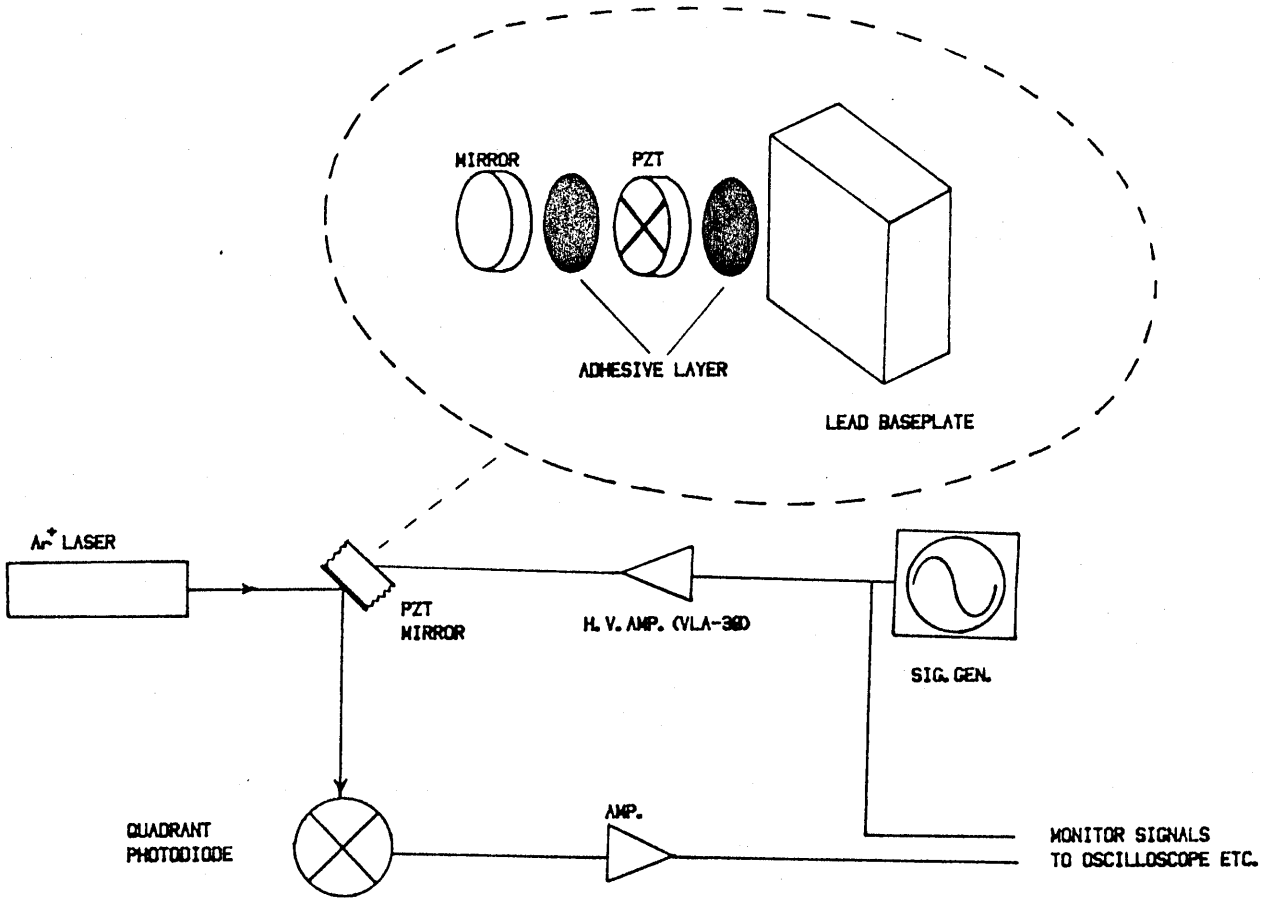

FIG 3.6. SCHEMATIC DIAGRAM OF APPARATUS FOR MEASUREMENT OF BEAM GEOM. FLUCTUATIONS SHOWING CONSTRUCTION OF PZT MIRROR.

$$dx(min) = \pi w(e/2P\eta)^{1/2} = \pi w(h\nu/2p\eta)^{1/2}$$
$$= \pi w(h\nu/2P\epsilon)^{1/2} . (\Delta f)^{1/2} \qquad (3.14)$$

where $\epsilon = (h\nu/e)\eta$ is the quantum efficiency of the photodiode, h is Planck's const., ν is the frequency of the light, and Δf is the observational bandwidth. For the parameters involved in this measurement dx(min) was the order of 10^{-11} $m/\sqrt{Hz}$ (using a power of a few milliwatts).

The analysed spectrum of the directional fluctuations was calibrated by using a piezoelectrically driven mirror in the path of the beam, to which was applied a sinusoidal signal of known amplitude. The construction of this mirror is also shown in fig.3.6. The piezoelectric element (Vernitron PZT-5H) is divided into four quadrants, and opposite quadrants may be driven differentially to allow an angular deflection to be induced in either dimension. For this measurement, however, it was sufficient to drive all elements together to produce a purely lateral translation.

A comparison of the directional fluctuations, with the original and rebuit resonators in use, is shown in fig.3.7. Again there is much improvement at low frequencies - approximately 20dB up to 1 kHz - and once more some of the peaks are related to the frequency of the mains power supply.

3.6 INTENSITY STABILITY OF THE FREE-RUNNING LASER.

The laser intensity spectrum is dominated by noise at the harmonics of 50Hz - the frequency of mains supply to

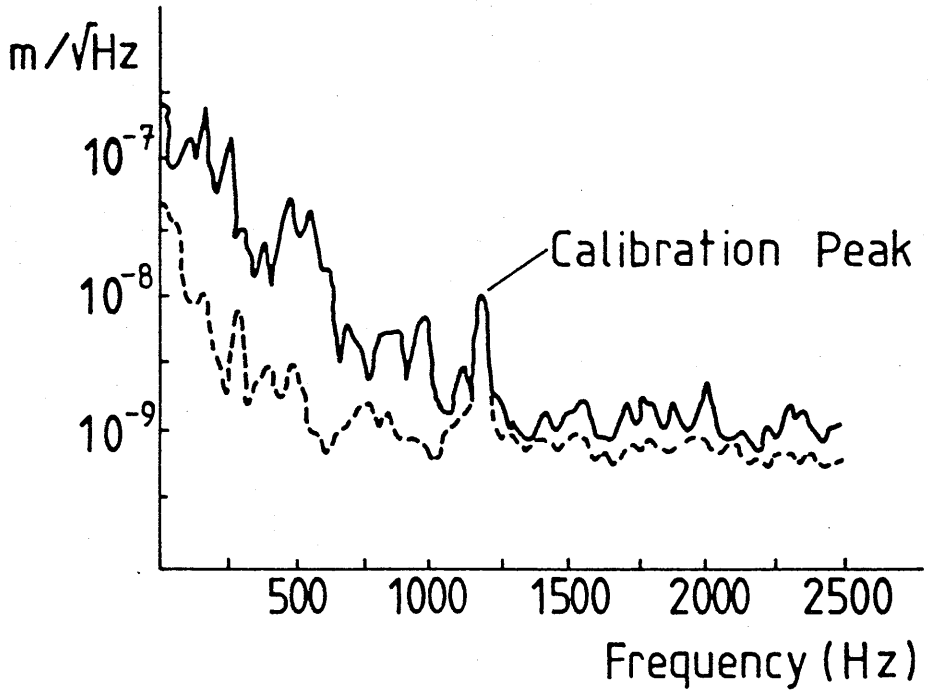

FIG.3.7: TYPICAL FOURIER SPECTRA OF POSITIONAL FLUCTUATIONS OF THE LASER BEAM (SPOT SIZE 10^{-3}m AT MEASURING POSITION). (SOLID CURVE: TUBE IN STANDARD RESONATOR, AND DOTTED CURVE: TUBE IN SEPARATELY BUILT RESONATOR).

the laser cathode. This is a common fault in most commercial, mainframe, argon lasers. As this noise is intrinsic to the laser, it is not reduced by the reconstuction of the resonator.

Several modifications to the laser power supply were made in an attempt to reduce the effects of switching transients. The most effective alterations were the insertion of extra smoothing capacitors on power rails, the magnetic shielding of the regulation circuits which control operation in current and light modes, and, most successfully, the installation of slower diodes in the rectifier circuits.

Fig.3.8 shows a comparison of fractional intensity noise spectra before and after the resonator and power supply modifications. Both spectra were measured with the laser running with similar operating parameters. The background level has dropped by more than 30dB, due in part to the new resonator, but it can be seen that the noise is still dominated by 50Hz harmonics which are visible 25dB above the background.

3.7 A SOUND-ATTENUATING LASER HOUSING.

As previously stated, the resonator rods are acoustically isolated by a polyurethane and lead covering. To further isolate the laser from laboratory noise, an enclosure, which completely covers the entire resonator, was constructed from perspex covered in the same material.

This housing attenuates the sound from laboratory

FIG.3.8: COMPARATIVE SPECTRA OF LASER INTENSITY NOISE.

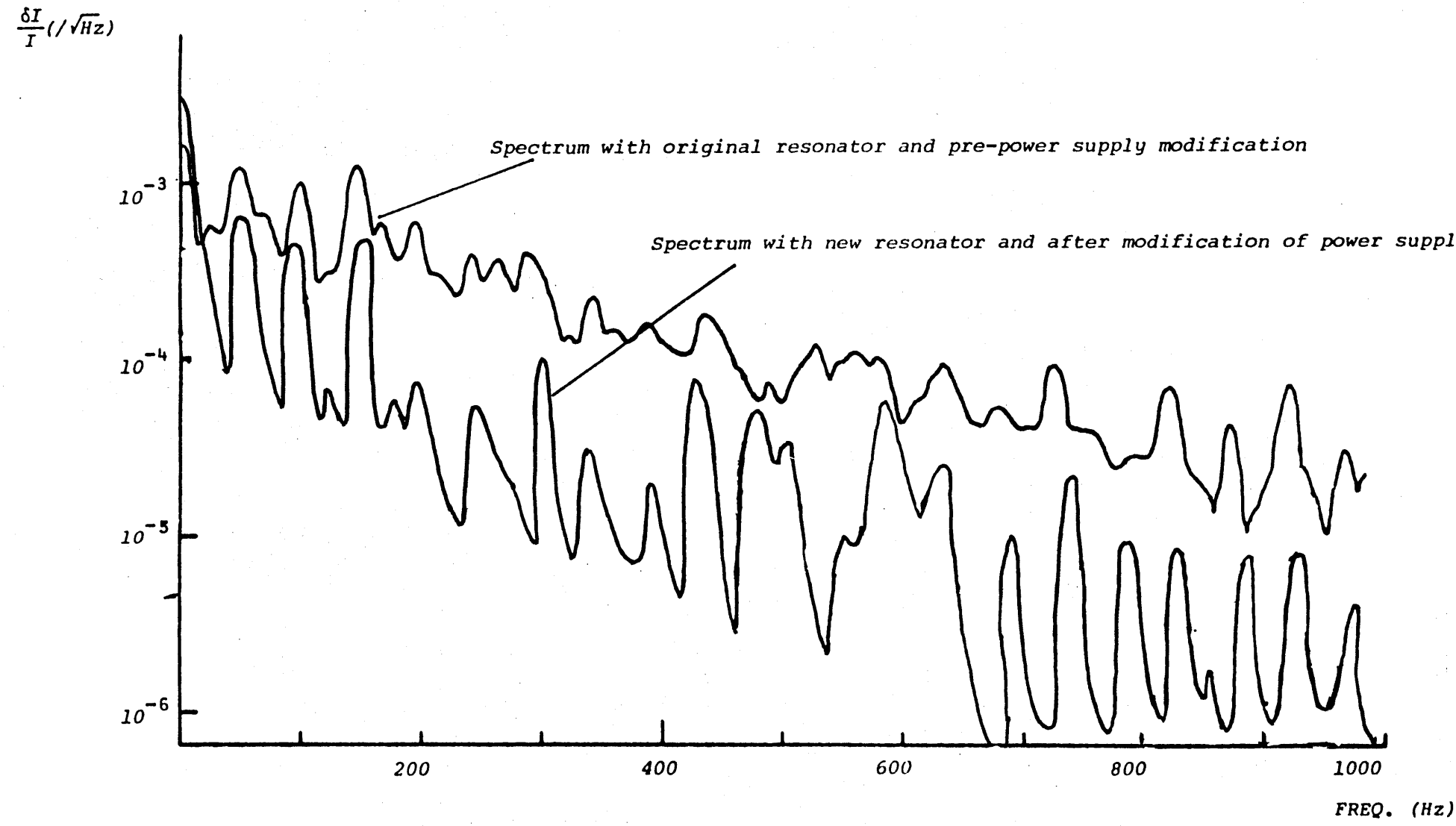

apparatus such as vacuum pumps which may contribute to laser noise, and is particularly useful for stopping sharp acoustical transients from disturbing the frequency lock of the laser when it is operated with the gravitational wave detector. The amount of acoustic isolation afforded by the box is shown in fig.3.9.

3.8 THE LIMIT TO INTRINSIC NOISE OF THE FREE-RUNNING LASER.

The inclusion of the acoustic housing for the laser meant that the amount of external acoustic coupling was small. To investigate the limiting contributions to the noise performance of the laser, the frequency fluctuations were studied in more detail.

The Tropel was locked to the laser as before and the pressure of the laser's circulating cooling water was gradually reduced. As low water pressure shortens the life of the plasma tube, the laser could only be run like this for a short time. Fig.3.10 shows the resulting frequency noise spectra. The reduction in the pressure of the water supply also reduces the residual laser frequency noise over most of the spectrum. As the laser resonator is effectively decoupled from the water noise, it seems likely that remaining noise is almost entirely due to excitation of the plasma tube. This would couple to the laser frequency in the following ways : (a) Physical deformation of the tube walls inducing pressure changes in the plasma (acoustic noise from the water being amplified by the plasma and causing pressure waves in the lasing medium).

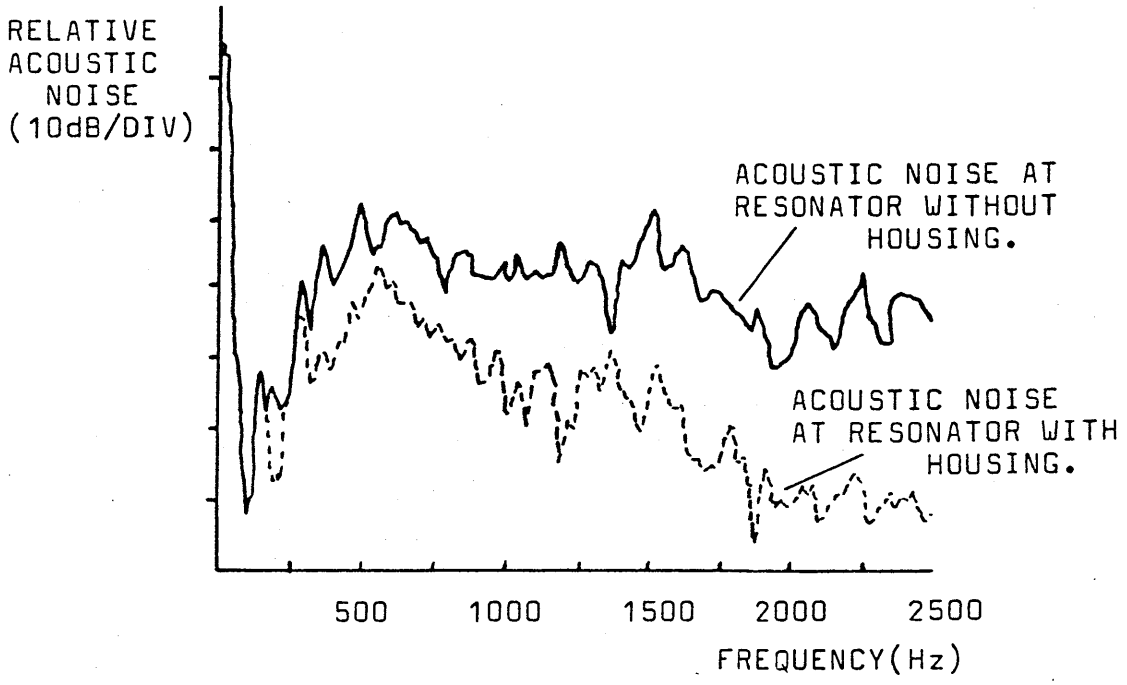

FIG.3.9: COMPARATIVE SPECTRA OF ACOUSTIC NOISE AT RESONATOR SHOWING ATTENUATION DUE TO HOUSING.

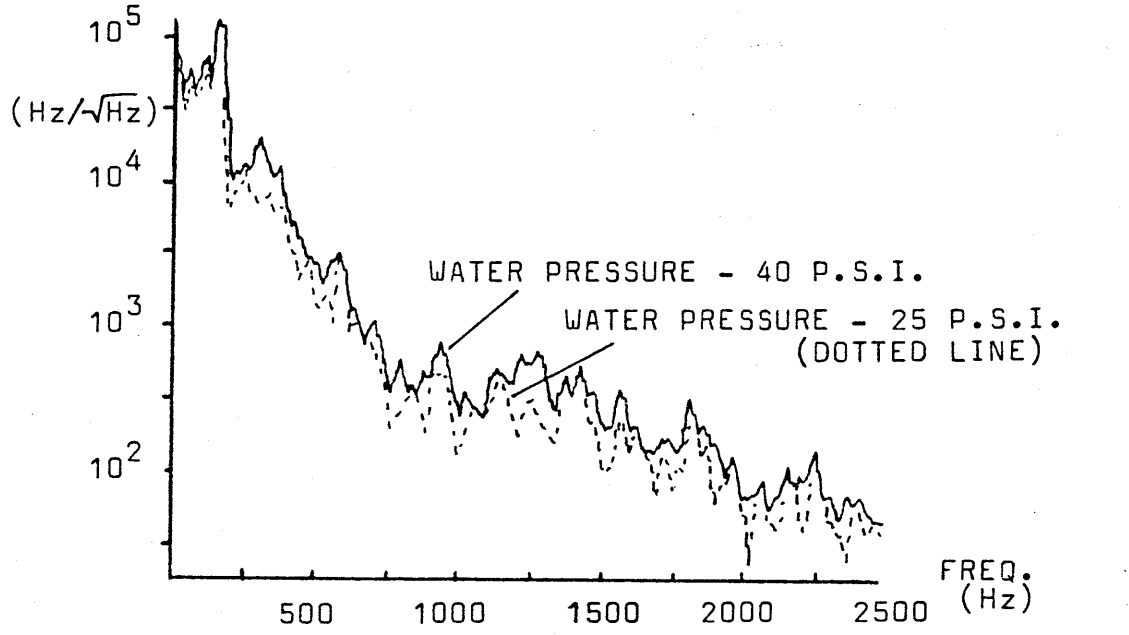

FIG.3.10: FREQUENCY NOISE OF LASER WHEN OPERATED WITH TWO DIFFERENT PRESSURES OF WATER COOLING.

(b) Excitation of the Brewster windows due to tube vibration and from the water-cooled collars which cover the windows. (c) Excitation of the intra-cavity etalon used to provide a single frequency output, and which is held in place in the original laser body.

It would seem difficult to alleviate this noise but some suggestions include mechanically damping the tube and the Brewster windows, and the introduction of trace detergents into the water circulation to "soften" the water. The noise contribution from the vibration of the etalon could probably be reduced by mounting it as part of the new resonator to isolate it from water noise. - (This is currently being undertaken).

3.9 CONCLUSION

The reconstruction of the argon laser significantly reduced the noise parameters of the laser and so provided an excellent base for the development of a new frequency stabilisation technique which will be discussed in chapter 5.

CHAPTER 4.

"LASER FREQUENCY STABILISATION."

4.1 INTRODUCTION.

Chapter 2 indicated that very high demands on the frequency stability of the illuminating laser light have to be met in order to realise the necessary sensitivity for a laser interferometer to be used as a gravitational wave detector. Chapter 3 showed the improvements that could be made with alterations to the laser resonator. This chapter deals with the active stabilisation of the laser frequency, and analyses the stabilisation scheme used at Glasgow.

As the frequency range of interest for gravitational waves lies around 1kHz, the required stabilisation scheme has to have highest performance in this region. Thus a factor such as long term stability, which is fundamentally important for aspects of metrology and spectroscopy, is not quite so important in this case.

4.2 METHODS OF FREQUENCY STABILISATION.

A laser may be stabilised by a feedback loop which makes use of an error signal derived from the laser itself, often using information provided by a modulation of the cavity length, or it can be derived from an external/internal reference cell which acts as a frequency discriminator. Three well established methods of frequency stabilisation will be briefly described here for purposes

of comparison and orientation.

4.2(a) SELF STABILISATION.

The most common method of self stabilising a laser is that used in most inhomogeneously broadened lasers such as helium-neon systems. These lasers have their lineshape broadened by Doppler effects in the plasma and exhibit the phenomenon of Lamb's Power Dip[64] in their output. The dip in laser power at Doppler centre frequency is usually 5-10% of the power, and up to 200MHz wide. The self stabilised laser holds the laser frequency to the centre of the dip.

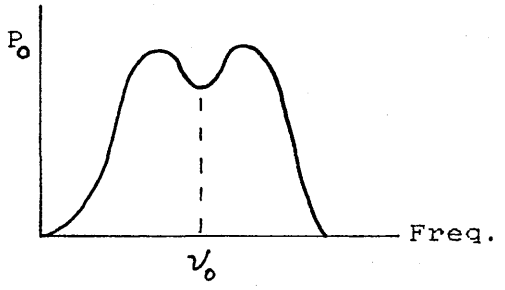

Fig.4.1 GAUSSIAN CURVE WITH LAMB DIP.

The method involves driving a PZT rear mirror with a modulating voltage such that the laser frequency varies by a small amount about ν_o. The ouput intensity is detected and compared with the original sweep signal by a phase sensitive detector (PSD) which gives an error signal, approximately equal to the derivative of the power curve,[65] which is then fed back to the PZT mirror to keep the frequency fixed at ν_o.

The advantages of this technique are its simplicity and ease of operation. Its disadvantages are that the laser is operated at slightly reduced power and, although it has reasonable performance for long term frequency drifts, it

is not good enough in short term stability for gravitational wave use. Also it has been shown that the operating frequency at the dip centre may be a function of discharge current under certain conditions.[66] This methods[1] main limitation to sensitivity lies in the width of the dip and its flatness near the centre.

4.2(b) FREQUENCY STABILISATION BY SATURATED ABSORPTION.

This technique involves placing inside the laser cavity a cell containing a molecular vapour (usually Iodine) which has an absorption line falling within the gain bandwidth of the laser.[67] The standing wave field inside the cavity produces a saturation of the absorption and a Lorentzian dip forms at the centre of the absorption line. This dip produces a corresponding increase in laser power as the frequency is tuned through it. The width of the dip is determined by the natural width of the line involved in the transition and not by the larger broadening effects of the laser (-similar to Lamb Dip in emission). An example of a stabilising loop for this type of scheme is shown below.

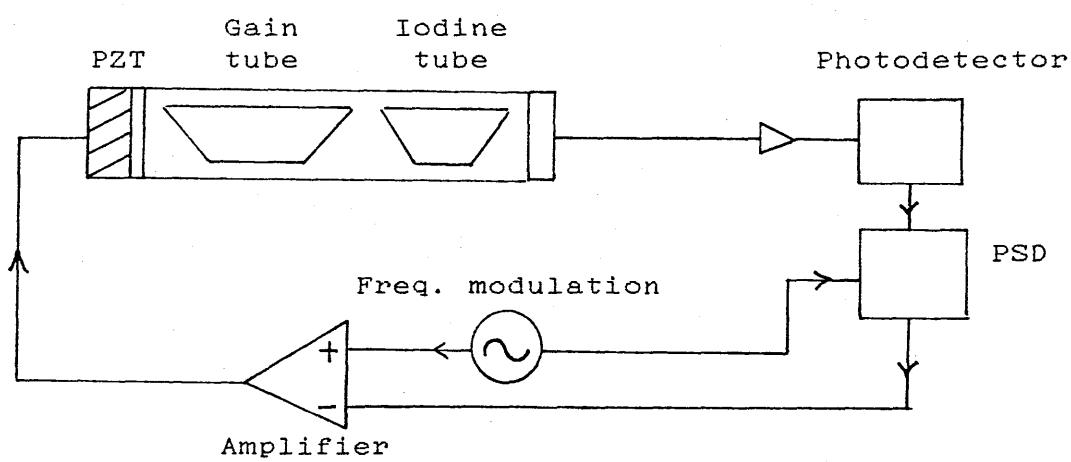

Fig 4.2 STABILISING LOOP FOR SATURATED ABSORPTION.

Again the main limitation to stability is imposed by the absorption linewidth which is typically $\sim$ 4MHz wide.

4.2(c) STABILISATION BY THE ZEEMAN EFFECT.

A technique first demonstrated by White[68], in 1964, involves the use of an external absorption cell in which a discharge is maintained. The application of an axial magnetic field to the discharge induces Zeeman splitting of the atomic levels, and the medium becomes dichroic for circularly polarised light. If light passing through the medium is right circularly polarised (RCP) it interacts with those atoms contributing to the low frequency absorption profile; if the light is left circularly polarised (LCP) it interacts with those of the high frequency profile. To convert the plane polarised laser output to circularly polarised light, a 1/4-wave plate electro-optic switch is used. This switch is modulated with a square wave, which changes the polarisation between left and right handed, and the resulting light output is phase sensitively detected with the modulation input to provide the error signal. The magnetic field does not affect the frequency of the light which remains close to ν_c (fig 4.3).

The servo loop used tries to stabilise as close to ν_c as possible. Response of a light detector situated beyond the absorption cell depends on the frequency shift due to the splitting. A change in the frequency from ν_c produces a change in the response. The separation of the absorption profiles can be $\sim$ 1GHz with a field of 350 gauss.

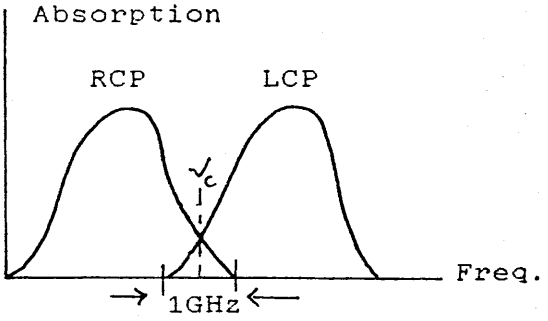

FIG. 4.3 DOUBLE ABSORPTION PROFILE PRODUCED BY ZEEMAN SPLITTING.

This technique has good long term stability but is poorer than the saturated absorption technique for short term fluctuations.

A method employed by Baer et al[69] involves applying an axial magnetic field to the laser medium itself to produce internal Zeeman splitting of the plasma, thus removing the need for an external cell.

Most work on the above schemes have taken place involving helium-neon lasers and table 4.4 shows some typical performance levels for these lasers.

A measure of the frequency stability, which may be calculated from the spectral density of the frequency fluctuations, is given by the Allan variance relationship,[70]

$$\sigma^2(\tau) = 2 \int_0^\infty \frac{S(f)}{\nu_0^2} \left(\frac{\sin^2 \pi f t}{\pi f t} \right)^2 . \, df \qquad (4.1)$$

where τ is the sampling time, S(f) is the power spectral density of the frequency fluctuations, and ν_0 is the mean optical frequency. This relationship is used to produce some of the comparitive statistics of table 4.4.

The unstabilised linewidth of a He-Ne laser is naturally narrower than that of argon lasers and so the levels of performance, indicated in table 4.4, are, in general, more difficult to achieve for an argon laser.

TABLE 4.4: SOME TYPICAL VALUES OF FREQUENCY STABILITY (ALLAN VARIANCE) FOR THREE STANDARD STABILISATION TECHNIQUES INVOLVING HELIUM-NEON LASERS OPERATING AT 633nm. [67, 69, 90]

LAMB DIP STABILISATION:

$\sigma \sim 10^{-8}$ for an averaging time $\tau \sim 10^{2}$s

(-Tends to free-running value at $\tau < 10^{-1}$s.)

STABILISATION BY ZEEMAN EFFECT:

σ	$5 \cdot 10^{-10}$	$2 \cdot 10^{-10}$	$5 \cdot 10^{-11}$
τ(s)	1	10	10^{2}

(-Tends to free-running value as $\tau \rightarrow 10^{-3}$s.)

STABILISATION BY SATURATED ABSORPTION OF IODINE^{127}:

σ	$2 \cdot 10^{-10}$ *	$1 \cdot 10^{-10}$	$3 \cdot 10^{-11}$	$1 \cdot 10^{-11}$	$3 \cdot 10^{-12}$	$1 \cdot 10^{-12}$
τ(s)	10^{-3}	10^{-2}	10^{-1}	1	10	10^{2}

* This would correspond to a fractional frequency deviation at 1kHz of $\frac{\delta\nu}{\nu} \sim 8 \cdot 10^{-10}/\sqrt{\text{Hz}}$.

REFLECTION LOCKING VERSUS SIDE-LOCKING.

Up until recently, stabilisation of lasers to cavities has mainly been carried out by locking the laser frequency to the side of the Fabry-Perot transmittance curve. The precise frequency stability required by gravitational wave detectors led to the introduction of a more flexible method which allows a greater stabilisation bandwidth to be used. This technique uses reflected light from the cavities combined with r.f. modulation of the input light. As indicated in the analysis of the reflection locking scheme (sect. 4.3), at frequencies above the cavity linewidth the transfer function has a gradient of around 6dB per octave. This is due to the fact that the reflected field signal is a modulated amplitude signal. With the side-lock technique, the locking signal used is that of the derivative of the intensity transmittance profile of the cavity which has a gradient of around 12db per octave at frequencies above the cavity linewidth and which, in practice, restricts the unity gain point of the servo loop to below this frequency. The possible bandwidth obtainable with the reflection locking technique can be up to twice the frequency of the phase modulation (see figure 5.4).

For a gravitational wave strain sensitivity of $\delta l/l \sim 10^{-21}/\sqrt{Hz}$, a laser frequency stability of $\Delta\nu/\nu \sim 10^{-21}/\sqrt{Hz}$, around the frequency range of observation, should be aimed for. Some shortfall in this can be made up by balancing the response of the cavites to give some common mode rejection of frequency fluctuations (see chapter 6).

4.3 STABILISATION BY THE REFLECTION LOCKING TECHNIQUE.

It is apparent that a common element in all frequency stabilisation methods is the use of an additional profile, of fixed linewidth, to which the frequency of the laser is stabilised. In general it is desirable to have this additional linewidth as narrow as possible to increase the signal to noise ratio. The introduction of narrow linewidth Fabry-Perot cavities[71] as the reference cell gave rise to a new technique which locks to the side of a cavity transmission fringe. However, the potential gain, that might have been expected of this technique, was restricted by its experimental limitations.[72] This will be expounded upon later.

The limitations of standard methods, such as those described above, led to the development of a new technique which uses the reflection signal derived from an external resonant optical cavity as the stabilising reference signal.[73] This was initially suggested by R.W.P. Drever and is similar to a related microwave technique used by R.V. Pound.[74] The advantages, in signal to noise ratio

terms, become apparent when considering reference linewidths of better than 500kHz. The narrowness of the linewidth does not inhibit the bandwidth of the servo loop, as it does with stabilisation to a cavity in transmission mode.

The technique itself involves putting phase modulation, at radio frequencies, onto the laser light, such that the frequency modulated (FM) sidebands produced lie far outside the linewidth of the reference cavity. Light reflected back from the cavity interferes with light that has been reflected directly from the input mirror of the cavity, producing an amplitude modulated beat signal that is proportional to the phase deviations of the output laser light from that which resonates in the reference cavity. The following analysis, which explores the sensitivity of a Fabry-Perot cavity to frequency fluctuations, will reveal this in detail.

Consider the amplitude field of light reflected from a cavity such as that in fig. 4.5.

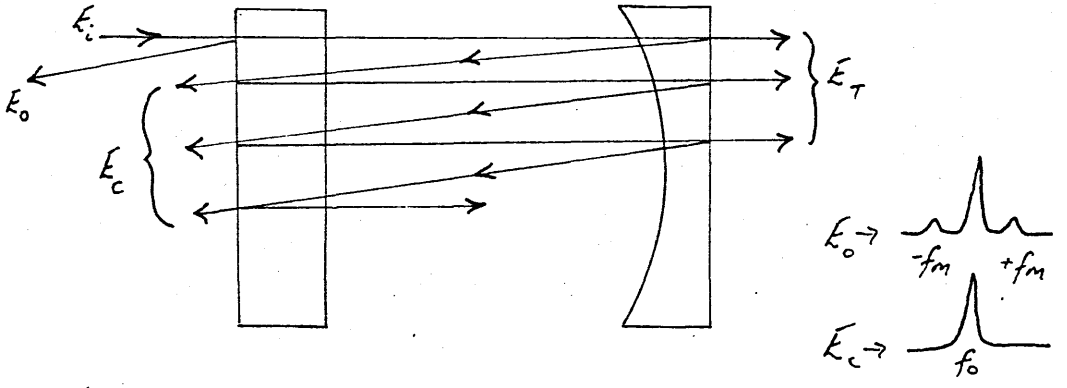

FIG 4.5 SCHEMATIC DIAGRAM OF LIGHT FIELD REFLECTED FROM AN OPTICAL RESONATOR. THE COMPONENT E_c EMERGING FROM THE CAVITY HAS LOST ITS FM SIDEBANDS.

The light can be considered to be made up of two components: E_0 , the light reflected directly from the front mirror, and E_C , the light emerging from the cavity. It is convenient to treat E_C as the superposition of the fields emitted from the cavity on each traversal.

$$E_C = E_1 + E_2 + E_3 + \ldots\ldots + E_N + \ldots\ldots \qquad (4.2)$$

If the incident field has the form $E_i = A_i e^{i\omega t}$ then

$$E_0 = A_i r_1 e^{i\omega t} \quad ; \quad E_N = -A_i t_1^2 r_2 (r_1 r_2)^{N-1} e^{i(\omega t + \phi_N)} \qquad (4.3a;b)$$

where ϕ_N is the phase of E_N and r_1 , t_1 and r_2 , t_2 are the reflection and transmission coefficients of the input and output mirrors respectively. Thus the total field is

$$E_R = E_0 + \sum_{N=1}^{\infty} E_N \ . \qquad (4.4)$$

Without loss of generality, consider only one fourier component of the noise spectrum of the light with angular frequency ω_n and amplitude $\Delta\omega$. Thus,

$$\omega = \omega_0 + \Delta\omega \sin \omega_n t \qquad (4.5)$$

The phase is then the integral of ω,

$$\phi = \omega_0 t - (\Delta\omega/\omega_n) \cos \omega_n t. \qquad (4.6)$$

If the cavity induces a phase offset δ each double-pass then after N double passes

$$\phi_N = N\delta + (\Delta\omega/\omega_n) \cos (\omega_n t + N\eta) \qquad (4.7)$$

where $\eta = 2l\omega_n/c$.

[Note that t here is travel time outside cavity and does not include cavity storage time which is part of $N\eta$.]

If the incident light is phase modulated at an angular frequency ω_m, then E may be described as

$$E_i = A_i e^{i\omega t} \cdot e^{i\phi_0 \sin\omega_m t}, \qquad (4.8)$$

where ϕ_0 is the index of modulation. Now $\exp(i\phi_0 \sin\omega_m t)$

may be expanded in terms of Bessel's functions of the first kind.

$$\exp(i\phi_0 \sin\omega_m t) = [J_0(\phi_0) + 2J_2(\phi_0)\cos 2\omega_m t + 2J_4(\phi_0)\cos 4\omega_m t + \ldots\ldots\ldots] + i[2J_1(\phi_0)\sin\omega_m t + 2J_3(\phi_0)\sin 3\omega_m t + 2J_5(\phi_0)\sin 5\omega_m t + \ldots\ldots\ldots] \quad (4.9)$$

If ϕ_0 is small then almost all the energy is distributed at the carrier frequency and the frequency of the first two sidebands.

i.e. $$\exp(i\phi_0 \sin\omega_m t) \simeq J_0(\phi_0) + 2iJ_1(\phi_0)\sin\omega_m t \quad (4.10)$$

So, $$E_0 = r_1 A_i \,\mathrm{expi}\{\omega_0 t - (\Delta\omega/\omega_n)\cos\omega_n t + \phi_0 \sin\omega_m t\} \quad (4.11)$$

As $(-\Delta\omega/\omega_n)\cos\omega_n t \ll 1$,

$$\mathrm{expi}\{-(\Delta\omega/\omega_n)\cos\omega_n t\} \simeq 1 - i(\Delta\omega/\omega_n)\cos\omega_n t \quad (4.12)$$

i.e. $$E_0 = r_1 A_i \,\mathrm{expi}(\omega_0 t + \phi_0 \sin\omega_m t).\ \{1 - i(\Delta\omega/\omega_n)\cos\omega_n t\} \quad (4.13)$$

The frequency of the phase modulation of the light is such that $\omega_m \ll \omega_c$, where $\omega_c = 2\pi\nu_c$ and ν_c is the free spectral range of the cavity. Thus the r.f. sidebands are almost totally reflected from the cavity. The emerging cavity field can then be written

$$E_c = -A_i t_1^2 r_2 e^{i\omega_0 t} J_0(\phi_0) \sum_{N=1}^{\infty} [(r_1 r_2)^{N-1} e^{iN\delta} \cdot \mathrm{expi}\{-(\Delta\omega/\omega_n)\cos(\omega_n t + N\eta)\}] \quad (4.14)$$

(Note that E_c is 180° out of phase with E_0).

The last exponential can again be expanded to the first two terms. And with the cosine expressed in exponential form, this gives

$$E_c = -A_i t_1^2 r_2 e^{i\omega_0 t} J_0(\phi_0) \left[\left(\frac{e^{i\delta}}{1-r_1 r_2 e^{i\delta}} \right) -i(\Delta\omega/\omega_n) \left(\frac{e^{i\omega_n t} . e^{i(\delta+\eta)}}{1-r_1 r_2 e^{i(\delta+\eta)}} + \frac{e^{-i\omega_n t} . e^{i(\delta-\eta)}}{1-r_1 r_2 e^{i(\delta-\eta)}} \right) \right] \qquad (4.15)$$

Defining coefficient of finesse,

$$F' = 4r_1 r_2/(1-r_1 r_2)^2 = 4F^2/\pi^2 \qquad (4.16)$$

where F is the cavity finesse, which is the ratio of the free spectral range to the cavity linewidth ($=\nu_c/\nu_{min}$), this is then

$$E_c = \frac{-A_i t_1^2 r_2 J_0(\phi_0)}{(1-r_1 r_2)^2} e^{i\omega_0 t} \left[\frac{(e^{i\delta} - r_1 r_2)}{1+F' \sin^2(\delta/2)} -(i\Delta\omega/2\omega_n) \left(\frac{e^{i\omega_n t} (e^{i(\delta+\eta)} - r_1 r_2)}{1+F' \sin^2((\delta+\eta)/2)} + \frac{e^{-i\omega_n t} (e^{i(\delta-\eta)} - r_1 r_2)}{1+F' \sin^2((\delta-\eta)/2)} \right) \right] \qquad (4.17)$$

As $\frac{1}{1+F' \sin^2(\delta/2)}$ is Airy's function which describes the transmittance of a Fabry-Perot cavity, the emerging cavity field carries with it the signature of the Lorentzian lineshape.

The total reflected light field is then,

$$E_R = A_i e^{i\omega_0 t}\left[r_1 e^{i\phi_0 \sin\omega_m t}\,(1-i(\Delta\omega/\omega_n)\cos\omega_n t) - J_0(\phi_0)\,\frac{t_1^2 r_2}{(1-r_1 r_2)^2}\left\{\frac{(e^{i\delta}-r_1 r_2)}{1+F'\sin^2(\delta/2)} - i(\Delta\omega/2\omega_n)\left(\frac{e^{i\omega_n t}(e^{i(\delta+\eta)}-r_1 r_2)}{1+F'\sin^2((\delta+\eta)/2)} + \frac{e^{-i\omega_n t}(e^{i(\delta-\eta)}-r_1 r_2)}{1+F'\sin^2((\delta-\eta)/2)}\right)\right\}\right] \quad (4.18)$$

The intensity incident on the photodiode is obtained by multiplying E_R with its complex conjugate. And if the signal reaching the photodiode is subsequently demodulated, then this has the effect of picking out the terms in $\sin\omega_m t$. The demodulated signal is then given by

$$\begin{aligned} I_R/I_i &= (4X/Y_1)\,[(\Delta\omega/\omega_n)\cos\omega_n t.(\cos\delta - r_1 r_2) - \sin\delta] \\ &\quad -(2X/Y_2)\,[(\Delta\omega/\omega_n)\cos\omega_n t.\{\sin(\omega_n t+\delta+\eta) - r_1 r_2 \sin\omega_n t\} \\ &\qquad +\{\cos(\omega_n t+\delta+\eta) - r_1 r_2\cos\omega_n t\}] \\ &\quad +(2X/Y_3)\,[(\Delta\omega/\omega_n)\cos\omega_n t.\{\sin(\omega_n t-\delta+\eta) - r_1 r_2 \sin\omega_n t\} \\ &\qquad -\{\cos(\omega_n t-\delta+\eta) - r_1 r_2\cos\omega_n t\}] \end{aligned} \quad (4.19)$$

where $X = \dfrac{t_1^2 r_1 r_2}{(1-r_1 r_2)^2} J_0(\phi_0)\,J_1(\phi_0) = \dfrac{T\bar{R}}{(1-\bar{R})^2} J_0(\phi_0)\,J_1(\phi_0)$

and $Y_1 = 1+F'\sin^2(\delta/2)$; $Y_2 = 1+F'\sin^2((\delta+\eta)/2)$;

$Y_3 = 1+F'\sin^2((\delta-\eta)/2)$.

Setting $\Delta\omega=0$ (i.e. zero noise case) gives the error signal obtained purely as a function of cavity offset δ.

$$I_R/I_i\,(\Delta\omega=0) = \frac{T\bar{R}}{(1-\bar{R})^2} J_0(\phi_0)\,J_1(\phi_0)\,\frac{\sin\delta}{1+F'\sin^2(\delta/2)} \quad (4.20)$$

$$\text{i.e.} \qquad I_R/I_i\,(\Delta\omega=0) \propto \frac{\sin\delta}{1+F'\sin^2(\delta/2)} \quad (4.21)$$

This is simply the product of the sine function of the cavity offset and the Airy function of the cavity. As F' is

a measure of the gradient or "sharpness" of the Fabry-Perot fringes, it can be seen that an increase in F' produces an increase in the sharpness of the demodulated, or "r.f.", fringes. Figure 4.6 shows how I_R/I_i varies with for various values of finesse. It is, primarily, this part of the overall error signal, that allows a servo loop to maintain the cavity on resonance.

With the cavity on resonance ($\delta=0$) the resulting signal is

$$\left.\frac{I_R}{I_i}\right|_{\delta=0} = \frac{4\bar{R}T}{(1-\bar{R})^2}\,(\Delta\omega/\omega_n)\,J_0(\phi_0)\,J_1(\phi_0)\left((1-\bar{R})\cos\omega_n t + \frac{\{\bar{R}\cos\omega_n t - \cos(\omega_n t+\eta)\}}{1+F'\sin^2(\eta/2)}\right) \quad (4.22)$$

To appreciate more clearly the form of I_R/I_i, consider two extreme cases.

(a) $\nu_n < \nu_{MIN}\,(=\nu_c/F)$: i.e. The frequency of the noise much smaller than the linewidth of the cavity.

Now,

$$\left.\frac{I_R}{I_i}\right|_{\substack{\delta=0\\ \nu_n<\nu_{MIN}}} = \frac{4\bar{R}T}{(1-\bar{R})^2}\,J_0(\phi_0)\,J_1(\phi_0)\,(1/\nu_c)\cdot\Delta\omega\sin\omega_n t \quad (4.23)$$

$$\propto \sin\omega_n t.$$

This is proportional to the frequency deviations of the light from the cavity. So in this regime the action is that of the desired frequency discriminator.

(b) $\nu_n > \nu_{MIN}$. Here the noise sidebands, like those of the phase modulation, are located wide of the resonator passband and are reflected by the input cavity mirror.

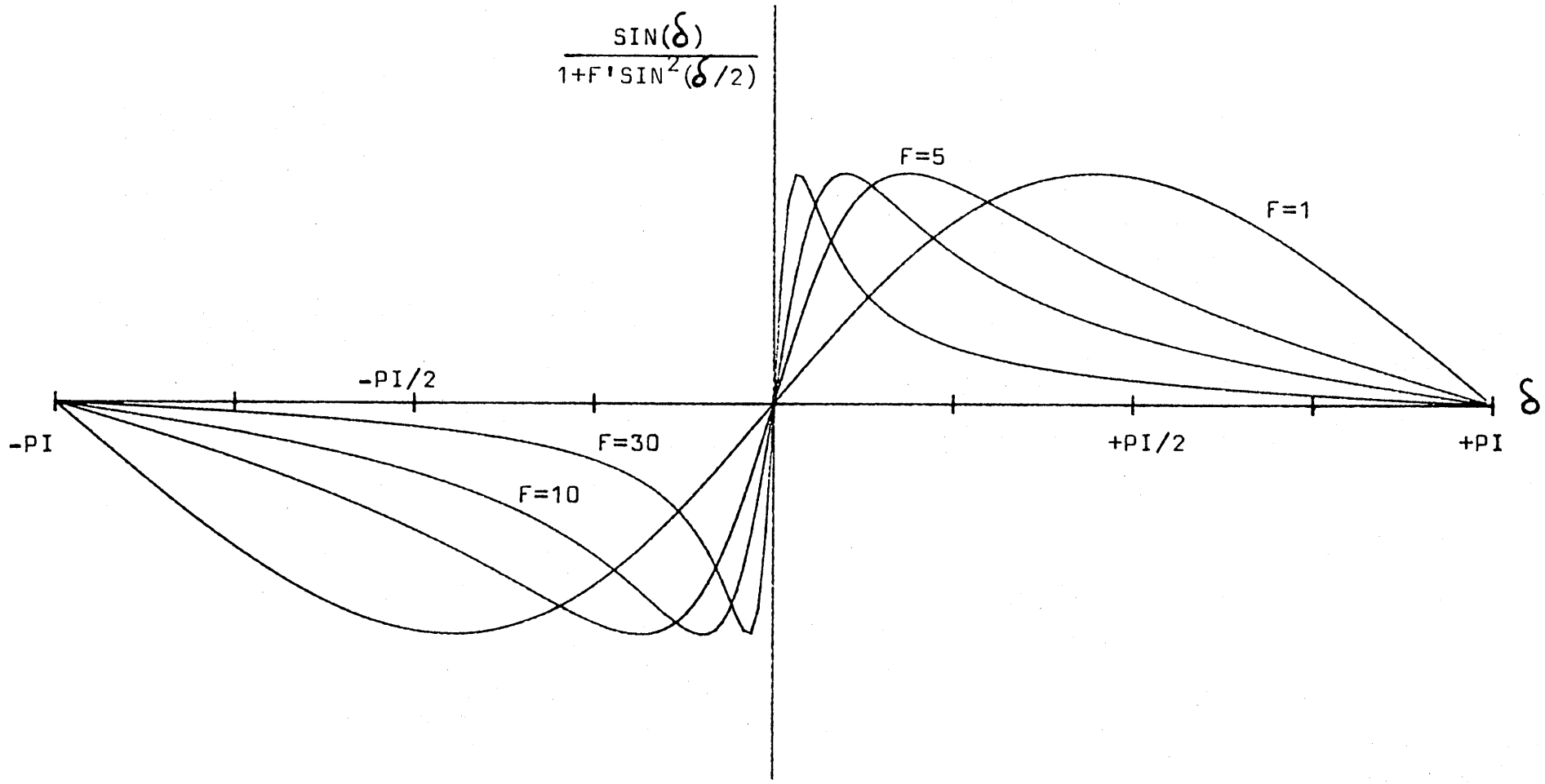

FIG.4.6: THEORETICAL CURVES OF DEMODULATED OUTPUT AS A FUNCTION OF CAVITY OFFSET δ FOR SEVERAL VALUES OF (LOW) FINESSE.

$$\left.\frac{I_R}{I_i}\right|_{\substack{\delta=0 \\ \nu_n > \nu_{MIN}}} = \frac{4\bar{R}T}{(1-\bar{R})} J_0(\phi_0)\, J_1(\phi_0)\, (\Delta\omega/\omega_n)\cos\omega_n t. \quad (4.24)$$

$$\propto (\Delta\omega/\omega_n)\cos\omega_n t.$$

Thus when $\omega_n > \omega_c/F$ the signal is proportional to the phase fluctuations of the light. Also the signal size is inversely proportional to ω_n and rolls off at 6dB per octave. The transfer function of the cavity thus behaves like that of an electronic integrator. The corner frequency, or 3dB point, is reached when $F'\eta^2/2 = 1$.

$$\text{i.e. } \nu_n(3\text{dB}) = \nu_c/2F = \nu_{MIN}/2. \quad (4.25)$$

It is interesting to note that when $\omega_n = n\omega_c$, where n is an integer, that the response of the cavity falls to zero.

$$\text{i.e. } \left.\frac{I_R}{I_i}\right|_{\substack{\delta=0 \\ \nu_n = n\nu_c}} = 0 \quad (4.26)$$

This means that the response of the stabilising servo will be zero at frequencies which are multiples of the free spectral range of the cavity. For high finesse cavities, these drops to zero are well outside the bandwidth of the servo loop. With the extension of cavity lengths to kilometre distances, however, the implication is that the servo bandwidth will encompass some of these sharp drops. This may pose some problems if the drops are asymmetric such that the phase is offset by the deviation.

The design of any servo circuit has to take into account the 6dB roll-off of the cavity if it is to produce good stabilisation performance. Thus, in the high speed domain, where the cavity is responding to phase (rather than frequency) of the light, the electronics can be so

arranged to enable a wide bandwidth to be achieved which is not limited by the response time of the cavity.

For practical purposes, it is often convenient to express the light output in terms of the amplitudes of the component fields at the photodiode: A_o, from the front of the input mirror, and A_c, from inside of the cavity. Then 4.23 and 4.24 can be rewritten as

$$\left.\frac{I_R}{I_i}\right|_{\nu_n < \nu_{MIN}} \simeq 4\left(\frac{A_c}{A_o}\right) J_o(\phi_o)\, J_1(\phi_o)\, \tau_s \cdot \Delta\omega \sin\omega_n t \qquad (4.27)$$

and

$$\left.\frac{I_R}{I_i}\right|_{\nu_n > \nu_{MIN}} \simeq 4\left(\frac{A_c}{A_o}\right) J_o(\phi_o)\, J_1(\phi_o)\, \frac{\Delta\omega}{\omega_n} \cos\omega_n t \qquad (4.28)$$

$$\text{where} \quad \tau_s = \frac{2Fl}{c\pi} = \frac{1}{\pi\nu_{MIN}} \qquad (4.29)$$

i.e. τ_s is the storage time of the cavity (- the time for intensity of transmitted light to fall to 1/e of its initial value).

If the contrast, or visibility, of the fringes, V, is defined as

$$V = \frac{I_{MAX} - I_{MIN}}{I_{MAX}} = 1 - \frac{(A_o - A_c)^2}{A_o^2} \qquad (4.30)$$

Then,

$$\left(\frac{A_c}{A_o}\right) = 1 \pm (1-V)^{1/2} \quad \begin{pmatrix} \text{+ve sign if } A_c > A_o \\ \text{-ve sign if } A_c < A_o \end{pmatrix} \qquad (4.31)$$

and

$$V_{MAX} = 1 - \left(r_1 - \frac{T_1 r_2}{1-\bar{R}}\right)^2 \qquad (4.32)$$

Visibility will only approach V_{MAX} with low absorption mirrors and good mode matching.

Similar, complementary, analysis to that above has

also been carried out by Ford (1981), Munley (1982), and Meers (1983).[75,58,48]

4.4 THE POWER LOSS ASSOCIATED WITH AN INTRA-CAVITY DEVICE.

As described in chapter 2, the control element, used to correct for the frequency deviations of the light, is an electro-optic modulator placed inside the cavity of the laser. An unfortunate side effect of this, is that it can result in a significant degradation of the output power of the laser light, and, in a high power laser, the modulator itself can be easily damaged.

The effect of internal cavity losses on laser output power has been shown to be dependent on both the gain factor of the lasing medium and the output coupling factor of the cavity.[76] Yariv (1975)[77] has shown that the useful output power of a laser has the form

$$P_o = K \left(\frac{g_o}{L_i + T} - 1 \right) . T \qquad (4.33)$$

where K is a constant dependent on the type of lasing medium, the cross-sectional area of the laser mode and the atomic transition involved in the lasing action. L_i is defined as the internal loss factor and g_o as the unsaturated gain factor per pass.(i.e. $g_o = \gamma_o l$, where γ_o is the gain constant at threshold and l is the length of the medium; and $L_i = \alpha l$ where α is the absorption coefficient due to all loss mechanisms except laser transition). T is defined as the useful coupling factor, and for all practical purposes is simply the transmittance of the

output mirror.

Maximising 4.33 for T results in an optimum value of mirror transmittance for a given loss.

$$T_{OPT} = - L_i + \sqrt{g_o L_i} \qquad (4.34)$$

The effect of introducing extra losses into the cavity (such as those due to an intra-cavity modulator) can be found by differentiation, with respect to L_i, of 4.33.

$$\frac{dP_o}{P_o} = \frac{-g_o dL_i}{(L_i+T)(g_o-L_i-T)} \qquad (4.35)$$

Assuming $g_o > L_i+T$ (i.e. well above threshold),

$$\frac{dP_o}{P_o} = \frac{-dL_i}{(L_i+T)} \qquad (4.36)$$

Now the <u>minimum</u> power loss that arises as a result of introducing extra losses dL_i is found by setting $T=T_{OPT}$ in 4.36. This gives

$$\left.\frac{dP_o}{P_o}\right|_{OPT} = \frac{-dL_i}{\sqrt{(g_o L_i)}} \qquad (4.37)$$

With an intra-cavity device installed the new internal loss factor is denoted L_i'. Then

$$L_i' = L_i + L_p \qquad (4.38)$$

where L_p is the loss due to the intra-cavity device.

If T is now optimized for the new internal loss factor then

$$\left.\frac{dP_o}{P_o}\right|_{OPT} = \frac{-dL_i}{L_i+[-L_i'+\sqrt{g_o L_i'}]}$$

$$= \frac{-L_p}{-L_p+\sqrt{g_o L_i'}} \qquad (4.39)$$

Letting n and m be dimensionless real numbers such that

$$L_i = nL_p \qquad (4.40)$$

$$\text{and} \quad g_o = mL_i \qquad (4.41)$$

$$\text{then} \quad \left.\frac{dP_o}{P_o}\right|_{OPT} = \frac{-1}{\sqrt{nm(n+1)} - 1} \qquad (4.42)$$

When T is optimized, P_o, as a function of L_i, approximates to a linear function for dL_i much less than L_i. For larger changes, it is necessary to use the large change formula which can easily be shown to be

$$\left.\frac{\Delta P_o}{P_o}\right|_{OPT} = \frac{-L_p}{L_p\sqrt{(L_i'/g_o)} - L_i' + \sqrt{g_o L_i'}} \qquad (4.43)$$

For the 514.5 nm line in a typical high power argon laser, a value of g_o may be around 2.5 (250%) [59] and a typical loss value L_i, well above threshold, of 0.1 (10%). For an intrinsic modulator loss of $\sim$ 5% then, 4.43 reveals that the minimum possible intra-cavity loss, for the above gain and loss factors, is $\sim$ 11%

While this mimimum change in power loss, from inside to outside the laser cavity, does not appear particularly severe itself, it should be borne in mind that the optimisation of the loss factor is very difficult in practice to achieve and even more difficult to maintain. In high power lasers intra-cavity devices often suffer a steady degradation in transmittance. And if the output mirror coupling is not close to its optimum value, then the insertion loss can increase dramatically. It is not unknown, for instance, for insertion losses as high as 50% to occur. It is, therefore, desirable to have a

stabilisation technique that does not involve the use of intra-cavity devices. Such a technique is described in the following chapter.

CHAPTER 5.

FREQUENCY STABILISATION USING AN EXTRA-CAVITY ELECTRO-OPTIC MODULATOR.

5.1 EXTERNAL STABILISATION.

The previous chapter outlined the motivation for developing a new method of frequency stabilisation which does not require the use of an intra-cavity device. This new technique, which is an extension of the reflection locking technique analysed in section 4.3, uses a fast piezoelectrically driven laser mirror and an extra-cavity electro-optic modulator as the control elements.

Previous experiments investigating external frequency stabilisation have concentrated on the use of acousto-optic modulators to control the laser frequency.[49,78] However, in acousto-optic modulators an unavoidable effect of the Bragg deflection of the light is to introduce fluctuations in the angle and shape of the laser beam - although the angular fluctuations can be reduced somewhat, at the expense of laser power, by "double-passing" the modulator.[49,78] Further, the use of acousto-optic modulators alone outside the laser cavity restricts the overall bandwidth of the servo loop as they have an associated time delay of microseconds due to the relatively slow travel time of acoustic waves. Hall and Hansch (1984)[79] have been able to overcome this time delay by using a combination of an electro-optic modulator and acousto-optic modulator to stabilise the frequency of a dye laser.

The essence of using external frequency stabilisation with an extra-cavity electro-optic modulator lies with the fact that phase fluctuations of the light are essentially integral forms of the frequency fluctuations, and so the frequency corrections ($\delta\nu$), required for stabilisation, are related to the phase corrections ($\delta\phi$) by

$$\delta\nu = \frac{1}{2\pi} \frac{d(\delta\phi)}{dt} \qquad (5.1)$$

Now a voltage U applied to the external modulator produces a change in the phase, $\delta\phi$, of the light. A frequency shift is obtained when the voltage changes at some rate dU/dt. To obtain a frequency shift $\delta\nu$, proportional to a voltage signal V(t), an integration is required such that

$$U = 1/\tau \cdot \int V(t)\, dt. \qquad (5.2)$$

where V(t) is the voltage signal that would normally be sent to an intra-cavity device and τ is the time constant of the integrator. Then

$$\delta\nu = \frac{1}{2U_o} \cdot \frac{dU}{dt}$$

$$= \frac{1}{2U_o\tau} V(t) \qquad (5.3)$$

where U_o is the half-wave voltage of the modulator.

Thus if an error signal proportional to laser frequency fluctuations is detected, the integral of this signal applied to the external modulator will produce a change in the phase of the light that is equivalent to these frequency fluctuations.

In practice, the correction signal is split between

two control elements. The phase modulator receives only the integrated form of the higher frequency correction signals, with the lower frequency signals being applied to a fast piezoelectric transducer (PZT) driving the rear laser mirror. This piezoelectric mirror assembly has a first resonance at 200kHz and, if the PZT alone is used as the control element, the bandwidth of the servo loop tends to be limited by this resonance. However, as will be seen, the introduction of the external modulator allows a considerable extension of the bandwidth and so permits the low frequency gain to be increased to a point where the system would previously have been unstable.

The stabilisation scheme is shown in figure 5.1. The intensity modulated light returning from the reference cavity is steered towards the photodetector by a polarising beamsplitter and quarter waveplate combination. The reference cavity, used as part of the reflection locking scheme, is a commercial item (Tropel model 216) with a free spectral range (ν_c) of 300MHz and a linewidth (ν_{MIN}) of 1.5MHz. This implies a finesse of 200 and a cavity roll-off frequency (ν_{3dB}) of 750kHz.

Phase modulation is applied to the light at 10MHz via a Brewster cut ADP crystal (Inrad) through a self-resonant, step-up transformer coupled from a 50Ω r.f. source. Approximately 1/4 watt of r.f. power is supplied to the crystal. The r.f. sidebands produced have a modulation index of $\sim$ 0.8. (As the intensity noise from an argon laser reaches its shot noise level above a few Megahertz, the 10MHz phase modulation also ensures that any fluctuations

in the level of the light do not have any adverse influence on the performance of the frequency stabilisation).

The 10MHz amplitude modulated light reflected from the cavity ($\sim 250\mu W$) is detected by a photodiode. The tuned preamplifier circuit (tuned for 10MHz) is shown in figure 5.2. It has a bandwidth in excess of 2MHz and a base noise level $\sim$ 4dB below the photoelectric shot noise in the detected light. The demodulated signal from the balanced mixer, shown in fig.5.1 provides the error signal input to the servo system.

The system has two main channels, one, the "slow" channel, driving the PZT transducer connected to the rear laser mirror, and the other, the "fast" channel, driving the external electro-optic modulator. The slow channel essentially operates below the resonant frequency of the PZT mount ($\sim$ 200kHz) and has a maximum roll-off of greater than 18dB around 1kHz. The laser control requires signals of up to 250 V at low frequencies but much smaller signals at high frequencies, and so for optimum performance a parallel amplifier combination is used to drive the PZT. The fast channel operates to give the whole system a unity gain point of approximately 2MHz, the signal from the error point being amplified and integrated at frequencies above 50kHz.

To limit propagation delay through the servoelectronics, the servo amplifier is designed in a "bypass" arrangement. The circuit diagram of this amplifier is shown in figure 5.3.

The parallel amplifier combination, which drives the

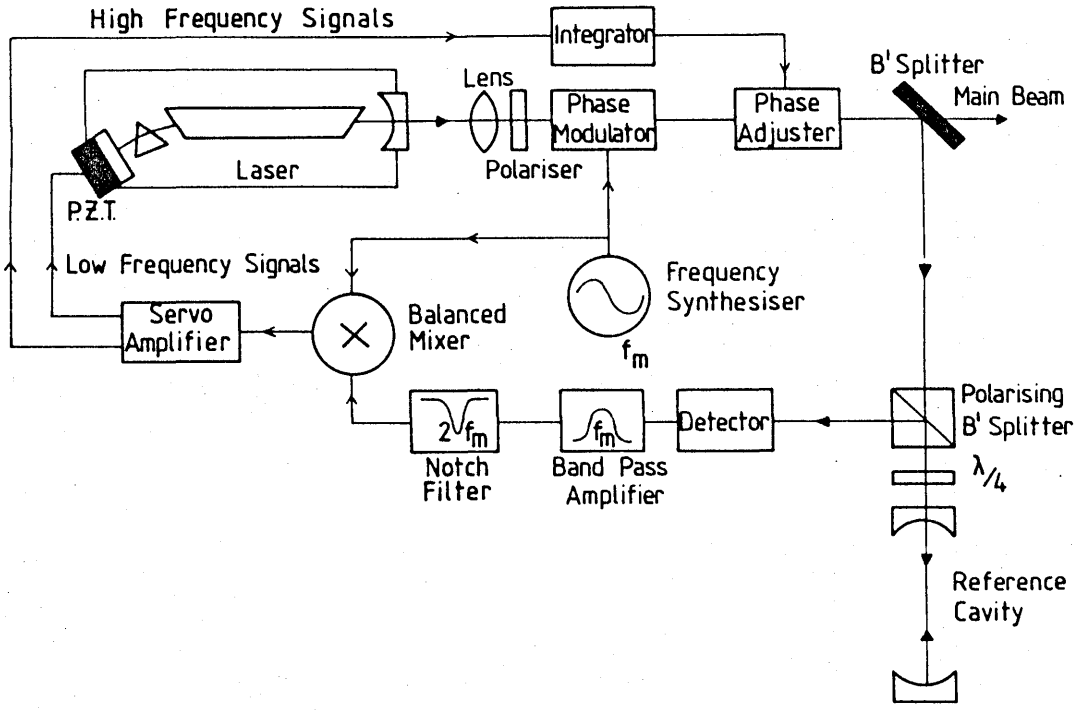

FIG.5.1: SCHEMATIC BLOCK DIAGRAM OF LASER STABILISATION SYSTEM. THE ERROR SIGNAL FROM THE DEMODULATOR, A MEASURE OF THE DETUNING OF THE LASER FROM A RESONANCE OF THE REFERENCE CAVITY, IS SPLIT INTO TWO PARTS. THE LOWER FREQUENCY PART IS AMPLIFIED AND FED BACK ONTO A PZT DRIVEN LASER MIRROR, AND THE HIGH FREQUENCY PART, AFTER AMPLIFICATION BY A HIGH VOLTAGE AMPLIFIER OF 6MHz BANDWIDTH AND SUITABLE INTEGRATION, IS FED BACK ONTO AN EXTRA-CAVITY ELECTRO-OPTIC MODULATOR.

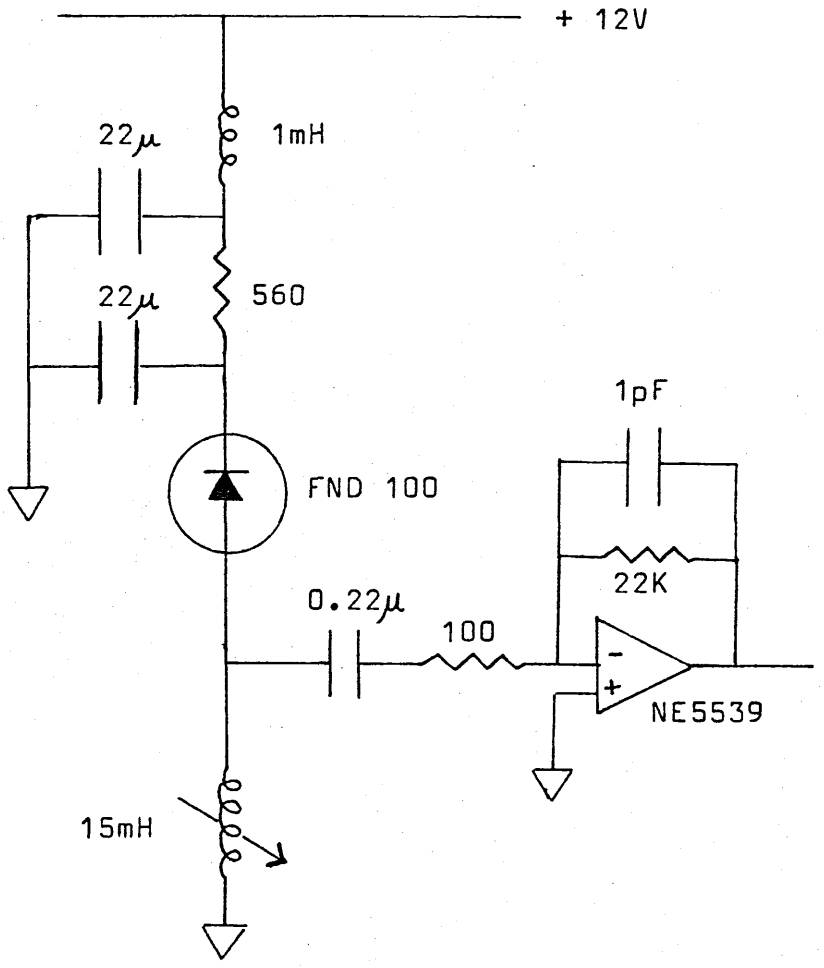

FIG.5.2: PHOTODIODE/PREAMPLIFIER CIRCUIT USED AS PART OF THE LASER FREQUENCY STABILISATION SCHEME.

PZT, has a crossover frequency of $\sim$ 8kHz. The slow signals, which dominate stabilisation below 8kHz, are fed through a high voltage amplifier, which has a gain of 24 and a bandwidth of 10kHz, to the piezo transducer itself which imposes a 6dB/octave roll-off from $\sim$ 100Hz. The intermediate signals are fed directly to the PZT which rolls-off from about 100kHz. The high frequency signals are fed via a VLA30 high voltage amplifier with a bandwidth of 6MHz and a gain factor of 130. These signals are integrated, by means of a passive integrator, and fed to the external electro-optic modulator. The crossover frequency between the slow/intermediate channel and the fast channel of the system arises at $\sim$ 100kHz, which means that the fast channel begins to dominate stabilisation before the resonant frequency of the PZT is reached. The circuit of the servo amplifier shows the inclusion of three variable resistors which allow the relative gains of the three channels to be altered.

The PZT transducer mounting (manufactured in Orsay, France) consists of a low mass mirror/PZT combination mounted on a Tungsten acoustic delay line to minimise structural resonances. The arrangement is damped by embedding it in a viscous, low vapour pressure, damping compound loaded with lead shot.

The phase adjusting electro-optic modulator is a transverse cut ADP crystal (Capacity $\sim$ 100pF) mounted in a housing filled with index matching fluid and fitted with anti-reflection coated windows. The modulator has a half-wave voltage of 255 V.

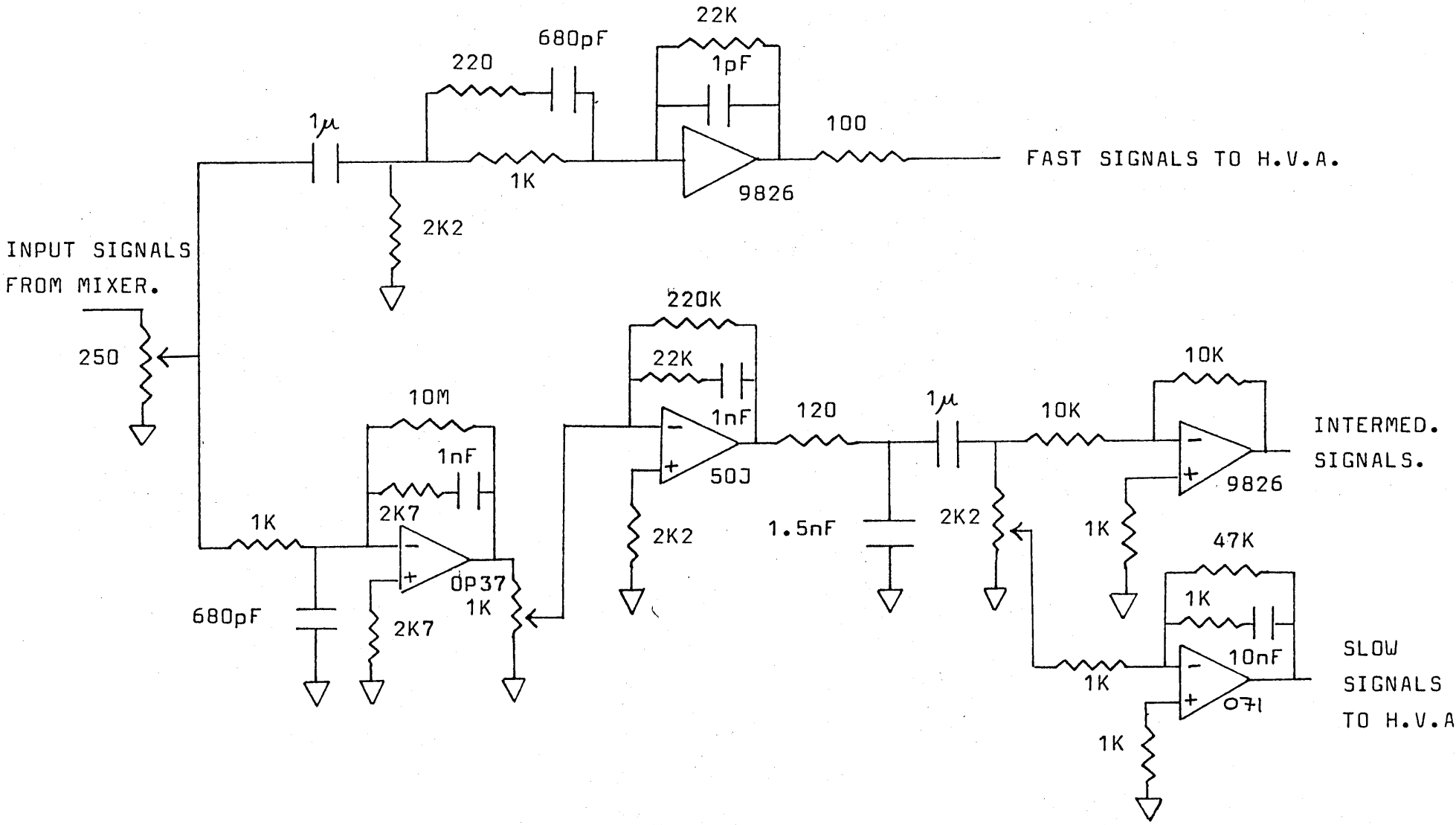

FIG.5.3: FINAL CIRCUIT ARRANGEMENT OF THE SERVO AMPLIFIER.

5.2 RESULTS AND DISCUSSION.

The reflection signals obtained with this type of system, which were analysed in section 4.3, are shown in figure 5.4. These traces show the observed signals as a function of cavity offset.

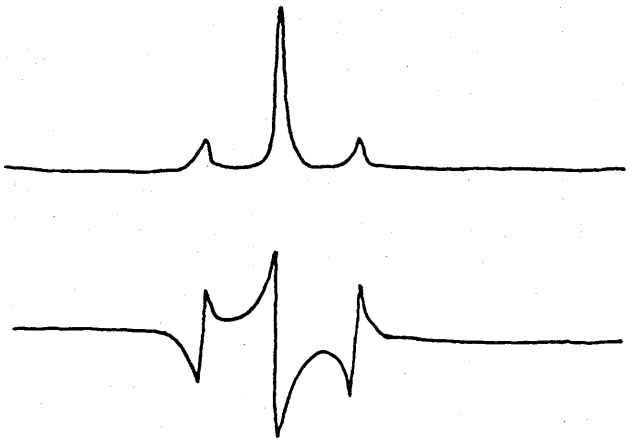

FIG. 5.4 FRINGE SIGNALS OBTAINED FROM THE FABRY-PEROT REFERENCE CAVITY.

The upper trace shows the cavity transmission signal or "d-c fringe" signal. The sideband peaks due to the 10MHz phase modulation being visible on either side of the central "Airy function" peak. The lower trace shows the reflected field signal ("r.f. fringe") after demodulation. The feedback loop locks the laser to the zero point of the r.f. fringe. This corresponds to the maximum cavity transmission point. Observe that the error point signal has the correct sign, to allow the servo to lock, over a range covering twice the modulation frequency.

It should be noted that a real advantage of locking to the maximum cavity transmission point is that it permits a bandwidth of servo loop greater than the cavity linewidth

to be employed. With a fringe "side-lock" scheme, a bandwidth greater than the cavity linewidth means that operating the servo with a low damping coefficient allows the transient response errors, characteristic of this scheme, to destabilise the loop.[72]

For practical purposes, the performance of the scheme was measured at the error point of the frequency stabilised loop. These error point measurements were calibrated by measurement of the gradient (in MHz/V) of the the error signal fringe shown in figure 5.4. The error point signals themselves are not a true measure of the residual frequency fluctuations of the laser since, for example, if the loop gain is high enough, the error signal may be reduced below the fundamental limit set by shot noise in the detected photocurrent. (Under these circumstances the shot noise in the photocurrent will be imposed on the laser frequency to produce the appropriate servo null). However, consideration of the error point signal allows a clear demonstration of the contribution of the extra-cavity modulator to the allowable gain/bandwidth of the loop, and is suitable for technical comparison of this stabilisation scheme with methods which use an intra-cavity device.

The amplitude spectral density of the error point signal was measured, for two different feedback arrangements, up to a frequency of 2.5kHz.

In the first arrangement the high frequency channel to the extra-cavity modulator was not used, and the gain of the feedback amplifier was increased until the system was

close to instability at the resonant frequency of the piezoelectric mirror drive on the laser. Typically, an error point of $\sim$ 0.06 Hz/$\sqrt{\text{Hz}}$ at 1kHz was achieved, as is shown in figure 5.5. In the second arrangement the high frequency channel was connected, and the gain of the low frequency channel could be increased by approximately 15dB to allow an error point signal level of $\sim$ 0.01 Hz/$\sqrt{\text{Hz}}$ to be typically achieved at 1kHz (fig. 5.5).

The unity gain point of the system, with the high frequency channel connected, was approximately 2MHz, thought to be limited by propagation delay through the high frequency amplifier chain, which causes a slight tendency towards instability around this frequency. This is illustrated in a wideband spectrum of the error point signal shown in figure 5.6, the small "wings" at the unity gain point being clearly visible. These come about as a result of a certain amount of transient overshoot which is acceptable in exchange for an increase in the overall gain. This is explained more fully in the next section.

It is interesting to note that, as the extra-cavity modulator dominates the situation at 200kHz, the phase change associated with the PZT resonance is much less important in determining the stability of the system.

This level of performance was obtained with a laser output power of up to 3.5 W.

With the extra-cavity electro-optic modulator and PZT driven laser mirror in use, the error point signal closely approached the level of measured stability being attained, at the same time, for the argon laser, on the

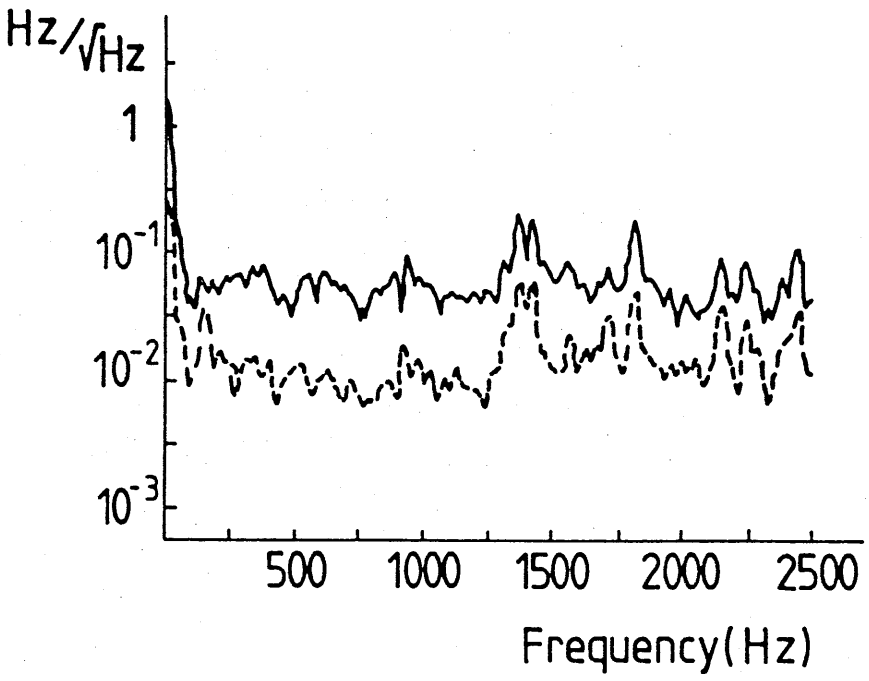

FIG.5.5: TYPICAL FOURIER SPECTRA OF THE APPARENT FREQUENCY FLUCTUATIONS OF THE LASER MEASURED AT THE ERROR POINT OF THE FEEDBACK LOOP. (SOLID CURVE: WITH ONLY THE PZT DRIVEN LASER MIRROR AS THE FEEDBACK ELEMENT, AND DOTTED CURVE: WITH THE ADDITION OF THE EXTRA-CAVITY ELECTRO-OPTIC MODULATOR). THE HEIGHT OF THE MAINS SUPPLY RELATED HUMP AT $\sim$ 1.5kHz WAS VARIABLE AND THE RESULTS HERE SHOW THE WORST CASE CONDITION OF THIS EFFECT. SUCH CURVES WERE OBTAINED WITH A LASER POWER OUTPUT OF UP TO 3.5W.

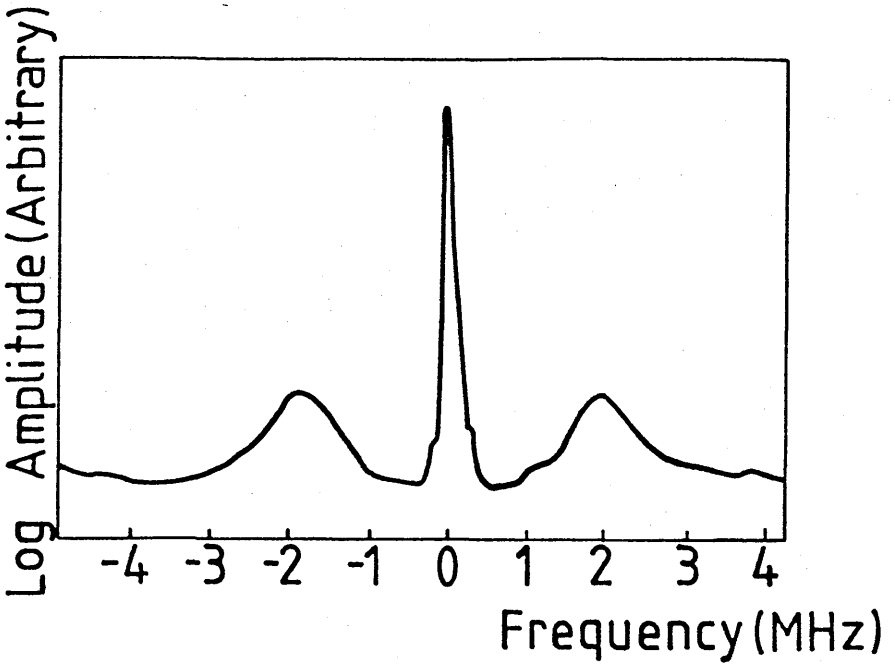

FIG.5.6: TYPICAL FOURIER SPECTRUM OF THE APPARENT FREQUENCY FLUCTUATIONS AT THE ERROR POINT OVER A WIDE BANDWIDTH. THE UNITY GAIN POINT AT ~ 2MHz IS CLEARLY SHOWN BY THE SLIGHT TENDENCY TO INSTABILITY AT THIS FREQUENCY. (NOTE THAT NEGATIVE FREQUENCIES TO THE LEFT OF THE ZERO PEAK ARE REDUNDANT).

Glasgow 10m detector, with an intra-cavity modulator.

Although, in this experimental arrangement, two electro-optic modulators have been used in front of the laser - one for applying the 10MHz phase modulation and one for the fast frequency correction - there is no reason, in principle, why a single modulator cannot be used for both purposes, with suitable arrangement of the driving circuitry.

In this stabilisation scheme, where a short (25cm) reference cavity is used, it is difficult to obtain a level of photon noise limited stability as small as the apparent error point achieved. In fact, with the amount of light used on the photodiode, the photon noise limited frequency fluctuations would be close to 0.4 $Hz/\sqrt{Hz}$ at 1kHz. However, this will not be a problem when the scheme is used with the 10m long reference cavity of the detector, since such a cavity has a sensitivity to frequency fluctuations much higher than that of a short cavity with the same finesse and fringe contrast.

5.3 SERVO ANALYSIS.

To appreciate the shortcomings of a feedback system, and to aid the development of future systems, it is worth analysing the performance in detail. This section, then, includes the servo analysis of the external laser stabilisation scheme.

The basis of any negative feedback loop can be

schematically represented by the block diagram in figure 5.7. The amount of gain available is represented by G. The frequency dependent filtering is represented by H, and the error signal measurements of the previous section are represented by E.

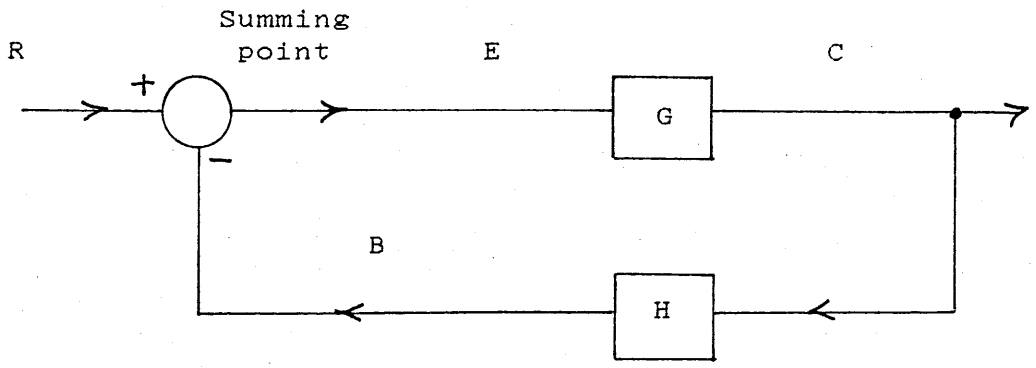

FIG. 5.7 BLOCK DIAGRAM OF A NEGATIVE FEEDBACK LOOP.

The following definitions will be used in this section:

G = Forward transfer function.

H = Feedback transfer function.

GH = Open-loop transfer function.

C/R = Closed-loop transfer function.

E/R = Error ratio.

and B/R = Primary feedback ratio.

It is straightforward to show that

$$\frac{C}{R} = \frac{G}{1+GH} \qquad (5.4)$$

$$\frac{E}{R} = \frac{1}{1+GH} \qquad (5.5)$$

$$\frac{B}{R} = \frac{GH}{1+GH} \qquad (5.6)$$

The two main design objectives of a feedback system

are high gain and stability of performance. As will be seen, it is sometimes permissable to have a system that is not unconditionally stable in exchange for extra gain performance.

The stability of a system is determined by its transient response. To assess the stability, it is usually necessary to convert the analysis from the time domain to the complex s-domain[80]. The mathematical tool used for this is the Laplace transform $\mathcal{L}$. A function f(t) is converted from the time domain to the s-domain by

$$F(s)=\mathcal{L}[f(t)]=\int_0^\infty e^{-st} f(t)\,dt \qquad (5.7)$$

where $s=\sigma+i\omega$ is the Laplace complex variable, and $i=\sqrt{-1}$.

In the s-domain a system transfer function, T(s), is given by

$$T(s) = \frac{\mathcal{L}[r(t)]}{\mathcal{L}[e(t)]} = \frac{R(s)}{E(s)} \qquad (5.8)$$

where r(t) is the time domain response function, R(s) is the s-domain response function, e(t) is the time domain excitation function, and E(s) is the s-domain excitation function.

Thus, the system response, to a given excitation is,

$$R(s)=T(s).E(s) \qquad (5.9)$$

Values of s which make the system output infinite are known as poles of the response function and are found by the solution of the equations

$$T(s)^{-1}=0 \qquad (5.10)$$

$$E(s)^{-1}=0 \qquad (5.11)$$

For transient response the excitation function may be considered to be a unit impulse at time t=0. The Laplace

transform E(s) is then 1, and so the stability of a system is determined by the poles of the system transfer function. The response function is then

$$r(t) = \mathcal{L}^{-1}[T(s)] \tag{5.12}$$

where $\mathcal{L}^{-1}$ denotes the inverse Laplace transform.

For complex systems, there may be several poles, $(s_1, s_2, \ldots, s_n)$, for a given transfer function. T(s) may be written as

$$T(s) = \frac{1}{(s_1+\alpha_1)(s_2+\alpha_2)\ldots(s_n+\alpha_n)} \cdot \frac{K}{F} \tag{5.13}$$

where K is known as the gain factor, and F contains those factors of the denominator which do not result in poles.

Now,

$$f(t) = \mathcal{L}^{-1}\left(\frac{1}{s_i+\alpha_i}\right) = e^{-\alpha_i t} \tag{5.14}$$

The transformation of equations of the form of 5.13 invariably result in functions containing products such as 5.14.

A pole occurs when $s = -\alpha_i = \sigma_i + i\omega_i$. Then,

$$f(t) = A\, e^{s_i t} . \tag{5.15}$$

Thus, it can be seen that the transient response will tend to infinity if a pole has a positive real part, $+\sigma$.

If the frequency response, for both positive and negative frequencies, is plotted on a polar plot, then all points inside the curve have positive values of σ. This is the basis of Nyquist analysis.

The characteristic equation of a closed loop transfer function can be written as

$$GH = -1 \tag{5.16}$$

and each root of this equation defines a signal $Ae^{s_i t}$ for which the gain around the servo loop is equal to 1. When a signal $Ae^{s_i t}$ originates, it is maintained indefinitely by the very nature of a feedback system. Thus the system will become unstable if s_i has a positive real part. If σ is negative, however, the signal dies away exponentially. When $\sigma=0$, the pole $s=\pm i\omega$, and there are oscillations of a constant amplitude introduced.

Nyquist's criterion states that the closed loop system is stable if, and only if, the area enclosed by the full open loop response curve does not include the point (-1,0). Under these circumstances, there can be no value of s with a positive real part such that GH=-1. An alternative form of the criterion states that the closed loop is stable if, and only if, when the full open loop frequency response is drawn, for frequencies varying between zero and infinity, the (-1,0) point lies on the left hand side of the locus, where positive direction corresponds to increasing frequency.

It follows from the above discussion that the damping of the system transient response depends on how negative σ is. Oscillations will decay with a time constant $\tau=\frac{1}{\sigma}$. The damping ratio ξ is defined as

$$\xi=\sigma/\omega_n. \qquad (5.17)$$

where ω_n = undamped natural frequency of the oscillation, and is related to ω_d, the damped natural frequency by

$$\omega_d=\omega_n(1-\xi^2)^{1/2}. \qquad (5.18)$$

The closer ξ is to 1, the better the oscillation is damped. If the system is not critically damped, then there will be

a certain amount of transient overshoot, and the system will be closer to instability. Total instability occurs when ξ =0. Obviously, there is a compromise to be reached between a reasonable system gain/bandwidth and how close to instability the system can afford to be run. If high gain performance is the main desirable quantity of the system, it may become worthwhile operating with a damping factor closer to 0 than 1, although such a system would become unstable rather easily.

As has been stated in the previous section, the introduction of the extra-cavity modulator allowed an extension of the overall bandwidth of the servo loop, of a factor of $\sim$ 10, from 200kHz to around 2MHz. This is illustrated in a graph of the open loop transfer function, GH, against frequency, shown in figure 5.8.

To enable the system to be locked stably with the PZT mirror alone, it was necessary to have the transfer function rolling off at $\sim$ 6dB/octave through the unity gain point, determined by the PZT resonance. This is evident in the slope of the lower half of the plot of GH. The flat region around 100kHz shows the point where the extra-cavity modulator begins to dominate, and the final slope of the curve is determined by the roll-offs of the Fabry-Perot cavity and the high frequency amplifiers.

Once the external modulator dominates the transfer function at $\sim$200kHz (the PZT resonance), the low frequency gain can be increased significantly (typically $\sim$ 15dB, as shown in figure 5.5). The open loop transfer function is shown for a gain G of 10^9. As will be seen,

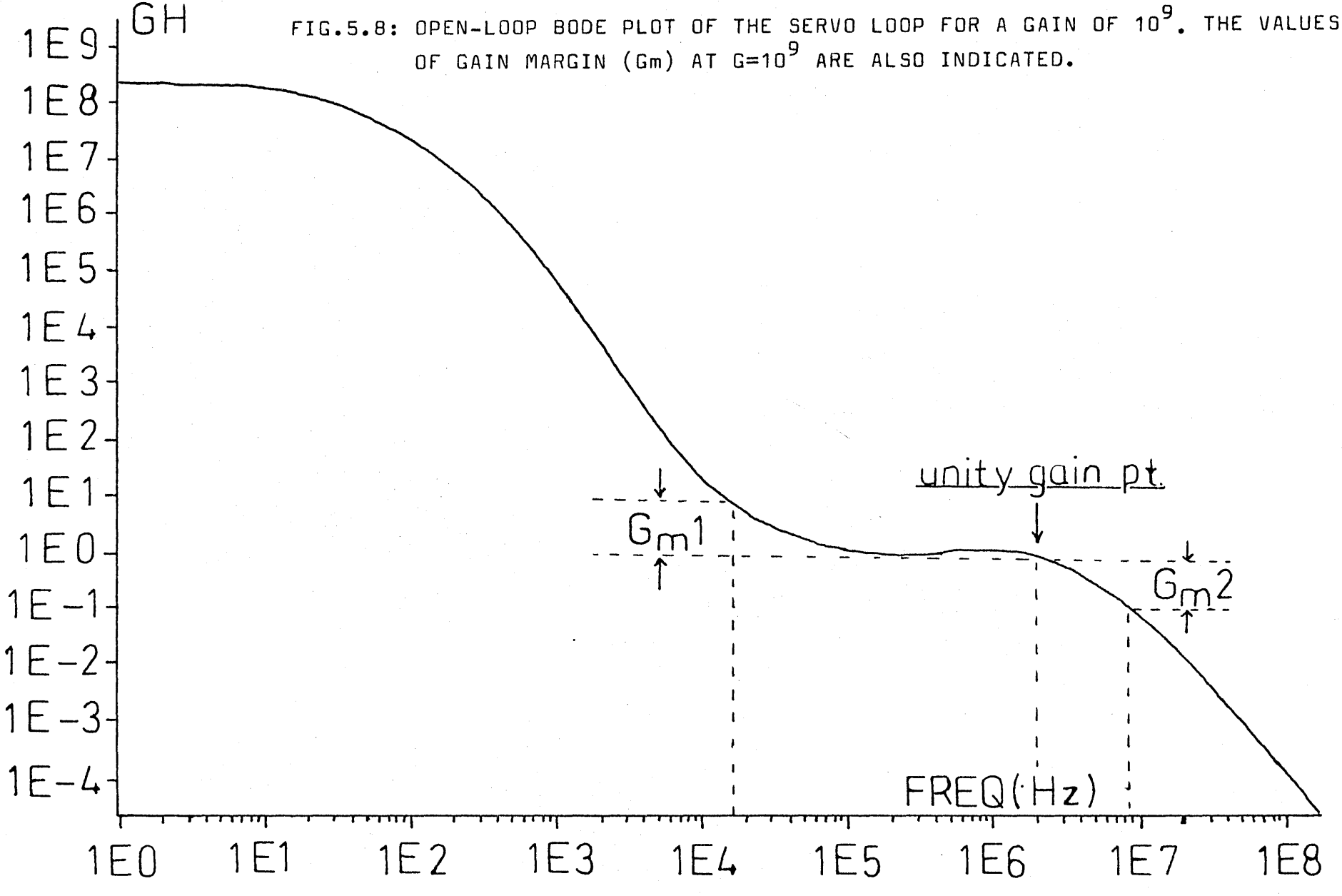

FIG.5.8: OPEN-LOOP BODE PLOT OF THE SERVO LOOP FOR A GAIN OF 10^9. THE VALUES OF GAIN MARGIN (Gm) AT G=10^9 ARE ALSO INDICATED.

this is a suitable region of gain for the operation of the system. If the gain is increased further, a point is reached where the system is unstable and oscillates at $\sim$8MHz. If the gain is reduced sufficiently, a second point of instability is reached, and the system oscillates at $\sim$15kHz. (Reduction of the high frequency gain alone results in oscillation at the PZT resonance of $\sim$200kHz). The system is therefore known as a conditionally stable system.

This situation, of stability over a limited region of gain, is best illustrated in a Nyquist plot of the open loop transfer function, shown in figure 5.9. Again, the graph is drawn for $G \sim 10^9$.

It can be seen that the system is stable under, the Nyquist criterion, as the (-1,0) point is always on the left hand side of the locus. Increasing the gain, however, moves the plot further towards $-\infty$ on the left hand side of the real axis, and the (-1,0) point passes to the right hand side of the locus, bringing on the oscillation at 8MHz. Similarly, reducing the gain moves that part of the plot with negative real values towards the origin, and the system again becomes unstable at 15kHz. The "kink" in the plot around the (1,-1) region of the graph is due to the fact that GH increases slightly, just after the crossover frequency between the PZT and the external modulator. This has no effect, however, on system stability.

A useful rule of thumb is that the further away from the (-1,0) point the locus cuts the real axis, the more stable the system is, and the closer to unity the damping

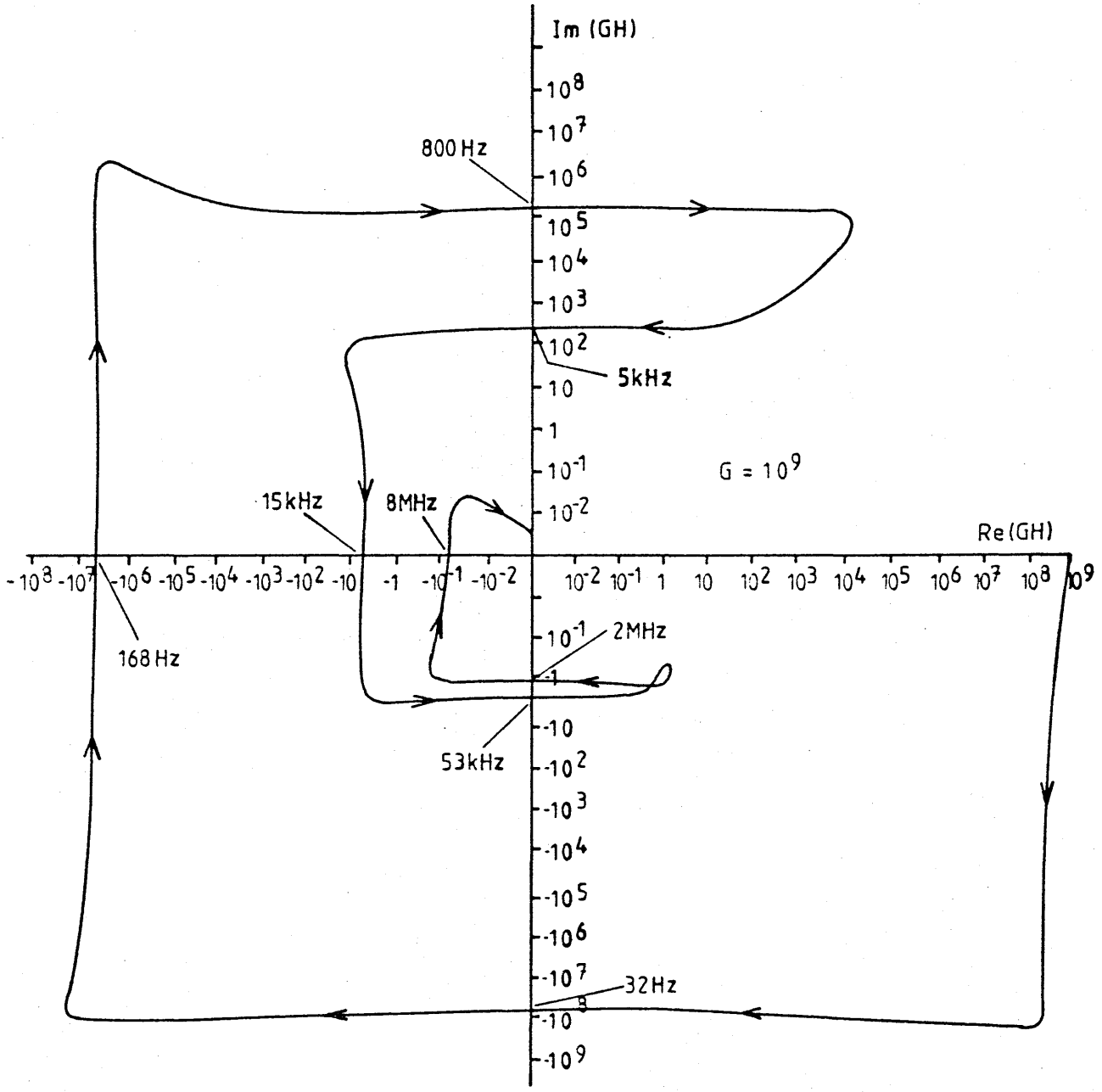

FIG.5.9: NYQUIST PLOT OF THE SERVO LOOP FOR A GAIN OF 10^9 ILLUSTRATING THE SITUATION OF CONDITIONAL STABILITY. THE FREQUENCY OF THE LOOP AT IMPORTANT AREAS IS ALSO INDICATED.

ratio ξ is. As the locus crosses closer and closer to (-1,0), the damping ratio decreases, transient overshoot occurs, and the closed loop transfer function develops "wings" at the frequency $\omega_d (= \omega_n \sqrt{1-\xi^2})$. As the wings become more prominant, they get classed as resonance peaks, M, and are defined by

$$\text{Resonance peak} \quad M = \frac{\text{max.} \left| \frac{C}{R} \right| (i\omega)}{\text{av.} \left| \frac{C}{R} \right| (i\omega)} \qquad (5.19)$$

i.e. the maximum factor of deviation of the closed loop gain from its average value. This can be used as a measure of relative stability.[80] As M increases, ω_d tends to ω_n, where the system eventually becomes unstable. Figure 5.10 shows this situation in several plots of the error ratio E/R for various values of gain G. This can be compared with the experimental graph of fig. 5.6.

These graphs show how the shape of the closed loop transfer function varies over the stable gain region. Note the changing frequency of the resonance peaks, and how the system tends to instability at the critical values of G.

It does not usually suffice that a system is mathematically stable, and so it is necesary to have a certain margin of stability to correct for sudden disturbances. A system, whose transient response is well damped, will respond better to sudden excitation. A measure of relative stability,[81] first introduced by Bode (1940), is defined as the magnitude of the reciprocal of the open loop transfer function at the frequency ω_π where the phase angle

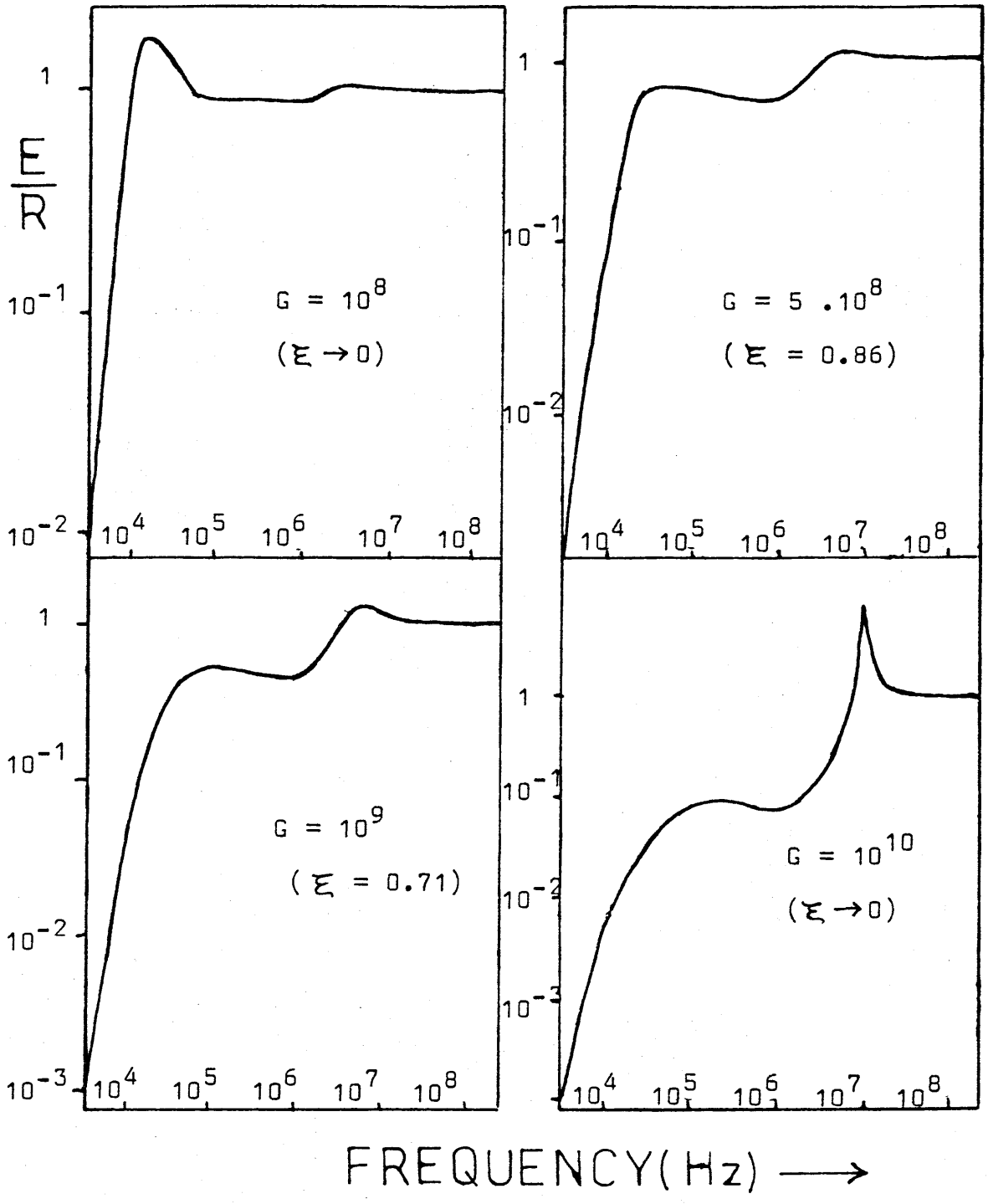

FIG.5.10: ERROR RATIO AGAINST FREQUENCY FOR SEVERAL VALUES OF GAIN. NOTE THAT AT GAINS OF 10^8 AND 10^{10}, THE DAMPING RATIO ξ TENDS TO ZERO AND THE SYSTEM BECOMES UNSTABLE.

is -180^{o}, for values of GH less than unity at this point, and the magnitude of GH for values greater than unity at $\omega_{\pi}=-180^{\circ}$.

$$\text{i.e. Gain Margin } G_M = \frac{1}{\left|GH(i\omega_{\pi})\right|} \qquad (5.20)$$

$$\text{if } \left|GH(i\omega_{\pi})\right| < 1.$$

$$\text{and Gain Margin } G_M = \left|GH(i\omega_{\pi})\right| \qquad (5.21)$$

$$\text{if } \left|GH(i\omega_{\pi})\right| > 1.$$

where $\arg.GH(i\,\omega_{\pi})=-180^{\circ}$ and ω_{π} is called the phase crossover frequency.

For the conditionally stable case here, there are two phase crossover frequencies determining the relative stability. The lower phase crossover frequency, $\omega_{\pi 1}$, is at 14.8kHz, and the upper, $\omega_{\pi 2}$, at 8.4MHz.

From figure 5.10, it can be seen that, at values of G close to 10^{8}, it is the lower phase crossover frequency which dominates, and the margin of stability is determined by $GH(i\,\omega_{\pi 1})$. At values above a few times 10^{8} the gain margin is determined by $GH(i\,\omega_{\pi 2})$. The value of gain where the stability influence crosses from $\omega_{\pi 1}$ to $\omega_{\pi 2}$ occurs at $1.13\ .10^{8}$.

Figure 5.11 shows the variation in gain margin as a function of gain. The range of gain over which the system is stable is ~ 60 (36dB). At its most stable position G can be varied by 18dB before becoming unstable. The point of maximum stability is at $9\ .10^{8}$. The gain margin for a gain of $G=10^{9}$ is indicated on figure 5.8, the graph of open loop transfer function.

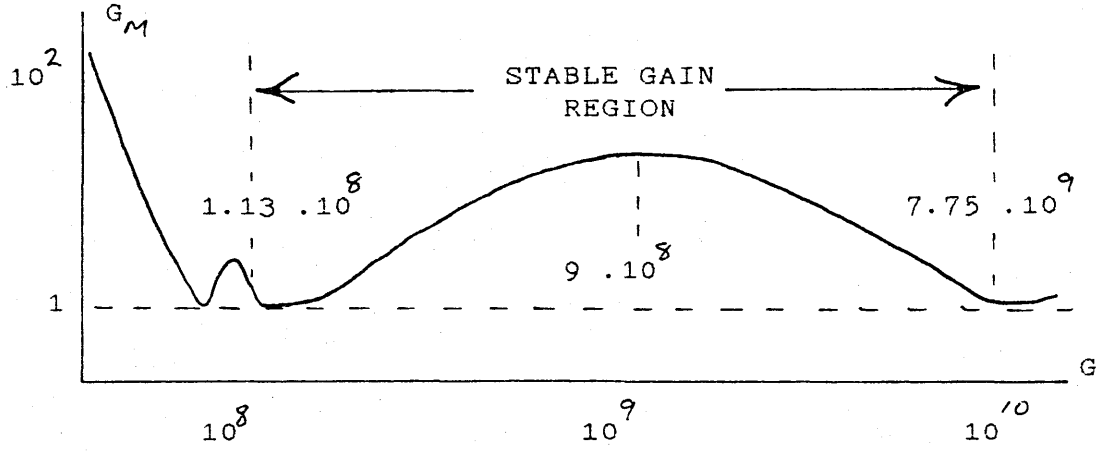

FIG. 5.11 SCHEMATIC GRAPH OF GAIN MARGIN G AS A FUNCTION OF GAIN G.

Another definition of relative stability, introduced by Bode, is the phase margin ϕ_{PM}. and is defined as 180° plus the phase angle ϕ_1 of the open loop transfer function at unity gain.

i.e. $\phi_{PM} = [180^\circ + \arg.GH(i\omega_1)]$ degrees. (5.22)

where $|GH(i\omega_1)| = 1$, and ω_1 is called the gain crossover frequency, or unity gain frequency.

At $G=10^9$, the unity gain frequency is 2MHz and $\arg.GH(i\omega_1)=-90^\circ$. So, the phase margin at a gain of 10^9 is $\phi_{PM}(G=10^9)=90^\circ$.

When the phase angle is zero, the system becomes unstable.

A graph of the phase angle of GH against frequency is shown in figure 5.12. The phase reaches its maximum value of $\sim 290^\circ$ at around 2kHz. The phase margin for a gain of 10^9 is indicated on the graph.

The amount of gain and phase margins required, depend on the particular application and running environment, but, for interest, it is noted that Bode

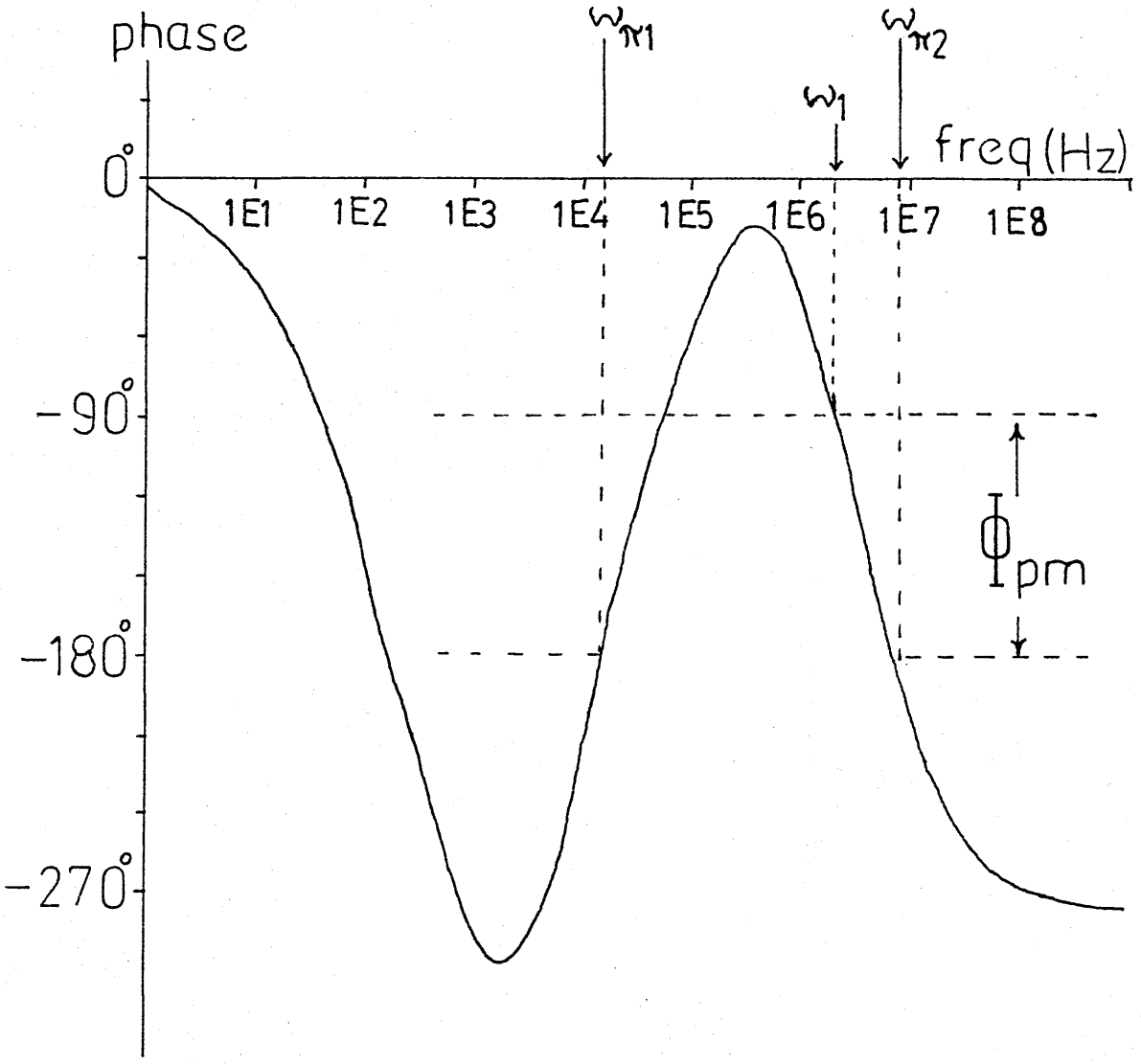

FIG.5.12: GRAPH OF PHASE ANGLE OF GH AGAINST FREQUENCY, FOR A GAIN OF 10^9. INDICATED ON THE GRAPH ARE THE UPPER AND LOWER PHASE CROSSOVER FREQS.($\omega_{\pi 1}$ & $\omega_{\pi 2}$), THE UNITY GAIN FREQUENCY (ω_1) AND THE PHASE MARGIN (Φ_{pm}).

suggests a gain margin of 9dB and a phase margin of 30° for amplifiers operating in the audio region.

As the overall gain of the system is desired to be as high as possible, for optimum frequency stabilisation, it is likely that the upper instability point will be most important in determining the stability of the system. One factor, which may lead the system to oscillation, is a long term drift in the absolute light level, which may change the overall gain of the servo loop sufficiently to make it unstable. For long operating times then, it may be advisable to make the gain independent of light intensity. This is fairly easily accomplished by the addition of some simple, extra circuitry.

The main limitation to performance, of this present system, is the requirement that the system be initially locked with the PZT alone. This means that the transfer function has to pass through the PZT resonant frequency at $\sim$6dB/octave. One method of improving performance then, would be to increase the rate of roll-off of the transfer function, around the PZT resonant frequency, to allow greater low frequency gain to be achieved. This would result, however, in a system difficult to lock with the PZT alone, but the extra time constants, necessary to increase the transfer function gradient, could be introduced by either a manual, or electronic, switch. Alternatively the system could be run without the possibility of stabilisation by PZT alone.

This system then, in conclusion, has shown to be potentially as good as those with intra-cavity devices, and

will be valuable at a time when laser power is at a premium, and detector sensitivity is limited by photon noise.

As the detector sensitivity was not yet photon noise limited, the immediate concern was the further reduction of laser frequency noise, and this is tackled in the following two chapters.

CHAPTER 6.

"SYSTEM PERFORMANCE WITH OPTICAL RECOMBINATION"

6.1 INTRODUCTION.

At this stage in the development of the prototype detector, the sensitivity was still limited at the level of chapter 2. Having identified laser frequency fluctuations as a possible limiting noise source, experimental investigations followed the direction of the two frequency subtraction techniques mentioned in section 2.4(b). This chapter deals with the first of these: the subtraction of residual frequency fluctuations by optical interference of the cavity output beams.

6.2 RECOMBINATION TECHNIQUE.

The amount of frequency noise subtraction is dependent on the symmetry of the slopes of the two cavity fringe profiles which, in turn, are mainly dependent on the finesse of the cavities. If the intensity of light in each cavity, and the visibility in each cavity, are the same then, from 2.29, the amount of subtraction obtainable, in principle, by this technique is given by a factor $\Delta F/F$, where F is the average finesse of the cavities and ΔF is the finesse difference between them. An additional improvement to sensitivity may be obtainable if the fringe contrast of the recombined output beam is greater than that of the individual cavity beams.

To reduce the amount of loss, and to improve the visibility of the fringes, the cavity mirrors were replaced with a set whose input couplers were 98% reflective. This reduced the cavity finesse from the chapter 3 figure of 600 to around 250 and improved the cavity visibility to close to 65% at best, and seldom less than 40%.

To examine the potential of the technique, the first experiments involved stabilising both cavities in the normal manner (with 10% of the output light) and observing error point signals derived from the stabilisation loop used in subsequently recombining the beams (which contain the remaining 90% of the output light). This allowed the easiest demonstration of the feasibility of the method.

With the primary and secondary cavities stabilised in the usual way, the output beams were recombined using the central mass area of the detector as a small Michelson interferometer. Figure 6.1, illustrating the arrangement, shows the central test masses along with the optical elements relevant to the recombination. Shown, on the central mass, are two phase modulators. The one through which the input beam passes was originally intended to apply the (24MHz) phase modulation for cavity stabilisation but, as this was applied by a modulator outside the vacuum tank, it was initially used, together with the output modulator, to alter the relative phase difference between the two orthogonal beam components, and so stabilise the Michelson interferometer.

The input beam has its electric vector defined by the input polariser such that the light entering each

FREQUENCY NOISE SUBTRACTION BY OPTICAL RECOMBINATION.

When sensitivity is limited by residual frequency errors in the laser cavity stabilisation loop, some improvement may be obtained by optical recombination of the two output cavity beams. Two cases are described in the text: subtraction at high frequencies and subtraction at low frequencies.

HIGH FREQUENCY CASE: In this arrangement the primary and secondary cavities are stabilised as described in chapter 2. As the unity gain point of the secondary cavity loop is around 8kHz, the cavity is effectively uncontrolled at frequencies above this. This means that any relative length changes in the cavity, at frequencies above 8kHz, will appear as direct phase change signals at the output of the recombining Michelson interferometer. At these frequencies the interference null is maintained by utilising the output phase modulator to alter the relative phase difference of the output beams. The resultant high frequency sensitivity of the detector may be monitored by observation of the Michelson error point.

LOW FREQUENCY SUBTRACTION: Fluctuations in the length of the cavity below 8kHz are controlled by the servo system for the secondary cavity and so no relevant signal appears at the output of the Michelson. For the required signals to be seen there, this output has to be used to control the secondary cavity length. Unfortunately, this output also contains a large low frequency signal relevant only to the Michelson interferometer, and this part is not suitable for feeding back to the secondary cavity. Thus, a hybrid signal has to be used, derived from the secondary cavity at low frequencies and from the Michelson output at higher frequencies. With the secondary cavity controlled by this combined signal, it provides a suitable measure of the detector sensitivity with frequency subtraction.

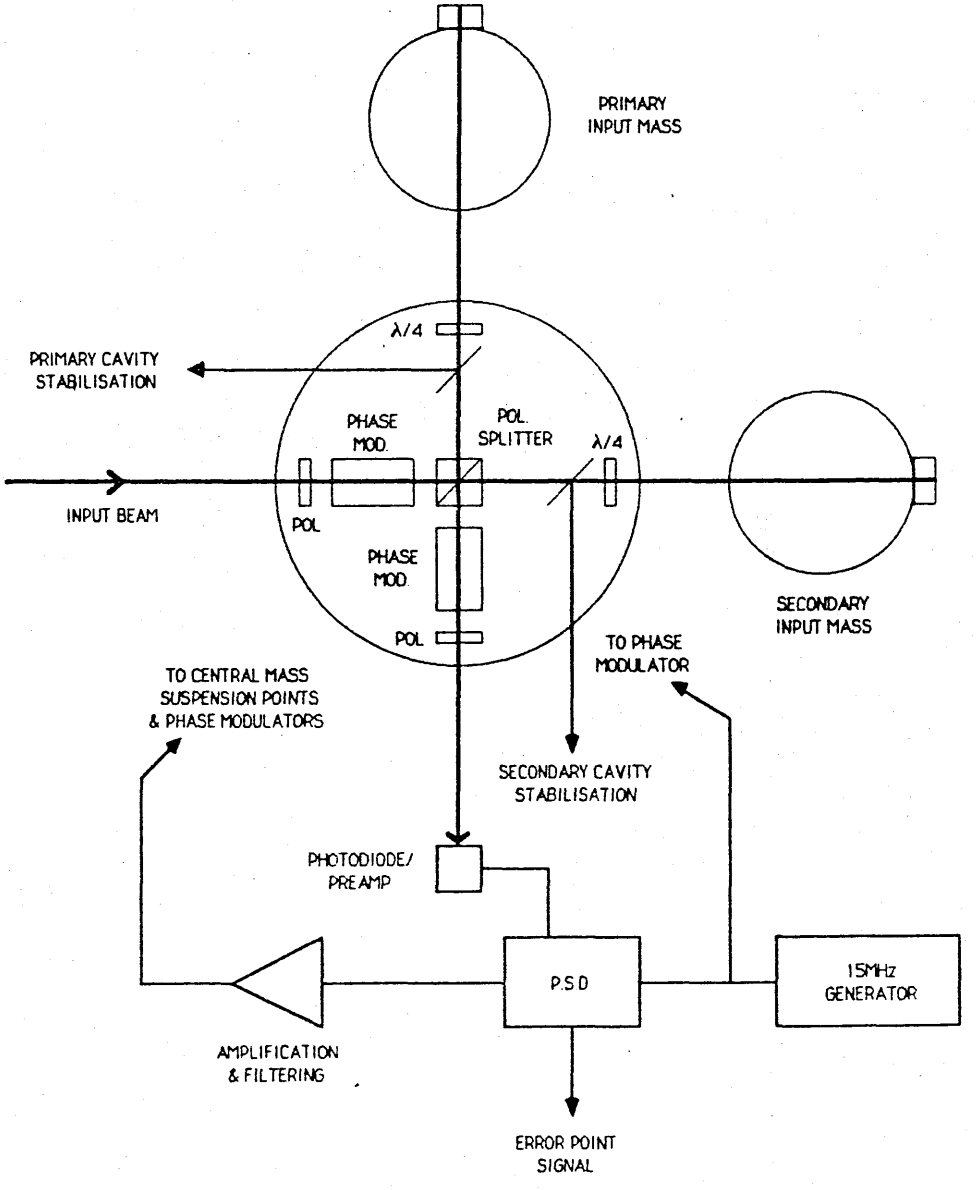

FIG. 6.1 CENTRE MASS MICHELSON ARRANGEMENT
FOR OPTICAL RECOMBINATION

cavity is split evenly. Phase modulation is applied, at 15MHz, to the light returning from the cavities by the output phase modulator. The output polariser is orientated at 45^{o} to the orthogonal electric vectors of the output beams for the recombination of these components (- see figure 2.1). The output light is coherently detected, and the error point signal obtained is a measure of the relative phase difference between the beams in each arm of the Michelson. The interfered output is stabilised to a null by feeding back to one, or both, phase modulators to alter the phase difference between the beams. The modulators used for this purpose are 4-crystal cells (Gsanger, Munich) which allow for differential modulation of the two light components. Some of the low frequency part of the feedback signal is applied (suitably amplified and filtered) to bimorph PZT pushers acting on the central mass, along the axes of the interferometer, to damp the low frequency motion of the mass.

A block diagram of the feedback cicuit for the Michelson loop is shown in figure 6.2. the photodiode/preamplifier is similar in design to that of figure 5.2. Tuned for 15MHz, it was intended to operate with a higher light output on the photodiode (type FND 200), and had a bandwidth of a few Megahertz. The circuit was operated with a typical d.c gain of $\sim 10^{5}$. The transitional integration (160Hz-240Hz) onto either side of the phase modulator was used to produce more stable operation. The signal to the PZT pushers was taken off after the PAR 113 amplifier, and fed through a driving

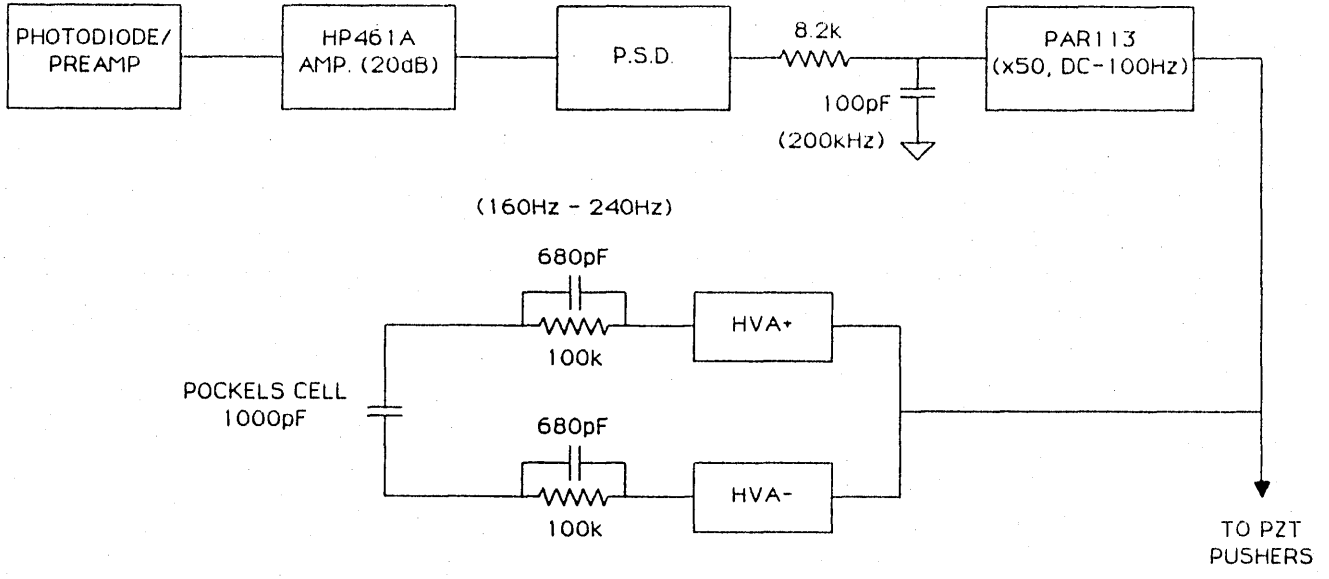

FIG.6.2 : BLOCK DIAGRAM OF MICHELSON FEEDBACK LOOP

amplifier (similar to that of fig. 2.4) and a high voltage amplifier.

6.3 SYSTEM OPERATION WITH POST-CAVITY MODULATION.

The Michelson loop was intially stabilised by feeding back to the output phase modulator only. The Michelson interferometer proved difficult to lock for long periods of time (>few minutes) and, although evidence for frequency subtraction was observed, the amount of subtraction was variable.

Figure 6.3 shows comparitive spectra of error point measurements from the secondary cavity p.s.d. output (normal high freq. sensitivity point) and the output from the Michelson p.s.d.. The two calibration peaks shown are a displacement peak, injected by the piezoelectric cavity mirror in the primary arm, and a frequency peak, injected onto the laser via the intra-cavity modulator. The amount of subtraction of the frequency peak is $\sim$ 5dB, and this is also the typical amount of subtraction over the background region. These were the best spectra obtained at this time.

In general, the level of background noise was variable and, although subtraction of the peak was observed fairly consistently, subtraction of the background noise was not always discernable. As the level of noise from the secondary cavity p.s.d., with the Michelson loop unlocked, did not vary, this suggested that the Michelson loop may have been introducing an extra noise source of varying severity.

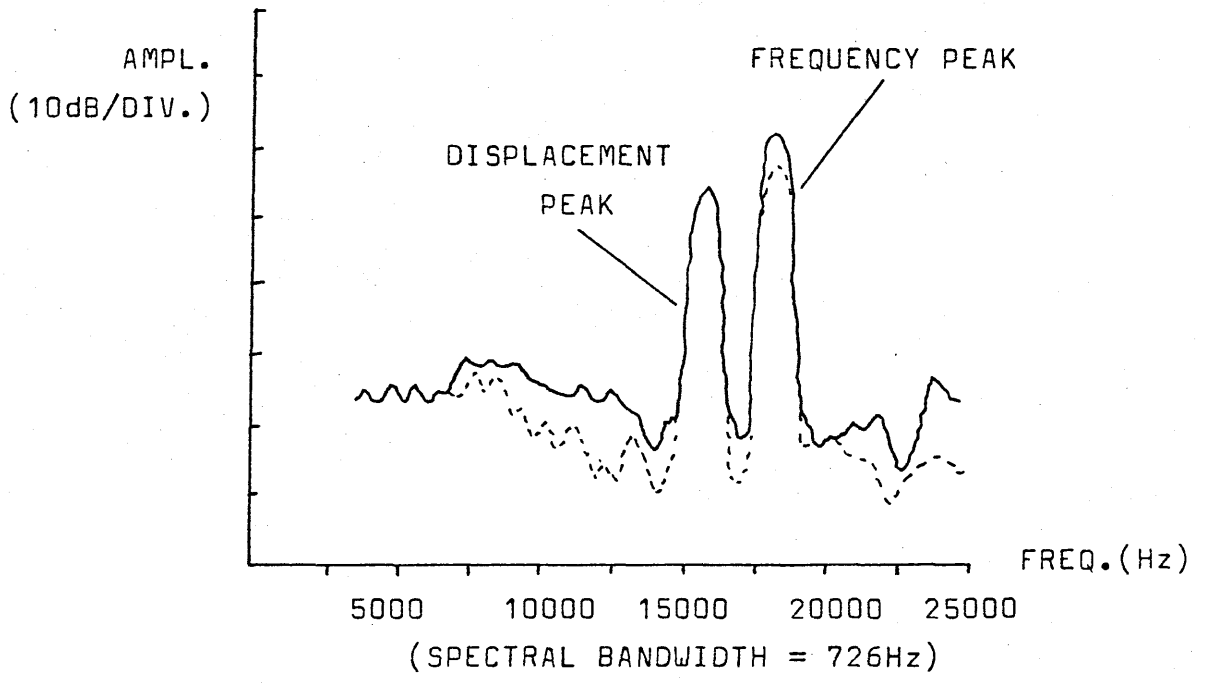

FIG.6.3: COMPARATIVE SPECTRA OF ERROR POINT SENSITIVITY MEASUREMENTS. (SOLID CURVE: SECONDARY CAVITY ERROR POINT, AND DOTTED CURVE: MICHELSON ERROR POINT). BOTH THE FREQUENCY PEAK AND THE BACKGROUND HAVE BEEN REDUCED BY $\sim$ 5dB. THE DISPLACEMENT PEAK IS INDUCED BY A MASS MOTION OF 1.6 $.10^{-13}_{m}$ r.m.s.

By measurement of the size of the "r.f." fringe signals, it was discovered that the finesses of the two cavities had become unbalanced by a factor of two, possibly due to a deterioration in the quality of one, or more, cavity mirrors. This meant that, to improve the amount of subtraction, a method had to be found whereby the gradients of the cavity fringes could be altered. This situation is apparent in the following analysis.

6.4 TUNING CONSIDERATIONS OF OPTICAL RECOMBINATION WITH DIFFERENT MODULATION SCHEMES.

(a) POST-CAVITY MODULATION.

If the phase offset in the overall interferometer is given by px in the primary arm and qx in the secondary arm, then, the component amplitudes in the Michelson can be broken down as follows:

Primary Arm:

$$\text{Amplitude from Michelson} = A_{01}\, e^{i\omega t} \qquad (6.1)$$

$$\text{Amplitude from cavity} = -A_{c1}\, e^{ipx}\, e^{i\omega t} \qquad (6.2)$$

Secondary Arm:

$$\text{Amplitude from Michelson} = -A_{02}\, e^{i\omega t} \qquad (6.3)$$

$$\text{Amplitude from cavity} = A_{c2}\, e^{iqx}\, e^{i\omega t} \qquad (6.4)$$

Applying differential phase modulation to the light at a frequency ω_m, on return from the cavities and before recombination, produces amplitude fields:

$$\text{Primary:} \quad (A_{01} - A_{c1}\, e^{ipx})\,\text{expi}(\omega t + \phi_m \sin\omega_m t) \qquad (6.5)$$

$$\text{Secondary:} \quad (-A_{02} + A_{c2}\, e^{iqx})\,\text{expi}(\omega t - \phi_m \sin\omega_m t) \qquad (6.6)$$

On recombination, the total field is

$$E_{TOT} = e^{i\omega t}[A_{01}\,\mathrm{expi}(\phi_M \sin\omega_M t) - A_{02}\,\mathrm{expi}(-\phi_M \sin\omega_M t) - A_{C1}\,\mathrm{expi}(px+\phi_M \sin\omega_M t) + A_{C2}\,\mathrm{expi}(qx-\phi_M \sin\omega_M t)] \quad (6.7)$$

Multiplying E_{TOT} by its complex conjugate, E^*_{TOT}, and letting $\alpha = \phi_M \sin\omega_M t$, $\beta = px$, $\gamma = qx$, gives the intensity at the output.

$$I_{OUT} = A_{01}^2 + A_{C1}^2 + A_{02}^2 + A_{C2}^2 - 2A_{01}A_{02}\cos 2\alpha - 2A_{01}A_{C1}\cos 2\beta - 2A_{02}A_{C2}\cos 2\gamma + 2A_{02}A_{C1}\cos(\beta+2\alpha) + 2A_{01}A_{C1}\cos(\gamma-2\alpha) - 2A_{C2}A_{C1}\cos(\beta+2\alpha-\gamma) \quad (6.8)$$

Assuming α, β, γ are all small, subsequent demodulation produces

$$I_{OUT}(\mathrm{demod}) = K_1[px(A_{C1}A_{C2} - A_{C1}A_{02}) - qx(A_{C1}A_{C2} - A_{01}A_{C2})] \quad (6.9)$$

where K_1 is a constant.

Optimum performance (i.e. perfect subtraction) implies

$$p(A_{C2}A_{C1} - A_{C1}A_{02}) = q(A_{C2}A_{C1} - A_{01}A_{C2}) \quad (6.10)$$

$$\text{i.e.} \quad \frac{p}{q} = \frac{1 - (A_{01}/A_{C1})}{1 - (A_{02}/A_{C2})} \quad (6.11)$$

From 4.31, $$(A_{C1}/A_{01}) = [1 \pm (1-V_1)^{1/2}] \quad (6.12)$$

and $$(A_{C2}/A_{01}) = [1 \pm (1-V_2)^{1/2}] \quad (6.13)$$

Thus, the only way of tuning the amount of subtraction is to tune A_{C1}/A_{01}, A_{C2}/A_{02} - i.e. alter the visibilities of the cavity fringes. This is obviously undesirable as it degrades the sensitivity of the interferometer.

(b) PRE-CAVITY MODULATION.

With the availability of the input phase modulator on the central mass, it was also possible to phase modulate the light before it enters the cavities. Then the component fields are given by:

Primary Arm:

$$\text{Amplitude from Michelson} = A_{01}\,\text{expi}(\omega t+\phi_m \sin\omega_m t) \quad (6.14)$$

$$\text{Amplitude from cavity} = -A_{c1}\,\text{expi}(\omega t+px) \quad (6.15)$$

Secondary Arm:

$$\text{Amplitude from Michelson} = -A_{02}\,\text{expi}(\omega t-\phi_m \sin\omega_m t) \quad (6.16)$$

$$\text{Amplitude from cavity} = A_{c2}\,\text{expi}(\omega t+qx) \quad (6.17)$$

Then,

$$E_{TOT} = e^{i\omega t}\,[A_{01}\,\text{expi}(\phi_m \sin\omega_m t)-A_{c1}\,\text{expi}(px) - A_{02}\,\text{expi}(-\phi_m \sin\omega_m t)+A_{c2}\,\text{expi}(qx)] \quad (6.18)$$

This produces a demodulated output signal

$$I_{OUT}(\text{demod}) = K_2[px(A_{01}A_{c1}+A_{c1}A_{02})-qx(A_{01}A_{c2}+A_{02}A_{c2})] \quad (6.19)$$

where K_2 is a constant.

For an output null,

$$\frac{p}{q} = \frac{A_{01}A_{c2}+A_{02}A_{c2}}{A_{01}A_{c1}+A_{c1}A_{02}} = \frac{A_{02}}{A_{01}} \cdot \frac{[1 \pm (1-V_2)^{1/2}]}{[1 \pm (1-V_1)^{1/2}]} \quad (6.20)$$

So with pre-cavity modulation, the amount of subtraction can be tuned, without altering the cavity visibilities, by adjusting the relative intensity of light entering each cavity.

6.5 SYSTEM OPERATION WITH PRE-CAVITY MODULATION.

To investigate the potential tuning capabilities of the pre-cavity modulation scheme, the 15MHz drive was applied to the input phase modulator, and the input polariser was mounted on a motorized optical mount which could be rotated, in the vertical plane, from outside the

vacuum tank. This latter step allowed the relative intensity of light entering each arm of the interferometer to be conveniently altered.

As with the post-cavity modulation scheme, the Michelson loop had a tendency to oscillate and, in general, would lock for only short periods of time, although some improvement was obtained by feeding back to both the input and output phase modulators. The system stability proved to be critically dependent on the orientation of the optic axis of the input phase modulator with respect to that of the central polarising beamsplitter. For differential modulation of orthogonal light components, the axis of the modulator was set at 45^{o} to that of the central splitter. Any slight offset resulted in amplitude modulation of the light at 15MHz which severely degraded the level of the output error signal.

With careful adjustment of the input polariser, however, the amount of frequency noise subtraction was demonstrated to be tunable. Figure 6.4 shows the best amount of subtraction that was obtained in these experiments. The artificial frequency peak has been reduced by $\sim$ 12dB, as has the background noise level. This is an improvement of $\sim$7dB over the best performance achieved with the post-cavity modulation scheme.

This level of performance was untypical, however, as instabilities in the Michelson loop tended to introduce extraneous noise into the system which often dominated the frequency noise background.

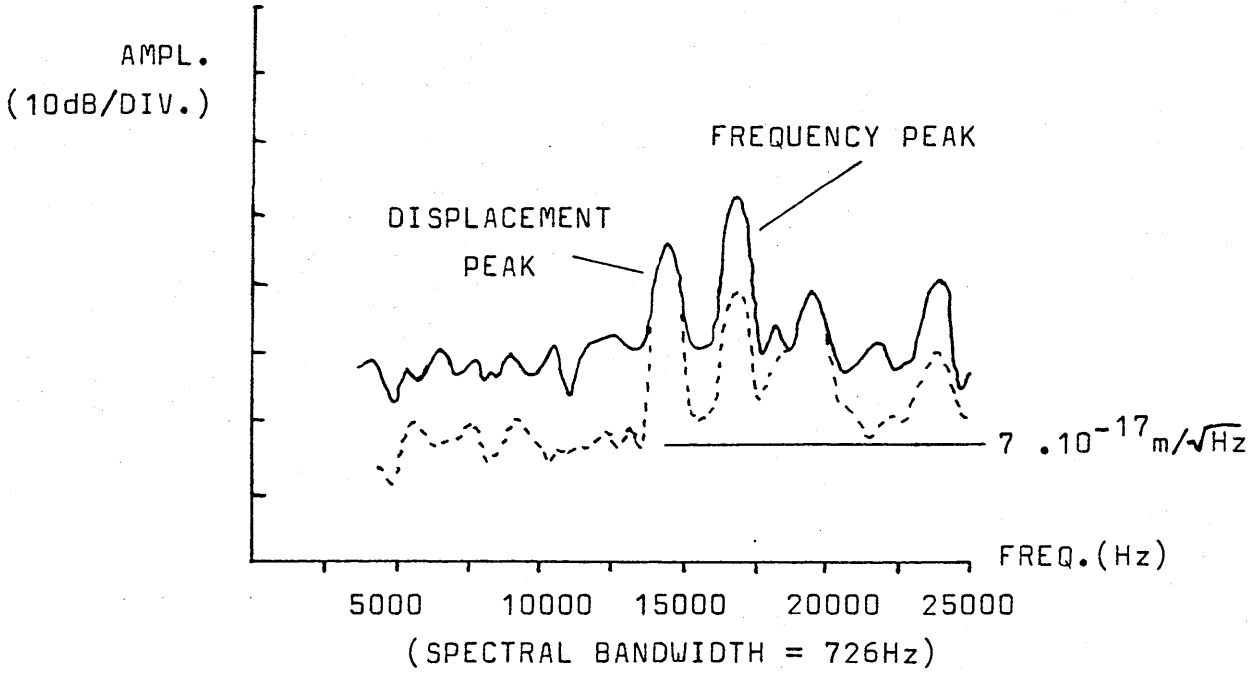

FIG.6.4.: COMPARATIVE SPECTRA OF ERROR POINT SENSITIVITY MEASUREMENTS USING THE PRE-MODULATION SCHEME. (SOLID CURVE: SECONDARY CAVITY ERROR POINT, AND DOTTED CURVE: MICHELSON ERROR POINT). BOTH PEAK AND BACKGROUND HAVE BEEN REDUCED BY $\sim$12dB.

6.6 SUBTRACTION TECHNIQUE AT LOW FREQUENCIES.

To examine the potential of optical subtraction in the frequency range covering 1kHz, it was necessary to derive a locking signal for the secondary cavity from the recombined output. The recombined output signal, however, contains a large amount of information about the low frequency motion of the Michelson interferometer (- due mainly to the relative 1Hz motions of the central, and input, test masses). To prevent this signal from corrupting the locking signal necessary to stabilise the secondary cavity, the overall signal was obtained from a combination of the high frequency part of the Michelson signal and the low frequency part of the normal secondary stabilisation signal (from the secondary p.s.d.). If the cross-over frequency, between the two signals, is arranged to be much less than 1kHz, then it should be possible to observe subtraction of frequency noise in the spectral range above this, covering 1kHz. This is represented in the schematic diagram of figure 6.5.

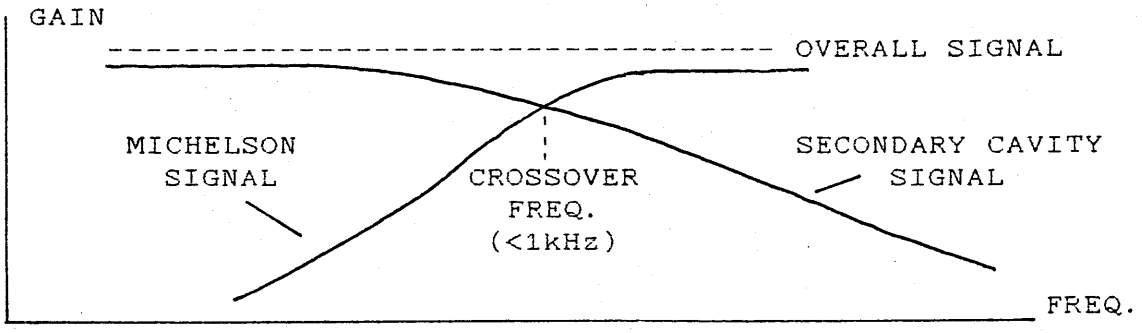

FIG. 6.5 SCHEMATIC REPESENTATION OF THE GAIN/FREQ. CONTRIBUTIONS TO COMBINED LOCKING OF THE SECONDARY CAVITY.

The Michelson contribution to the locking signal was

obtained by summing parts of the Michelson error point and feedback signals. This resulted in a signal which gave a suitable measure of the phase deviations of the (off-resonance) light in the secondary cavity.

The circuit diagram of the electronic arrangement, used to combine the Michelson, and secondary cavity, signals is shown in figure 6.6. The Michelson error point signal is taken off after the p.s.d and the 200kHz integration. The Michelson feedback signal is taken from one side of a phase adjusting modulator on the central mass.

To ease the acquisition of lock of the secondary cavity, the relative gains of the signals, represented in fig.6.5, could be adjusted such that the overall response was almost entirely made up of the normal secondary cavity stabilisation signal. This could be achieved by adjusting the 1kΩ "combining" potentiometer shown in figure 6.6. Once the cavity had been stabilised, the gains could be readjusted such that the crossover frequency was once more below 100Hz or so. As the level of the overall signal is undisturbed, cavity resonance should be capable of being maintained.

6.7 LOW FREQUENCY SUBTRACTION PERFORMANCE.

While the secondary cavity locked well when the combined stabilisation signal was dominated by the normal cavity signal, it proved extremely difficult to maintain lock with the combined Secondary/Michelson signal. Typical

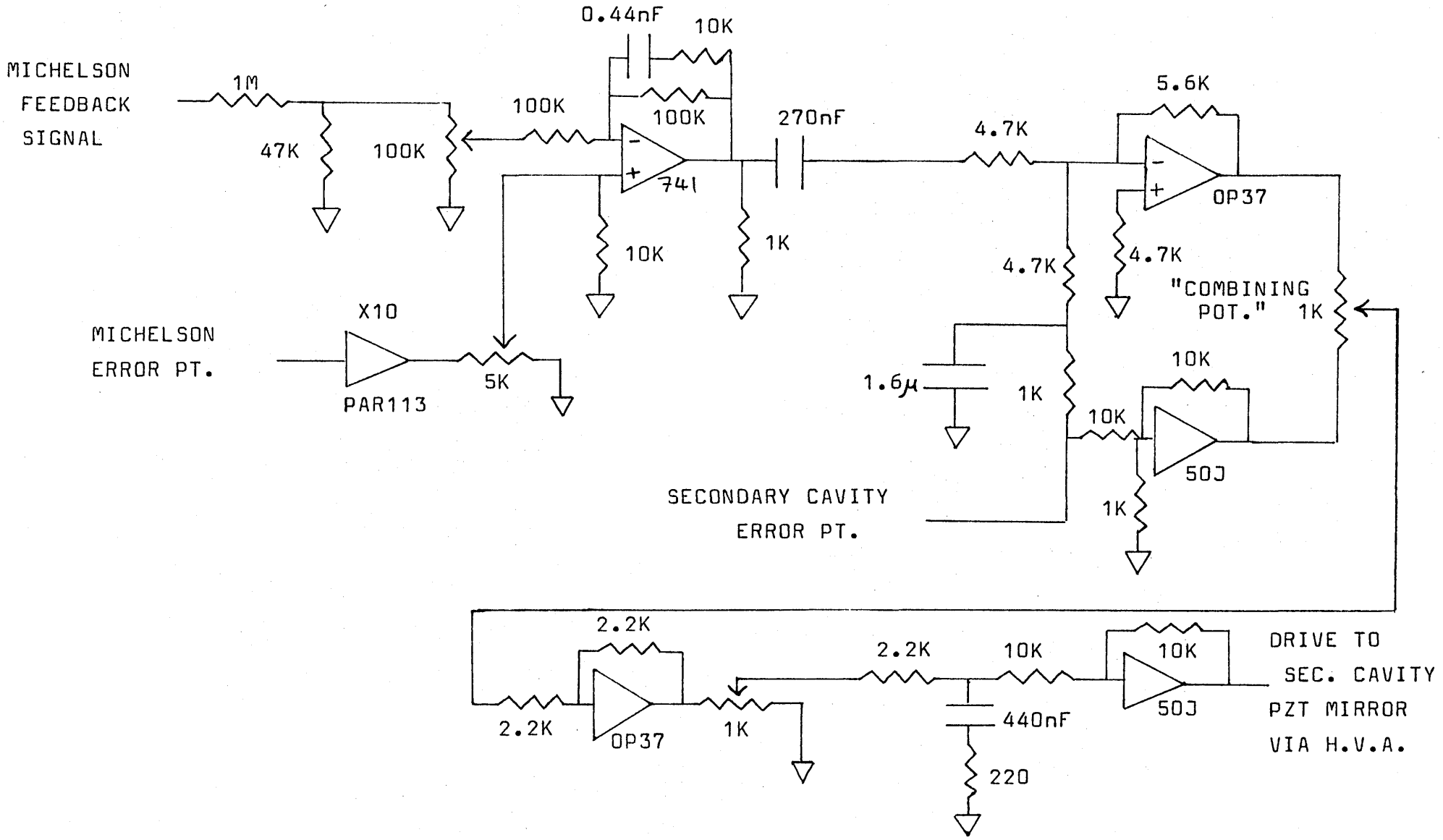

FIG.6.6: "COMBINATION" CIRCUIT USED TO STABILISE SECONDARY CAVITY FOR LOW FREQUENCY SUBTRACTION.

locking periods achieved were no longer than a few seconds at a time. Consequently, it was difficult to investigate the low frequency subtraction performance of the combined output, as most effort was spent on trying to improve the stability of the system. Figure 6.7 shows one of the few sensitivity spectra comparisons that was obtained during one of the short locking periods. Both spectra are measures of the feedback signals used to maintain cavity resonance from the different outputs. As can be seen, the background noise, when the cavity is locked with the combined signal, is a few decibels higher than with the normal stabilisation signal. The noise difference is especially noticable below 500Hz. While the background noise continued to be slightly greater with the combined signal, some reduction in the size of an artificially induced frequency peak was observed.

The reason for the poor sensitivity performance with the recombined output, here, was probably due to the influence of an extraneous noise source (possibly excess amplitude modulation introduced by the electro-optic modulator), similar to that often observed in the high frequency subtraction case, that dominated the Michelson signal, and, as a result, degraded the recombined output sensitivity.

Both pre-cavity, and post-cavity, modulation schemes were tried in an attempt to improve the stability of the combined locking loop, but no real improvement was discernable.

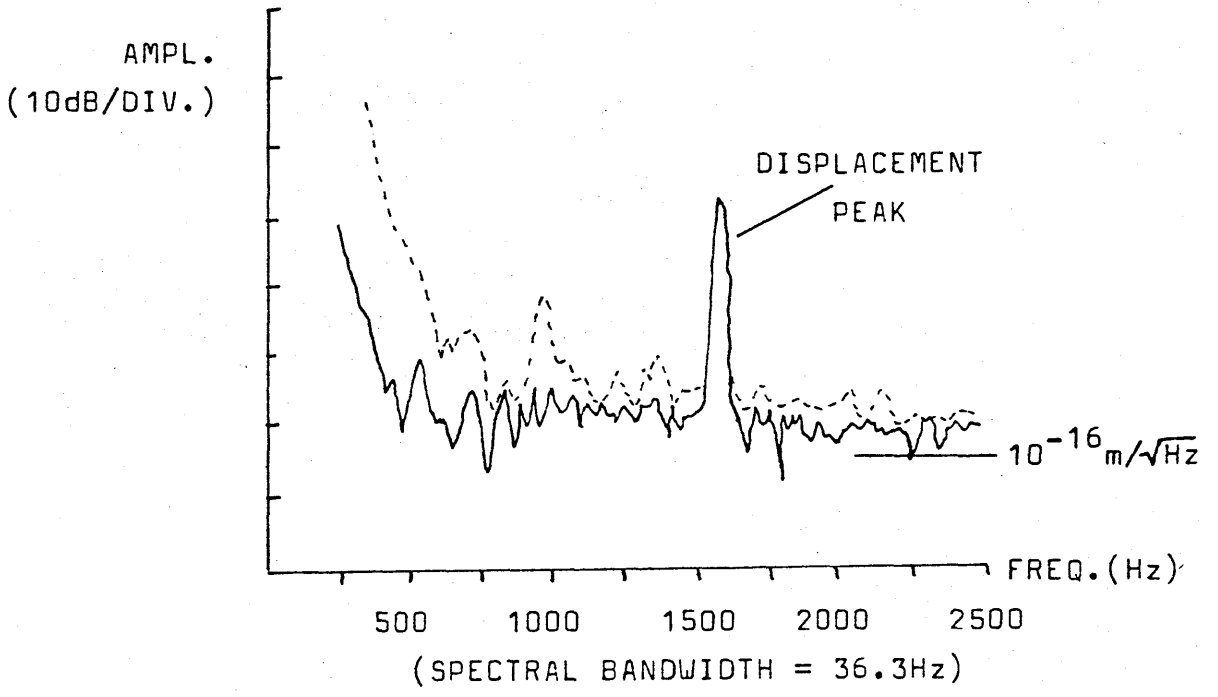

FIG.6.7: COMPARATIVE SPECTRA OF LOW FREQUENCY SENSITIVITY MEASUREMENTS TAKEN DURING ONE OF THE SHORT LOCKING PERIODS. (SOLID CURVE: SECONDARY CAVITY FEEDBACK SIGNAL USING NORMAL 10% OUTPUT, AND DOTTED CURVE: SECONDARY CAVITY FEEDBACK SIGNAL WHEN MOST OF THE LOCKING SIGNAL (> 100Hz) IS DERIVED FROM THE MICHELSON OUTPUT).

6.8 LOCKING OFFSET CONSIDERATIONS.

The instabilities, associated with the Michelson loop, may have been due, in part, to an inability of the Michelson servo to cope with (fast) offsets from its null locking point. This is revealed in an extension to the analysis of section 6.4.

If there exists a fast locking error, ϕ_o, in the Michelson interferometer, in a similar direction (say) to that of a fast cavity offset px, then equations 6.1 to 6.4 become

POST-CAVITY MODULATION

Primary Arm:

$$\text{Amplitude from Michelson} = A_{o1}\,\text{expi}(\omega t+\phi_o) \qquad (6.21)$$

$$\text{Amplitude from cavity} = -A_{c1}\,\text{expi}(\omega t+px+\phi_o) \qquad (6.22)$$

Secondary Arm:

$$\text{Amplitude from Michelson} = -A_{o2}\,\text{expi}(\omega t-\phi_o) \qquad (6.23)$$

$$\text{Amplitude from cavity} = A_{c2}\,\text{expi}(\omega t+qx-\phi_o) \qquad (6.24)$$

Following the method of section 6.4, applying differential phase modulation before recombination, and subsequently demodulating the recombined output, produces signal components as functions of ϕ_o, px and qx.

$$I_{OUT}(\text{demod}) = K_1[2I_1\phi_o + I_2 px + I_3 qx] \qquad (6.25)$$

where $I_1=(A_{o1}A_{o2}-A_{o1}A_{c2}-A_{c1}A_{o2}+A_{c1}A_{c2})$, $I_2=(A_{c2}A_{c1}-A_{c1}A_{o2})$, and $I_3=(A_{o1}A_{c2}-A_{c2}A_{c1})$.

Assuming $A_{o1} > A_{c1}$, $A_{o2} > A_{c2}$, and using 4.31 implies, for visibilities less than unity,

$$I_1 = [(1-V_1)^{1/2}(1-V_2)^{1/2}].A_{o1}A_{o2}$$

$$= (1-V).A_{o1}A_{o2} \quad (\text{letting } V_1 = V_2 = V) \qquad (6.26)$$

$$I_2 = [(1-V_1)^{1/2}(1-V_2)^{1/2} - (1-V_1)^{1/2}].A_{01}A_{02}$$

$$= [(1-V) - (1-V)^{1/2}].A_{01}A_{02} \qquad (6.27)$$

and $$I_3 = [(1-V_1)^{1/2} - (1-V_1)^{1/2}(1-V_2)^{1/2}].A_{01}A_{02}$$

$$= [(1-V)^{1/2} - (1-V)].A_{01}A_{02} \qquad (6.28)$$

Inspection of 6.26, 6.27 and 6.28 reveals that I_1 and I_3 will always be positive, whereas I_2 will always be negative. This implies that, in order to compensate for the locking offset ϕ_0, the Michelson servo has to oppose px and qx (and vice versa).

For frequencies within the bandwidth of the secondary cavity loop, px and qx may be assumed to be small (i.e. cavities on resonance). Any trouble will arise for ϕ_0, px and qx at frequencies greater than the secondary loop bandwidth (but less than the bandwidth of the Michelson loop). Thus if the Michelson servo has the correct sign (negative) to compensate for ϕ_0, and px is of significant magnitude, positive feedback for px will result, and the loop will become unstable at that frequency. This would result in a system which had a tendency to oscillate, and it would also limit the bandwidth of the Michelson loop.

Similarly,

PRE-CAVITY MODULATION.

$$I_1 = (2A_{01}A_{02} - A_{01}A_{C2} - A_{C1}A_{02})$$

$$= [(1-V_2)^{1/2} + (1-V_1)^{1/2}].A_{01}A_{02} = 2(1-V)^{1/2}.A_{01}A_{02} \qquad (6.29)$$

- always positive.

$$I_2 = -(A_{01}A_{C1} + A_{C1}A_{02}) \text{ -always negative.} \qquad (6.30)$$

$$I_3 = (A_{01}A_{C2} + A_{02}A_{C2}) \text{ -always positive.}$$

Both modulation schemes are equally sensitive to a

fast locking offset, in that the relative sizes of I_1 to I_2, I_3 are similar for comparable values of visibility. However, with increasing visibility I_1/I_2, I_1/I_3 decrease, reducing the sensitivity of the servo loop to ϕ_0.

(The experiments in this chapter were performed with typical cavity visibilities of ~ 0.4).

6.9 CONCLUSIONS.

The recombination experiments were characterized by instabilities in the Michelson servo loop. Some of this trouble may be attributable to conflicting error signals in the Michelson loop when fast fluctuations from the locking point are present. This may partially explain the oscillatory tendencies of the loop, and the restrictive locking periods.

Subtraction of a residual frequency noise background was seen at high frequencies ($\sim$ 10-25kHz) with an improvement of $\sim$ 12dB being observed.

Using the combined output, and the low frequency (>100Hz) component of the original secondary feedback signal, to simultaneously control both the Michelson interferometer and the secondary cavity proved difficult. No subtraction of residual background frequency noise was demonstrated, over the kilohertz region, due mainly to the introduction of excess noise by the (unstable) Michelson loop.

To achieve a definite and reliable improvement, in this region, it will probably be necessary to minimise

servo locking errors in the Michelson by improving cavity visibility and introducing a separate servo loop (using an extra He-Ne laser, perhaps) to maintain the Michelson interferometer in adjustment.

Residual frequency noise can also be diminished, however, by an alternative electronic technique, and this is examined in the following chapter.

CHAPTER 7.

"SYSTEM PERFORMANCE WITH ELECTRONIC SUBTRACTION OF FREQUENCY NOISE."

7.1 INTRODUCTION.

Instead of optically recombining the beams from the Fabry-Perot cavities and looking at the difference signal, it is possible to electronically subtract the photodiode signals obtained from each cavity, and use this signal to maintain the secondary cavity resonance. This is easier to do, as it requires no additional servo control, but some of the advantages of recombination are lost. -(For instance, with optical recombination some subtraction of intensity noise and beam geometry fluctuations are also potentially obtainable).

The principle of the technique is as follows: if the laser is stabilised, in frequency, to the primary cavity, to some level such that there is a remaining residual frequency error, $\Delta\nu$, between the primary cavity and the laser, then this excess frequency error also appears on the correction signal to the secondary cavity where it will set a limit to the sensitivity of the detector of $h \sim \Delta\nu/\nu$ (cf. section 2.2(b)). As the noise is common to both cavities, it will appear on both error signals from the two cavities. Assuming that the primary error signal is dominated by laser frequency noise (and not by electronic noise, say), then, when the primary error signal is subtracted from the secondary error signal, and the

difference used to stabilise the secondary cavity, the sensitivity limit due to frequency noise will be reduced by the factor of the subtraction, G.

7.2 EXPERIMENTAL ARRANGEMENT.

To make more use of the available light power, the 10% beamsplitters, on the central mass, were replaced by polarisation beamsplitters so that all of the light, returning from the primary and secondary cavities, could be taken to their respective photodiodes. To enable them to take light powers of up to $\sim$ 30mW, the photodiode/preamplifiers, for primary and secondary stabilisation, were correspondingly upgraded. The phase modulators, used for optical subtraction, were removed from the central mass to simplify the mechanical structure.

The arrangement is shown in figure 7.1. Also, shown is the differential amplifier (PAR 113) used to subtract the error point signals. The common mode rejection of this amplifier allows for a potential noise subtraction of greater than 40dB. The 5kΩ "combining" potentiometer allowed the relative sizes of the error point signals to be adjusted for optimum subtraction. After the differential amplifier, the signal was fed to the secondary cavity PZT through the remainder of the secondary loop electronics.

7.3 SUBTRACTION PERFORMANCE.

The stability of the secondary cavity, when locked

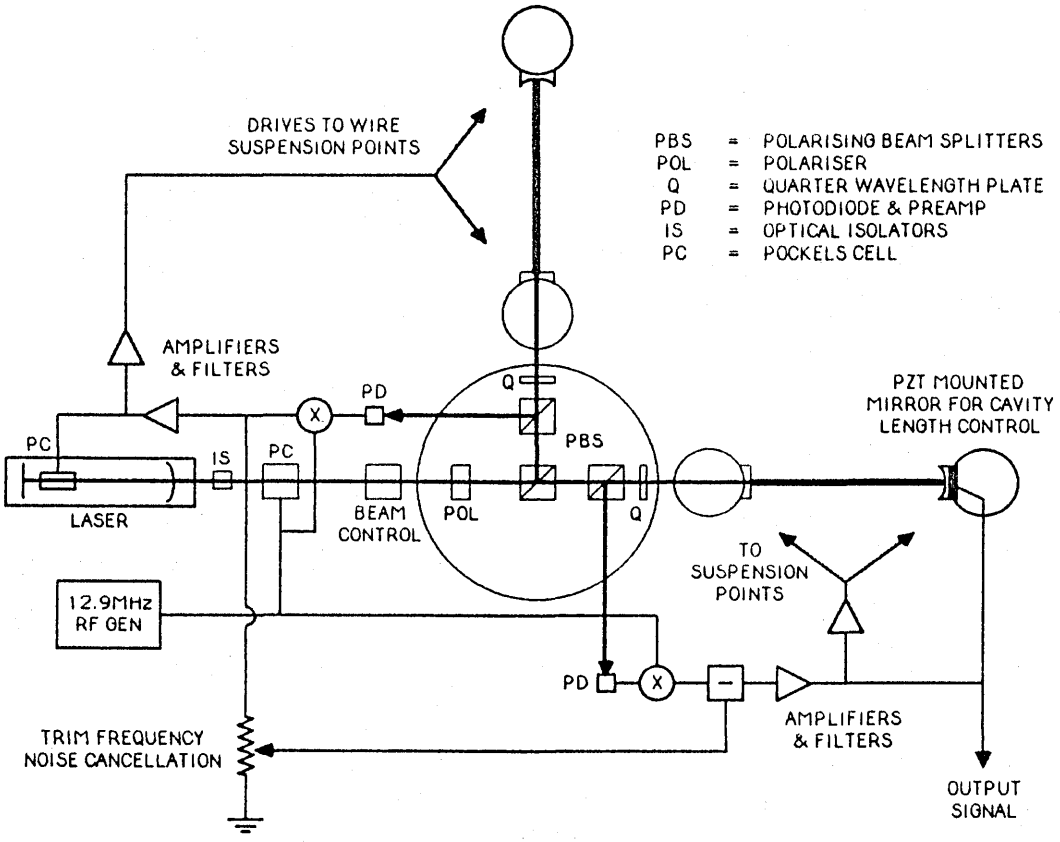

FIG.7.1 : INTERFEROMETER ARRANGEMENT WITH ELECTRONIC SUBTRACTION OF RESIDUAL FREQUENCY NOISE

with the subtracted signal, was equal to that when locked with its normal cavity signal.

To ensure that the relative sizes of the error point signals were correct for optimum subtraction, an artificial frequency induced peak was imposed on the spectrum of sensitivity and the height of this peak was minimised by adjustment of the "combining" potentiometer. In general, it was found that this frequency peak could be reduced by $\sim$ 15-20dB.

The displacement sensitivity of the interferometer, with subtraction, over a frequency range of $\sim$ 2kHz is shown in figure 7.2. Above 1kHz the sensitivity is reasonably flat. An expanded section, centred on 1440Hz is shown in figure 7.3. The upper trace shows a displacement sensitivity of $2 \ .10^{-16}$ $m/\sqrt{Hz}$ which was obtained without electronic subtraction. The lower trace, obtained when the difference signal is used to maintain the secondary cavity resonance shows a displacement sensitivity of $6 \ .10^{-17}$ $m/\sqrt{Hz}$. - 10dB of background frequency noise subtraction. (Both spectra were obtained with $\sim$ 10mW of light on the cavity photodiodes).

As an artificial frequency peak was reduced by an amount greater than this, other noise sources were investigated. By increasing the gain of the servo control dealing with lateral beam geometry fluctuations, and lessening the effects of electrical pickup, a further improvement was made to the sensitivity, as shown in figure 7.4. This spectrum shows the displacement sensitivity in a region covering 1.5-2kHz at a level of $\sim 3 \ .10^{-17}$ $m/\sqrt{Hz}$.

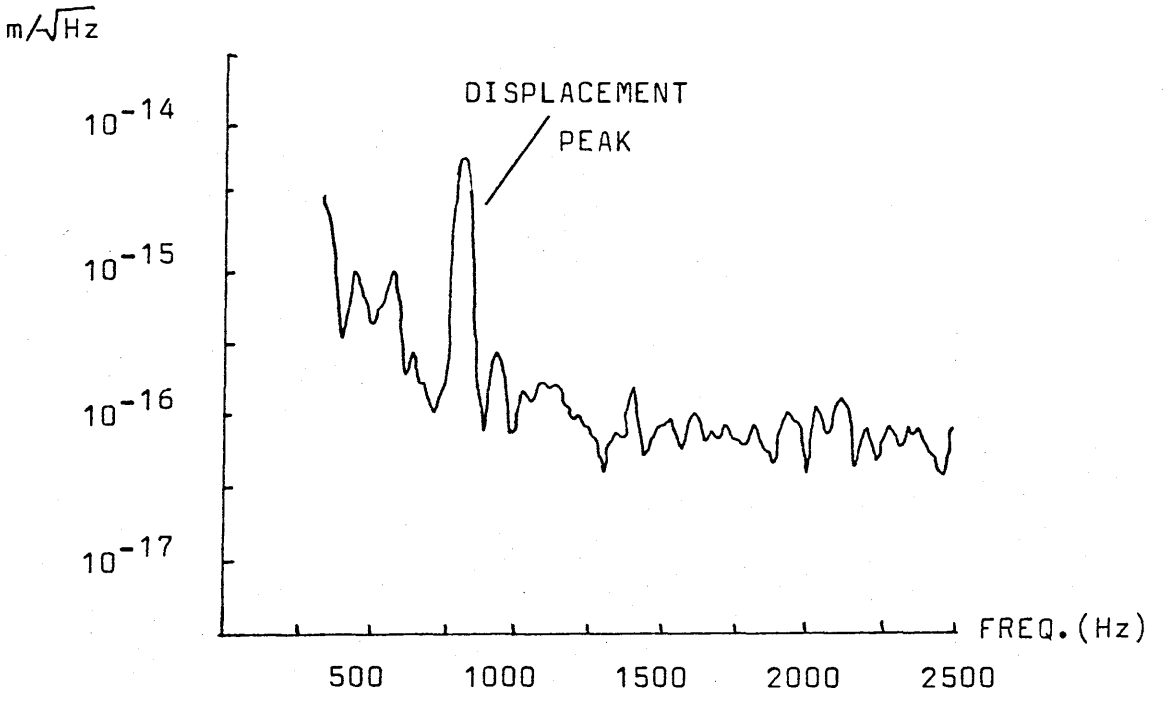

FIG. 7.2: PRELIMINARY SPECTRUM OF THE DISPLACEMENT NOISE OF THE DETECTOR USING ELECTRONIC SUBTRACTION OF RESIDUAL FREQUENCY FLUCTUATIONS.

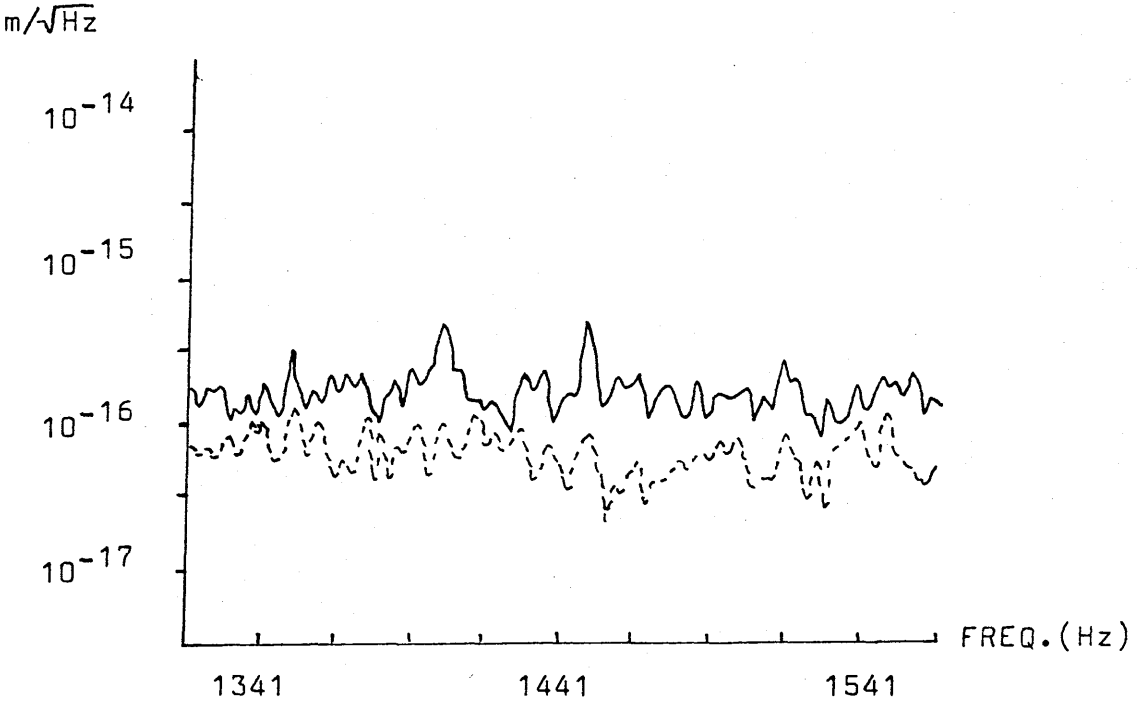

FIG.7.3: COMPARATIVE SPECTRA OF DISPLACEMENT NOISE OVER A 200Hz FREQUENCY INTERVAL CENTRED AT 1441Hz. (SOLID CURVE: WITHOUT ELECTRONIC SUBTRACTION, AND DOTTED CURVE: WITH ELECTRONIC SUBTRACTION).

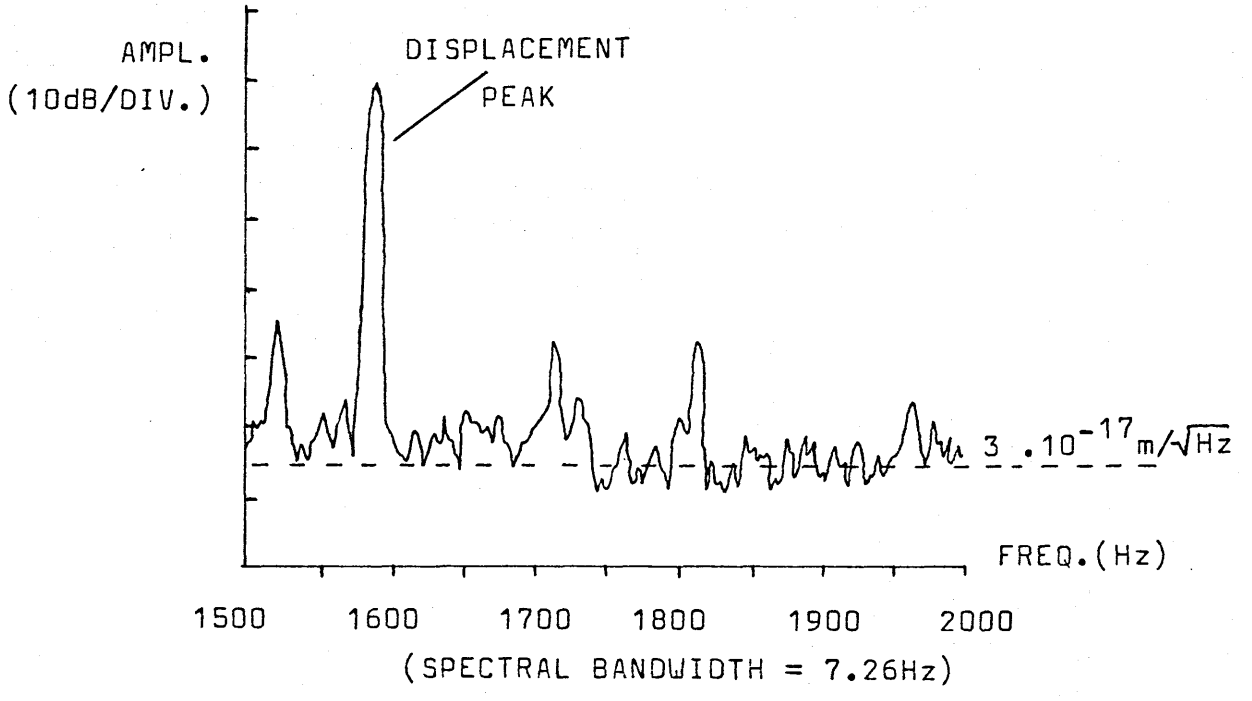

FIG.7.4: EXPANDED SECTION OF SENSITIVITY SPECTRUM. THE DOTTED LINE CORRESPONDS TO A STRAIN SENSITIVITY OF $\sim 3 \cdot 10^{-18}/\sqrt{Hz}$.

This is an improvement of five times the displacement sensitivity obtained in chapter 2.

CHAPTER 8.

"CONCLUDING REMARKS AND FUTURE PROSPECTS."

The work described in this thesis has been aimed at improving the sensitivity of the Glasgow prototype detector, and developing techniques that will be applicable to a longer baseline instrument which, hopefully, will have the necessary sensitivity for the observation of astrophysical phenomena (at reasonable rates). During the course of this work, the sensitivity of the interferometer has been improved by a factor of 100 in the kilohertz region. This has mainly been due to progress in the reduction of two main noise sources: mechanical noise from the test masses and their suspensions, and laser frequency noise.

The mechanical improvements, described in chapter 2, produced a reduction in the displacement noise of the interferometer from $3 \cdot 10^{-15}$ m/$\sqrt{\text{Hz}}$ to $1.5 \cdot 10^{-16}$ m/$\sqrt{\text{Hz}}$. However, the main emphasis of the remainder of the thesis has been on the fast frequency stabilisation of the laser, and the reduction of residual frequency fluctuations, and their effects, in the interferometer.

The reduction of frequency fluctuations intrinsic to the free running argon laser, described in chapter 3, by the reconstruction of the laser with an external resonator, provided a platform for the active stabilisation of the laser frequency by the reflection locking technique analysed in chapter 4 and extended in chapter 5.

The frequency noise subtraction techniques,

demonstrated in chapters 6 and 7, produced further improvements in the sensitivity of the detector. By optical recombination of the cavity beams, the sensitivity of the interferometer (at frequencies around 15kHz) was improved by factors up to 15dB. And with the electronic subtraction of residual frequency noise, the sensitivity, in the kilohertz region of the spectrum, was improved from $\sim 1.5 \cdot 10^{-16}$ m/$\sqrt{\text{Hz}}$ to $\sim 3.5 \cdot 10^{-17}$ m/$\sqrt{\text{Hz}}$.

The present detector has also been shown to operate in a stable condition for prolonged periods of time. - In April 1985, the system was operated continuously, for close to an hour (at a sensitivity of $\sim 2 \cdot 10^{-16}$ m/$\sqrt{\text{Hz}}$), without losing lock in the resonance of either cavity.

Most immediate improvements to sensitivity are likely to come from further mechanical improvements in test mass design (-this may even include the removal of piezoelectric elements from the masses themselves, and the use of electromagnetic forces to drive the masses for cavity stabilisation), and increased frequency stabilisation. Greater gain factors in the frequency stabilisation servo may be achieved by the use of a "2-loop" system whereby the laser is "pre-stabilised" to an auxiliary Fabry-Perot cavity before the light enters the detector. Noise introduced by beam geometry fluctuations may be further reduced by the adoption of a fibre optic coupling to the interferometer, and the use of a cavity alignment scheme should ensure that cavity visibility is optimised.[85]

The present prototype detector might expect to reach

an optimum sensitivity of around $h \sim 5 .10^{-20}/\sqrt{Hz}$. However, to reach a really significant level of sensitivity, it will be necessary to increase the baseline of the detector to kilometre lengths in order that the background noise effects, which do not scale with length, become acceptably small.[82]

In chapter 1, it was shown that a strain sensitivity of $10^{-21} - 10^{-22}$, over a kilohertz bandwidth, should give a good opportunity for the detection of fast pulsed sources, and 10^{-27}, over a narrow bandwidth, for periodic sources. To achieve this target sensitivity will require a great deal of technical effort to reduce the fundamental limit set by photon noise. For a constant measuring time, and cavity storage times less than the gravitational wave period, the photon noise limit, from 2.21, is dependent on four parameters as follows

$$h \propto [1F]^{-1} . [\lambda/I_0]^{1/2} \qquad (8.1)$$

If the sensitivity is optimised for a storage time equal to half the period of the gravitational wave then the limit due to photon noise can only be improved (or impaired) by altering two parameters.

$$\text{i.e.} \qquad h \propto [\lambda/I_0]^{1/2} \qquad (8.2)$$

From this viewpoint it is desirable to have available laser powers of greater than 20W, or so. The development of the frequency stabilisation technique, described in chapter 5, should reduce the degree of light loss and allow more of the available light power to enter the interferometer. Methods of achieving higher laser powers are also under consideration. For instance,

Neodymium-Yag (slab) lasers have recently been demonstrated to operate with extremely high powers (>100W) at their natural wavelength of 1.06 μm.[83] The efficiency of these lasers far exceeds that of present argon lasers. However, the longer wavelength means that any potential sensitivity improvement would be offset by a factor of $(1.06\,\mu m/514.5nm)^{1/2} \simeq \sqrt{2}$, and diffraction effects would result in a spot size also greater by a factor $\sqrt{2}$. This would increase the size of mirrors and vacuum pipes necessary in a long baseline detector. It is possible to frequency-double the light to 532nm but this would reduce the available power. Also, the laser would require to be operated in a single longitudinal mode (or modelocked) before being stabilised. This, again, would further reduce the output power.

An alternative approach, to the problem of achieving stable lasers with high ouput powers, is being investigated in Orsay.[60] Here a large argon laser has been stabilised by injection from a low power, stable, argon laser. The larger laser does not then, in principle, require an intra-cavity etalon, and should therefore produce a greater power output. A natural progression of technique is the coherent summation of several argon lasers, and the practicalities of this are also under investigation.

Even with increased laser powers, to reach the target sensitivity will require the additional technique of "recycling", mentioned briefly in chapter 1. This innovative idea, proposed by R.W.P. Drever,[82] involves

recycling the light, rejected at the output beamsplitter (figure 8.1), such that the overall intensity of light in the interferometer is increased. This is advantageous when the cavity mirrors used have losses so low that the storage times achievable are far in excess of the gravitational wave period.

The idea can be summarised as follows: when the interferometer is optimally operated with an interference null at the output, and the efficiency of the interference is such that the fringe null is essentially black, then most of the light leaves the interferometer through the other side of the output polariser/beamspliter. This light may be fed back to the interferometer such that it adds coherently to the initial laser beam via an additional mirror in front of the laser (figure 8.1). The reflectivity of the input mirror of each cavity is chosen to give a cavity storage time approximately equal to half the period of the expected source. The sensitivity gain, achievable with this technique, is limited by the losses of the optical elements.

If the intensity loss in each cavity mirror is A, then the total loss from each cavity is $2AN_{EFF}$, where N_{EFF} is the effective number of double-passes of the cavity made by the light.

$$\text{i.e.} \quad N_{EFF} = \frac{\text{cavity storage time}}{\text{round trip time}} = \tau_s \cdot \frac{c}{2l} \qquad (8.3)$$

This implies that the total loss per cavity, ρ , is given by

$$\rho = \frac{c\,\tau_s\,A}{l} \qquad (8.4)$$

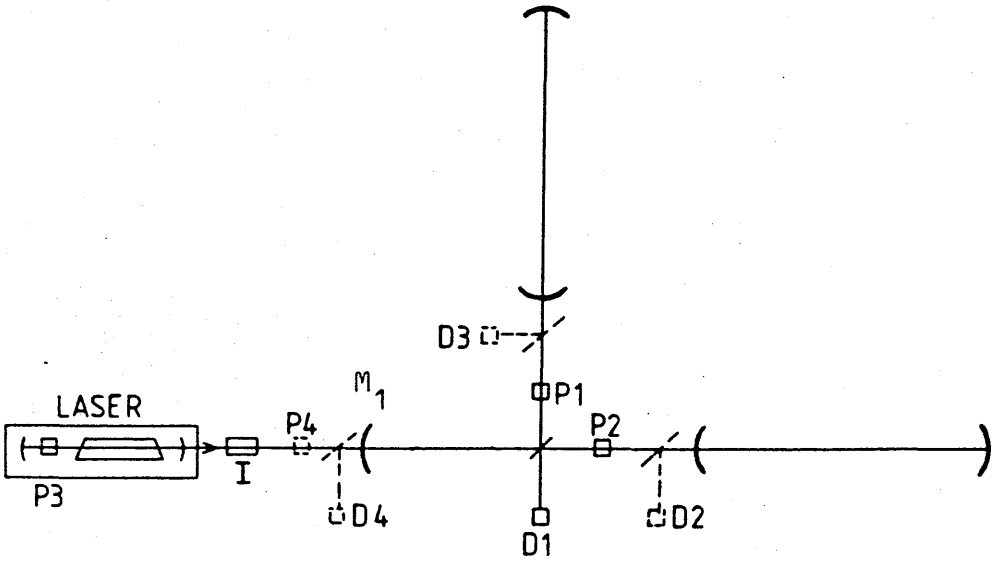

FIG.8.1: AN OPTICAL ARRANGEMENT OF A CAVITY INTERFEROMETER USING RECYCLING. THE "RECYCLING MIRROR" M_1 REFLECTS BACK INTO THE INTERFEROMETER ANY LIGHT RETURNING TOWARDS THE LASER. BY MINIMISING THE LIGHT AT D_1 THE LIGHT POWER WITHIN THE INTERFEROMETER IS INCREASED BY A FACTOR APPROXIMATELY EQUAL TO THE RECIPROCAL OF THE LOSSES.

Assumimg the cavity losses dominate, the increase in light intensity, produced by recycling, is approximately equal to $1/\rho$.

$$\text{i.e. Intensity gain} \simeq \frac{1}{c\tau_s A} \qquad (8.5)$$

which implies, from 8.2, that

$$\text{Sensitivity gain} \simeq \left(\frac{1}{c\tau_s A}\right)^{1/2} \qquad (8.6)$$

So, for mirrors with losses $A=10^{-4}$, a kilometre detector, searching for millisecond pulses, would have its sensitivity enhanced by a factor of ~ 8 with recycling.

If the end mirrors, of the cavities, have reflectivity R, such that $A \simeq (1-R)$, then 2.24 and 8.6 produce an optimum shot noise limit (with recycling) of

$$h_{MIN} \simeq \left(\frac{\hbar\lambda\,(1-R)}{2\pi\epsilon I_0 l\tau^2}\right)^{1/2} \qquad (8.7)$$

This reveals that, to reach a strain sensitivity $h \sim 10^{-22}$ in a kilohertz bandwidth, will require laser powers of the order of 100W, or so.

The recycling scheme, described above, is intended to be used in the search for short gravitational wave pulses. However, an alternative recycling technique - known as "periodic recycling" - may be used for searches for continuous sources, at a specific frequency, using integration times much longer than the source period.[82] This scheme, like the previous one, depends on the use of a very low loss interferometer capable of very long light storage times. The optical arrangement is schematically illustrated in figure 8.2. The initial input beam is split evenly into

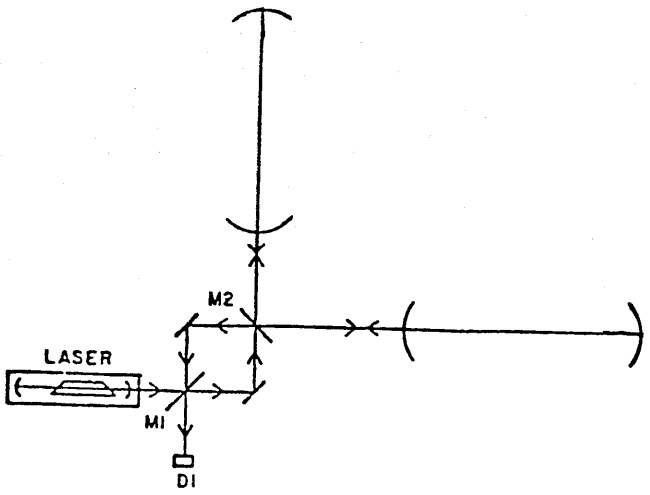

FIG.8.2: AN INTERFEROMETER ARRANGEMENT WHICH USES "PERIODIC RECYCLING". IF THE CAVITY STORAGE TIMES ARE ARRANGED TO BE EQUAL TO HALF THE PERIOD OF THE GRAVITATIONAL WAVE, THE LIGHT IS CYCLED BETWEEN THE CAVITIES WITH AN OVERALL PERIOD EQUAL TO THAT OF THE GRAVITATIONAL WAVE.

two separate parts by mirror M_1, and these beams pass through mirror M_2 before entering the orthogonal cavities which have their storage times arranged to be approximately equal to half the period of the gravitational wave. The light in each cavity experiences a phase shift due to the action of the gravitational wave, and each phase shifted cavity output is redirected (by means of M_2) into the opposite cavity where its phase is further shifted in the same direction. The cycle is repeated continuously, with a period equal to that of the source, until the losses due to the optical elements become dominant. Thus, there is a large overall phase shift, due to the gravitational wave, built up over the total storage time of the system.

The improvement in sensitivity, gained by periodic recycling over the conventional interferometer, is given by a factor approximately equal to the ratio of the total storage time to the period of the gravitational wave (i.e. τ_s / τ_g). The storage time of the system is approximately given by

$$\tau_s \simeq \frac{1}{c(1-R)} \qquad (8.8)$$

which implies

$$\text{Sensitivity Gain} \simeq \frac{c(1-R)\tau_g}{1} \qquad (8.9)$$

For a kilometre detector with low loss mirrors ($A=10^{-4}$), and source period of a millisecond, the sensitivity improvement is approximately 30.

The sensitivity limit (with periodic recycling) due to photon noise now becomes

$$h_{MIN} \simeq \left(\frac{c\hbar\lambda(1-R)^2}{2\pi\epsilon I_0 \tau l^2} \right)^{1/2} \qquad (8.10)$$

where τ is the total integration time.

Thus, a kilometre detector illuminated with 20W of laser light might expect to reach a photon noise limited strain sensitivity of $h \sim 10^{-27}$ with an integration time of $\sim$ 1 month.

This limit suggests that, with long integration times, it would be straightforward to detect gravitational radiation from a "weak" source such as the Crab pulsar. In practice however the limiting factors are likely to come from other noise sources such as thermal noise and (eventually) the quantum limit.

Both of the above recycling schemes can also be used, equally effectively, with delay-line interferometers.[82]

A long baseline detector then, in conclusion, would have the potential to reach levels of sensitivity where current theoretical estimates would predict observable signals at reasonable rates. There already exist design proposals for such interferometers in Britain, West Germany and the United States, with suggested detector baselines of up to 4km. Obviously the total cost of a detector is likely to be the most prohibitive barrier to its complexity, but the proposals include some elaborate design schemes. For example, a detector based on optical cavities allows for the possibility of operating multiple interferometers in the same vacuum housing. These interferometers (2 or more) could be of varying length such as to provide some local discrimination against certain noise sources, or they could

be dedicated to specific ranges of the gravitational wave frequency band.

The prospects for the future, then, are very exciting. Although there can be no guarantee of success, the potential for scientific discovery is so great that, hopefully, the programmeof gravitational wave research will come to full fruition.

APPENDIX.

"DIRECT OBSERVATIONAL UPPER LIMIT TO GRAVITATIONAL RADIATION FROM MILLISECOND PULSAR PSR1937+214."

The discovery, in late 1982, of the millisecond pulsar PSR1937+214, with its exceptionally high rotational rate (642Hz), led to excitement in the gravitational wave field and the initial hope that it was a potentially strong source of gravitational radiation. This was, in part, encouraged by early suggestions of a high slowdown rate which might have resulted in the dissipation of energy as a large flux of gravitational waves. Even though subsequent reports [86,87,88] suggested a very small slowdown rate, there were still possible circumstances in which a large flux of gravitational waves could have been produced. For example, continuing accretion might provide additional energy for gravitational radiation; and the Earth/pulsar distance may have been shorter, than was indicated by the dispersion measure, if there was large local dispersion. This encouraged a search for radiation, from the pulsar, with a divided-bar detector, originally developed at Glasgow for pulse searches. This detector was designed to have a relatively wide bandwidth (several hundred hertz) which included, at near maximum sensitivity, the frequency 1.284kHz - twice the pulsar rotation frequency. This would be a probable frequency for gravitational wave generation from this particular source.

The detector itself is a room temperature bar, sensed by piezoelectric transducers between the bar-halves,

with a total mass of 300kg, a coupling coefficent of 0.18, a mechanical quality factor of 2200, and an overall noise temperature of less than 5K.

The experimental arrangement is schematically shown in figure A.1. The detector output, after filtering by bandpass and notch filters,[24] was heterodyned, in a lock-in amplifier, to a frequency of around 1.7Hz, in order to ease the data handling problems. The reference signal was derived from a 5MHz crystal oscillator, referenced to the 60kHz MSF standard frequency transmission.

The quadrature components of the heterodyned signal were synchronously averaged in 26-minute batches by a digital spectrum analyser (HP3582A). The trigger timing for the analyser was also derived from the crystal clock, referenced to the MSF frequency standard, by a system of preset scalars operating in "leap-year" mode.[89]

To compensate for the apparent (Doppler) shift in the pulsar frequency, resulting from the motion of the Earth, small adjustments had to be made to the trigger period (- which was around 12.57 seconds). The trigger could be finely adjusted by changing the setting of the scalars. This ensured that any resulting phase errors were less than 0.1 cycle at all times.

The 26-minute data averages were down-loaded onto magnetic tape by a microcomputer (HP85), and added together with appropriate phase shifts inserted between batches. This allowed for a signal scan over 10 adjacent frequency channels around the expected frequency. Subsequent folding of the data, and analysis by the least squares method,

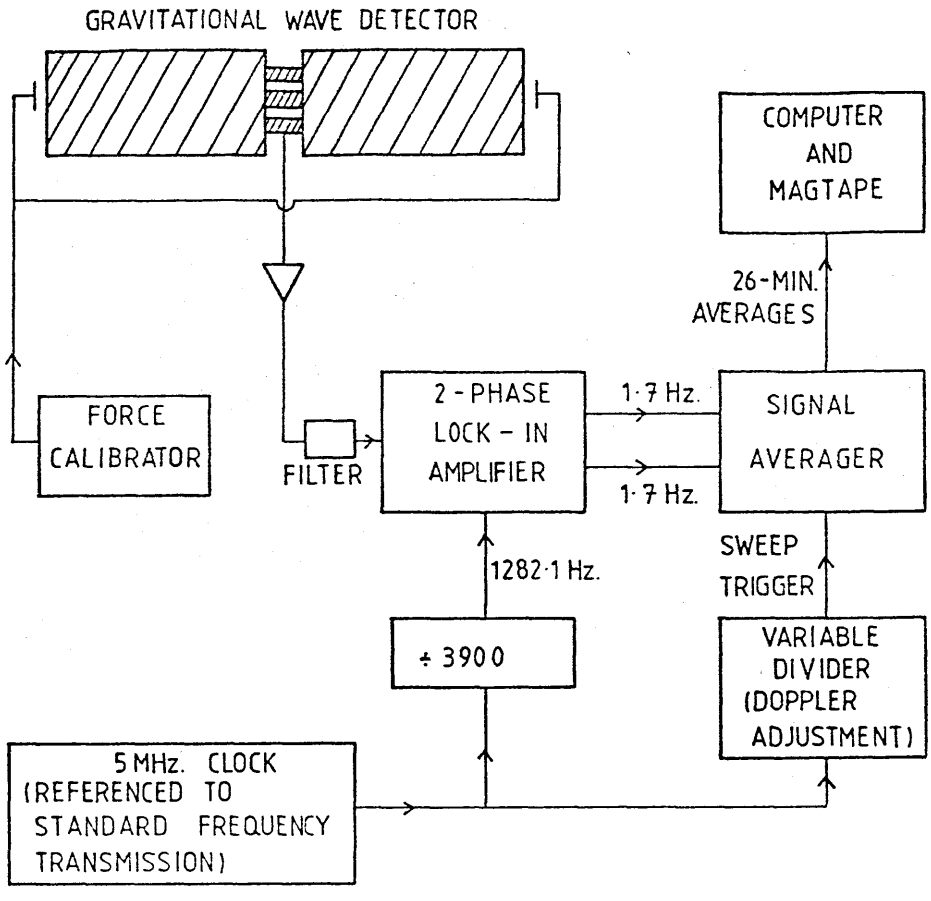

FIG.A.1: SIMPLIFIED SCHEMATIC DIAGRAM OF DETECTOR AND DATA RECORDING SYSTEM.

allowed the amplitudes of each frequency component to be obtained.

The resulting spectral output of the detector , over an 8-hour run from 20.15 6 Dec. to 04.15 7 Dec. 1982, is shown in figure A.2. The signal amplitude is expressed in terms of the equivalent gravitational wave amplitude, averaged over polarisation and accounting for the sensitivity variation due to the relative angular deviations of the detector and pulsar. The sensitivity calibration was obtained by applying known sinusoidal forces to the ends of the bar with capacitor plates.[24]

As can be seen, there is no statistical evidence for a signal at twice the pulsar frequency. At this frequency, the detector output power, corrected for noise power observed at other frequencies, corresponds to a gravitational wave amplitude of $h \sim 0.8^{+1.5}_{-0.8} .10^{-20}$.

The negative result of the search is not surprising, given the limited sensitivity of the detector. However it does provide an interesting and direct observational constraint on pulsar PSR1937+214.

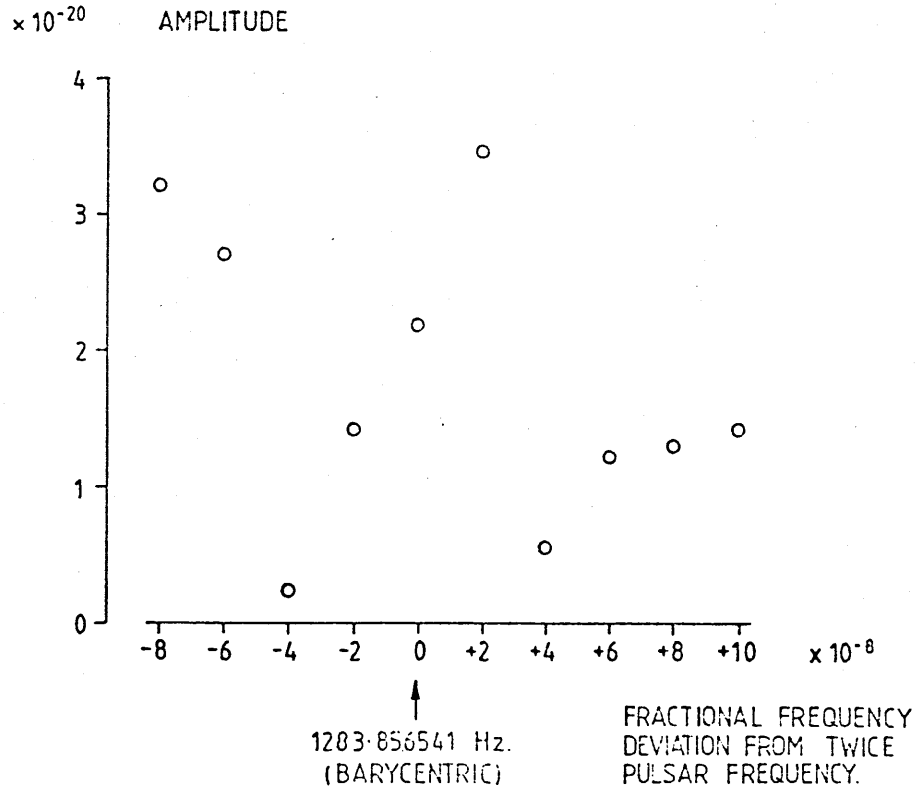

FIG.A.2: ANALYSIS OF DETECTOR OUTPUT FROM 8-HOUR RUN, WITH OUTPUT VOLTAGE COMPONENTS AT 10 DISCRETE BARYCENTRIC FREQUENCIES EXPRESSED IN TERMS OF EQUIVALENT GRAVITATIONAL WAVE AMPLITUDE AVERAGED OVER POLARISATION.

REFERENCES.

1. EINSTEIN, A., Sitzber. Preuss, Akad. Wiss., Berlin, K1. Math. Physik. UTech, 688, (1916).
2. EINSTEIN, A., Sitzber. Preuss, Akad. Wiss., Berlin, K1. Math. Physik. Utech, 154, (1918).
3. MISNER, C.W., THORNE, K.S. & WHEELER, J.A., "Gravitation", (W.H. Freeman, San Francisco), (1973).
4. PRESS, W.H. & THORNE K.S., Ann. Rev. Astron. Astrophys., 10, 355, (1972).
5. DAVIES, P.C.W., "The search for gravity waves", (Cambridge), (1980).
6. THORNE, K.S., O.A. Series, Nuc. Atomic and Nuc. Astrophys., 575, (1979).
7. KOPVILLEM, U.Kh. & NAGIBAROV, V.R., Sov. Phys. JETP., 38, 215, (1974).
8. GRISHCHUK, L.P. & SAZHIN, M.V., Sov. Phys. JETP., 38, 215, (1974).
9. ZIMMERMANN, M. & THORNE, K.S., in "Essays in General Relativity: a Fentschrift for Abraham H. Taub", Ed. F.J. Tipler, Academic, New York, (1980).
10. (e.g.) HILLEBRANDT, W., Ann. N.Y. Acadamy Sci., 422, 197, (1984).
11. EARDLEY, D.M. in "Gravitational Radiation", Eds. Deruelle, N. & Piran, T., (North-Holland, Amsterdam), (1983).
12. CLARK, J.P.A. & EARDLEY, D.M., AP.J., 215, 311, (1977).
13. TAYLOR, J.H. & WEISBERG J.M., AP.J., 253, 9081, (1982).

14. PINES, D., SHARMAN, J. & RUDERMAN, M., Nature Phys. Sci., 237, 83, (1972).

15. BOND, J.R. & CARR, B.J., Mon. Not. R. Asron. Soc., 207, 585, (1984).

16. HIRAKAWA, H., TSUBONO, K. & FUJIMOTO, M., Phys. Rev., D17, 1919, (1977).

17. WAGONER, R.V., Astrophys. J., 278, 345, (1984).

18. SKINNER, G.K., BEDFORD, D.K., ELSNER, R.F., LEAHY, D., WEISSKOPF, M.C. & GRINDLAY, J., Nature, 297, 568, (1982).

19. CARR, B.J., Astron. Astrophys., 89, 6, (1980).

20. HOUGH, J., PUGH, J.R., BLAND, R. & DREVER, R.W.P., Nature, 254, 498, (1975).

21. WEBER, J., Phys. Rev. Lett., 117, 306, (1960).

22. WEBER, J., Phys. Rev. Lett., 22, 1320, (1969).

23. BRAGINSKII, V.B., MANUKIN, A.B., POPOV, E.I., RUDENKO, V.N. & KHOREV, A.A., JETP. Lett., 16, 108, (1972).

24. DREVER, R.W.P., HOUGH, J., BLAND, R. & LESSNOFF, G.W., Nature, 246, 340, (1973).

25. ALLAN, W.D. & CHRISTODOULIDES, C., J. Phys. A. Math. Gen., 8, 1726, (1975).

26. APLIN, P.S., J. Gen. Rel. Grav., 3, 111, (1972).

27. BILLING, H., KAFKA, P, MAISCHBERGER, K., MEYER, F. & WINKLER, W., Lett. Al. Nuovo. Cim., 12, 111, (1975).

28. FORWARD, R.L., ZIPOY, D., WEBER J., SMITH, S. & BERIOFF, H., Nature, 189, 473, (1961).

29. MAST, T.S., NELSON, J.E. & SAARLOOS, J.A., Astrophys. J., 187, L49, (1974).

30. SADEK, D. & MEIDEV, M., Nature, 240, 136, (1972).

31. HOUGH, J., PUGH, J.R., EDELSTEIN, W.A. & MARTIN, W., J. Phys. E. Sci. Instrum., 10, 993, (1977).

32. EDELSTEIN, W.A., HOUGH, J., PUGH, J.R. & MARTIN, W., J. Phys. E., 11, 710, (1978).

33. HEFFNER, H., Proc. I.R.E., 50, 1604, (1962).

34. GIFFARD, R.P., Phys. Rev., D14, 2478, (1976).

35. UNRUH, W.G., Phys. Rev. D., 19, 2888, (1979).

36. CAVES, C.M., DREVER, R.W,P., SANDBERG, V.D., THORNE, K.S., & ZIMMERMANN, M., Rev. Mod. Phys., 52, 341, (1979).

37. MOSS G.E., MILLER, L.R. & FORWARD, R.L., Appl. Opt., 10, 2495, (1971).

38. FORWARD, R.L., Phys. Rev. D., 19, 2888, (1978).

39. WEISS, R., MIT Progress Report 105, Res. Lab. Electron., 54, (1972).

40. DREVÉR, R.W.P., HOUGH, J., MUNLEY, A.J., LEE, S-A, SPERO, R., WHITCOMB , S.E., WARD, H., PUGH, J.R., NEWTON, G.P., MEERS, B.J., BROOKS III, E.D. & GURSEL, Y., in "Quantum Optics, Expt. Grav. & Meas. Theory", Eds. Meystre, P. & Scully, M.O., (Plenum press), (1981).

41. CAVES, C.M., Phys. Rev., D23, 1693, (1981).

42. SCHILLING R., SCHNUPP, L., WINKLER, W., BILLING, H., MAISCHBERGER, K. & RUDIGER, A., J. Phys. E. Sci. Instrum., 14, 65, (1981).

43. ESTABROOK, F.B. & WAHLQUIST, H.D., GRG6, 439, (1975).

44. HELLINGS, R.W., in "Gravitational Radiation", Eds. Deruelle, N., & Piran, T., (N. Holland, Amsterdam), (1983).

45. WEISS, R., BENDER, P.L., MISNER, C,W. & POUND, R.V., Report on the sub-panel on Relativity and Gravitation, Management & operations working group for shuttle astronomy, NASA, (1976).

46. BRAGINSKII, V.B. & THORNE, K.S., Nature, 316, 610, (1985).

47. MICHELSON, P.F. & TAUBER, R.C., Phys. Rev., D29, 2149, (1984).

48. MEERS, B.J., PhD Thesis, Univ. of Glasgow, (1983).

49. HALL, J.L., LAYER, H.P. & DESLATTES, R.D., IEEE J. Q-E, 13, 45D, (1977).

50. BILLING, H., MAISCHBERGER, K., RUDIGER, A., SCHILLING, R., SCHNUPP, L. & WINKLER, W., J. Phys. E.: Sci. Instrum., 12, 1043, (1979).

51. RUDIGER, A., SCHILLING, R., SCHNUPP, L., WINKLER, W., BILLING, H. & MAISCHBERGER, K., Journal de Physique, 42, C8-415, (1981).

52. MEERS, B.J., NEWTON, G.P. & DREVER, R.W.P., To be published.

53. SHOEMAKER, D., WINKLER, W., MAISCHBERGER, K., RUDIGER, A., SCHILLING, R., SCHNUPP, L., Max-Planck institute internal report MPQ 100, (1985).

54. MAN, C.N., BRILLET, A. & CEREZ, P., J. Phys. E.: Sci. Instrum., 11, 19, (1978).

55. SCHNUPP, L., WINKLER, W., MAISCHBERGER, K., RUDIGER, A. & SCHILLING, R., J. Phys. E.: Sci. Instrum., 18, 482, (1985).

56. MARTIN, W., PhD Thesis, Univ. of Glasgow, (1978).

57. ROBERTSON, N.A., DREVER, R.W.P., KERR, I. & HOUGH, J., J. Phys. E.: Sci. Instrum., 15, 1101, (1982).

58. MUNLEY, A.J., PhD Thesis, Univ. of Glasgow, (1982).

59. BRIDGES, W,B., CHESTER, A.N., HALSTED, A.S., PARKER, J.V., Proc. IEEE., 59, 724, (1971).

60. MAN, C.N. & BRILLET, A., Opt. Lett., 9, 502, (1984).

61. JASEJA, T.S., JAVAN, A., MURRAY, J. & TOWNES, C.H., Bull. Am. Phys. Soc. 7, 553, (1962).

62. JASEJA, T.S., JAVAN, A. & TOWNES, C.H., Phys. Rev. Lett., 10, 165, (1963).

63. (e.g.) McLachlan, "Theory of vibrations", (Dover publications, N.Y.), (1951).

64. LAMB. W.E. Jnr., Phys. Rev., 134, 6A, A1429, (1964).

65. BLOOM, A.L. & WRIGHT, D.L., Proc. IEEE, 54, 1290, (1966).

66. SZOKE, A. & JAVAN, A., Phys. Rev., 145, 137, (1966).

67. WALLARD, A.J., J. Phys. E., 5, 926, (1972).

68. WHITE, A.D., GORDON, E.I. & LABUDA, E.F., Appl. Phys. Lett., 5, 97, (1964).

69. BAER, T., KOWALSKI, F.V. & HALL, J.L., Appl. Opt., 19, 3173, (1980).

70. ALLAN, D.W., SHOAF, J.H. & HALFORD, D., "Time and Frequency: Theory and fundamentals", NBS Monograph 140.

71. WHITE, A.D., IEEE J. Q-E., 1, 349, (1965).

72. HELMCKE, J., LEE, S-A. & HALL, J.L., Appl. Opt., 21, 1686, (1982).

73. DREVER, R.W.P., HALL, J.L., KOWALSKI, F.V., HOUGH, J., FORD, G.M., MUNLEY, A.J. & WARD, H., Appl. Phys. B., 33, 179, (1984).

74. POUND, R.V., Rev. Sci. Instrum., 17, 490, (1946).

75. FORD, G.M., PhD Thesis, Univ. Of Glasgow, (1981).

76. LAURES, P., Phys. Lett., 10, 61, (1964).

77. YARIV, A., "Quantum Electronics", 2nd ed., (Wiley, New York), (1975).

78. CAMY, G., PINAUD, D., COURTIER, N., CHIAN, H.C., Rev. Physique Appl., 17, 357, (1982).

79. HALL, J.L. & HANSCH, T.W., Opt. Lett., 9, 502, (1984).

80. (E.g.) DI STEFANO III, J.J., STUBBERUD, A.R. & WILLIAMS, J.J., "Feedback and control systems", (McGraw-Hill), (1967).

81. BODE, H.W., Bell System Journal, 19, 421, (1940).

82. DREVER, R.W.P., in "Gravitational Radiation", Eds. Deruelle, N. & Piran, T., (N. Holland, Amsterdam), (1983).

83. EDELSTEIN, W.A., Private Communication.

84. GIBBONS, G.W. & HAWKING, S.W., Phys. Rev. D., 4, 2191, (1971).

85. ANDERSON, D.Z., Appl. Opt., 23, 2944, (1984).

86. BACKER, D.C., KULKARNI, S.R., HEILES, C., DAVIES, M.M. & GROSS, W., Nature, 300, 615, (1982).

87. ASHWORTH, M., LYNE, A.G. & SMITH, F.G., Nature, 301, 313, (1983).

88. BACKER, D.C., KULKARNI, S.R. & TAYLOR, J.H., Nature, 301, 314, (1983).

89. HOROWITZ, P., Rev., Sci. Instrum., 40, 369, (1969).

90. LAYER, H.P., IEEE Trans. Instrum. Meas., IM-29, 358, (1980).